# NEURAL CONTROL OF REACHING AND STEERING



DONDERS S E R I E S Milou van Helvert

RADBOUD UNIVERSITY PRESS

Radboud Dissertation Series

# Neural control of reaching and steering

Milou van Helvert

The research presented in this thesis was carried out at the Radboud University, Donders Institute for Brain, Cognition and Behaviour, and was made possible by an internal grant from the Donders Centre for Cognition.

**Author:** Milou van Helvert

Title: Neural control of reaching and steering

#### **Radboud Dissertations Series**

ISSN: 2950-2772 (Online); 2950-2780 (Print)

Published by RADBOUD UNIVERSITY PRESS Postbus 9100, 6500 HA Nijmegen, The Netherlands www.radbouduniversitypress.nl

Design: Proefschrift AIO | Annelies Lips Cover: Proefschrift AIO | Guntra Laivacuma

Printing: DPN Rikken/Pumbo

ISBN: 9789465150307

DOI: 10.54195/9789465150307

Free download at: https://doi.org/10.54195/9789465150307

© 2025 Milou Johanna Louise van Helvert

# RADBOUD UNIVERSITY PRESS

This is an Open Access book published under the terms of Creative Commons Attribution-Noncommercial-NoDerivatives International license (CC BY-NC-ND 4.0). This license allows reusers to copy and distribute the material in any medium or format in unadapted form only, for noncommercial purposes only, and only so long as attribution is given to the creator, see http://creativecommons.org/licenses/by-nc-nd/4.0/.

# Neural control of reaching and steering

Proefschrift ter verkrijging van de graad van doctor
aan de Radboud Universiteit Nijmegen
op gezag van de rector magnificus prof. dr. J.M. Sanders,
volgens besluit van het college voor promoties
in het openbaar te verdedigen op
vrijdag 7 maart 2025
om 10.30 uur precies

door

Milou Johanna Louise van Helvert

geboren op 24 september 1994 te Eindhoven

#### Promotor:

Prof. dr. W.P. Medendorp

## Copromotoren:

Dr. R.J. van Beers Dr. ing. L.P.J. Selen

## Manuscriptcommissie:

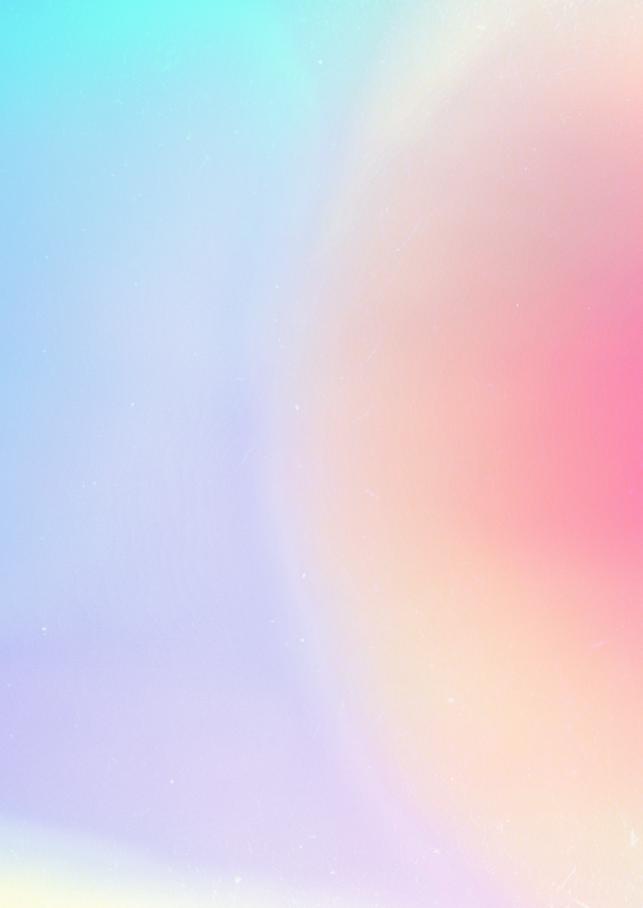
Prof. dr. U. Noppeney

Prof. dr. P. Lefèvre (Université catholique de Louvain, België)

Dr. P.A. Forbes (Erasmus MC)

# **Table of contents**

Chapter 1	General introduction	7
Chapter 2	Cortical beta-band power modulates with uncertainty in effector selection during motor planning	27
Chapter 3	Predictive steering: integration of artificial motor signals in self-motion estimation	51
Chapter 4	Vestibular-derived internal models in active self-motion estimation	79
Chapter 5	General discussion	107
Appendices	References Dutch summary Research data management About the author Donders Graduate School	120 131 133 135 136
	Acknowledgements	138



# Chapter 1

# General introduction

We seem to move our bodies with ease. This feeling of effortlessness makes sensorimotor control and learning seem simple, but beneath the level of consciousness is a prodigious control system at work. It decides on the movement to make, prepares the movement, and activates the muscles that execute the movement. During the movement, it responds to unexpected perturbations and learns from these events to improve future movements if needed. How does the central nervous system so smoothly control our movements in rich and dynamic natural environments?

Over the past decades, many studies have examined the control processes underlying our actions. Behavioral experiments have been used to investigate the interaction between sensory inputs and motor output (Tresilian, 2012). By manipulating the sensory feedback and recording the responses of the participants, researchers have tried to infer the control system's computational mechanisms that govern the behavior (Franklin & Wolpert, 2011). With the development of modern techniques to record brain activity, researchers have additionally mapped these computational mechanisms onto areas and circuits of the brain (Kandel & Hudspeth, 2000).

Most of these studies used straightforward experimental tasks with well-controlled stimulus-response behaviors that unnaturally constrain the body. In natural environments, stimuli are contextually embedded and continuously changing, and responses are more complex and heterogeneous. Most natural behaviors depend on closed action-perception loops: continuous interactive processes in which an action affects the sensory input and the sensory input affects the action (Fig. 1.1A) (Gordon et al., 2011). This allows us to actively explore our environments to search for useful information, also known as active sensing (Little & Sommer, 2013; Schroeder, Wilson, Radman, Scharfman, & Lakatos, 2010).

Some of the processes that are thought to underlie sensorimotor behavior are shown in Figure 1.1B. Forward internal models, which simulate the relationship between motor commands and the consequences of the movement without actually executing the movement, play an important role in the action-perception loop (Gordon et al., 2011; Kawato, 1999; von Holst & Mittelstaedt, 1950; Wolpert et al., 2000). The sensory input from the body and environment is thought to be continuously compared to sensory predictions that are computed by the forward internal model based on an efference copy of the motor commands. Based on

an estimate of the state of the body and the environment, the action is in turn updated if needed (Scott, 2004), closing the action-perception loop.

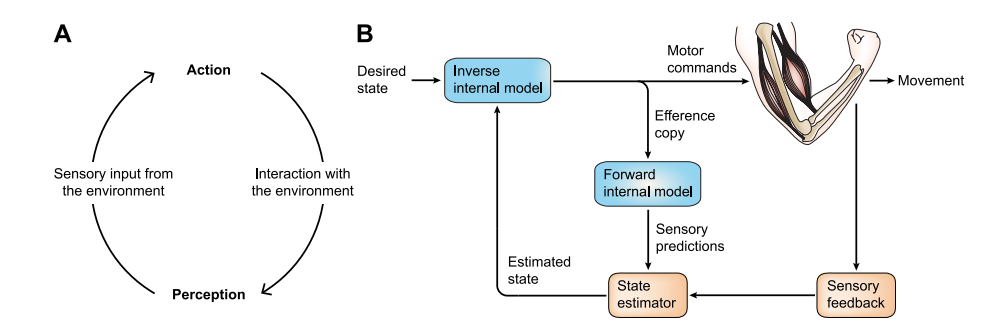


**Figure 1.1.** Interaction between action and perception in natural environments. A) Most natural behaviors depend on closed action-perception loops, in which there is a continuous interaction between action and perception. B) This interaction is also reflected in some of the processes that are thought to underlie sensorimotor behavior. To execute a movement, an inverse internal model determines the required motor commands. These motor commands are sent to the muscles to generate the necessary forces. An efference copy of the motor commands is sent to a forward internal model, which predicts the sensory consequences of the movement by simulating the interaction of the motor system and the environment. These predictions are compared to the actual sensory feedback to estimate the state of the body and the environment, and, depending on the control policy, the movement is adjusted if needed. Adapted from Scott (2004) and Wolpert et al. (2000).

In this thesis, I will study two natural behaviors, reaching and steering, to examine the processes that underlie the smooth control of our movements in rich and dynamic environments in more detail. In the following sections, I will first describe how the central nervous system selects and plans actions in rich environments. I will focus on reaching, and more specifically on hand choice (Chapter 2). After this, I will describe the online control of movements based on sensory feedback and sensory predictions, followed by a section about motor learning and adaptation. I will focus on the role of vestibular sensory feedback and predictions during the control of self-motion in dynamic environments (Chapter 3 and 4). Finally, I will provide an outline of the thesis.

# 1.1 Action selection and movement planning

## 1.1.1 Serial and parallel processing

Natural environments give rise to many action opportunities (Cisek, 2007). How do we decide what to do and how to do it? Action decisions are thought to

be based on the desirability and the costs of the possible actions (Shadmehr, Huang, & Ahmed, 2016; Trommershäuser, Maloney, & Landy, 2009; Wolpert & Landy, 2012). If you are very thirsty for example, it might be more desirable to take a sip of your drink instead of reaching for some food. And if there are two jugs of your favorite drink on the table, you will probably reach for the one that is closest to you because it is easiest to reach, minimizing the energetic costs of the movement (Cos, Bélanger, & Cisek, 2011).

When you determine what to do and how to do it has been a topic of debate. Traditional views of cognition state that the brain processes information in a serial manner, with temporally separable perceptual, cognitive and motor processes (Donders, 1869/1969). The perceptual system is thought to transform the incoming sensory information into an internal representation of the environment (Marr, 1982). The cognitive system in turn decides what action to execute based on this representation, and provides the motor system with the movement plan to be implemented. However, neural data has shown substantial overlap in brain regions associated with perceptual, cognitive, and motor processes (for a review, see Cisek & Kalaska, 2010). This suggests that the processes are more integrated than proposed by the serial processing model.

As an alternative to this serial processing model, the parallel processing model has been proposed, in which multiple possible movement plans are defined in parallel that compete for execution (Cisek & Kalaska, 2005). This idea is based on an experiment in which nonhuman primates were instructed to reach towards one of two targets. Before the actual reach target was specified, neural activity in the motor cortex was found to represent both targets. After the reach target was specified, neural activity increased in the neural population representing the selected target and decreased in the neural population representing the unselected target. This was taken to suggest that the brain specifies multiple potential movement plans before reaching a decision, although some suggest that these findings are the result of averaging neural activity across trials (see Dekleva, Kording, & Miller, 2018).

## 1.1.2 Hand choice experiments

If deciding between two possible reach targets evokes multiple movement plans, deciding between the left and right hand to reach to a single target may similarly lead to the specification of parallel movement plans that compete for execution. I will focus on this question in Chapter 2 of this thesis. When

choosing which hand to use, in general people select the hand closest to the target (Bryden, Pryde, & Roy, 2000). However, this choice is biased by handedness and expected task success (Schweighofer et al., 2015). During body motion, hand choice is also influenced by the inertial forces on the arm, modulating the biomechanical costs of the reaching movement (Bakker, Selen, & Medendorp, 2019; Bakker, Weijer, van Beers, Selen, & Medendorp, 2017; Oostwoud Wijdenes et al., 2022).

Preferences in hand choice can be studied psychometrically, e.g., using a paradigm in which the target is presented at different locations relative to the body (Fig. 1.2A, from Oliveira, Diedrichsen, Verstynen, Dugue, & Ivry, 2010). The targets appear one at a time at various locations on a semicircle and participants are instructed to reach to the target as guickly as possible with either hand. Reaches towards the same target location are repeated multiple times to compute the probability of left and right hand choices for each target location (Fig. 1.2B). The target location for which participants have an equal probability of using the left or the right hand can be determined by fitting a psychometric function to the choice data, and is called the point of subjective equality (PSE). The PSE provides information about biases in hand choice, and will for example be slightly shifted towards the left of the body midline in right-handed participants.

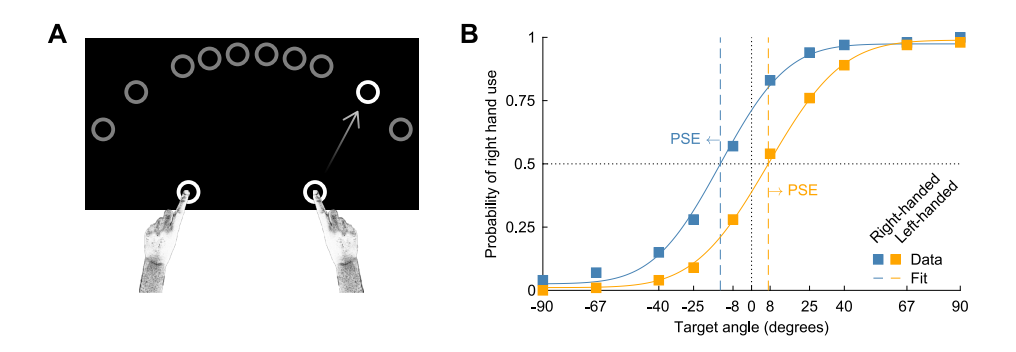


Figure 1.2. Experimental paradigm used to study hand choice (adapted from Oliveira et al., 2010). A) Experimental setup. Participants place their hands on the start locations and reach for a target that appears on a semicircle. B) Hand choice as a function of target angle for two fictional participants. The point of subjective equality (PSE; dashed vertical colored lines) is the target angle for which participants have an equal probability of choosing the left or the right hand (dotted horizontal line), and can be determined by fitting a psychometric function (solid colored lines) to the hand choice data (colored squares). Relative to the body midline (dotted vertical line), in general, the PSE will be slightly shifted to the left for a right-handed participant (blue data) and slightly shifted to the right for a left-handed participant (orange data).

It is unclear whether hand choice is governed by a competition between reach plans or by serial processing of hand choice and subsequent reach implementation. Some behavioral and neural findings suggest that hand choice relies on a competitive process between movement plans for the left and right hand. Reaches toward targets that are close to the PSE, at which the competition between the left and right hand is expected to be highest, have longer reaction times (Oliveira et al., 2010; Stoloff, Taylor, Xu, Ridderikhoff, & Ivry, 2011) and are associated with greater neural activity in the parietal cortex, a brain region important for movement planning and control, than reaches toward lateral targets (Fitzpatrick, Dundon, & Valyear, 2019).

However, results of other studies are at odds with the idea that hand choice relies on a competitive process between movement plans for the left and right hand. Bernier et al. (2012) found neural activity in the parietal and motor cortex only after the reach target had been presented and the reaching hand had been instructed by the color of the target or a preceding cue. Similarly, in nonhuman primates, Cui and Andersen (2011) studied eye and reaching movements and found that some neurons in the parietal cortex only became active after the effector was chosen or instructed by the color of the target. These results could be interpreted as if the brain first determines the effector to move and then defines the movement plan, as in serial processing.

In Chapter 2, I will examine whether deciding between the left and right hand leads to the specification of parallel movement plans that compete for execution. For this we use a paradigm similar to the paradigm described by Oliveira et al. (2010), and measure neural activity during hand choice using electroencephalography, or EEG (see Box 1). In the analysis of the EEG data, we focus on neural oscillations in the beta band, which have a frequency of 13 to 30 Hz. It has long been known that the power of oscillations in the beta band over the sensorimotor cortex changes before and during voluntary movements of the hand (Jasper & Penfield, 1949; Pfurtscheller, 1992). During movement planning, the beta-band power decreases contralateral to the hand that is used for the subsequent movement (for a review, see Kilavik, Zaepffel, Brovelli, MacKay, & Riehle, 2013). Modulations of this decrease have been shown to be predictive of the upcoming action (Pape & Siegel, 2016), and might therefore similarly reflect hand choice. If hand choice is reflected in beta-band power during movement planning, we expect the power to decrease less with more uncertainty about the hand to use for the upcoming movement, either due to the location of the target or the task instructions.

#### Box 1: Electroencephalography

Electroencephalography (EEG) is a method used to record electrical activity in the brain. By placing electrodes on the scalp using an EEG cap (Fig. 1.3A), synchronized activity of groups of neurons, also called field potentials, can be measured (Westbrook, 2000). The signal mainly reflects the activity from neurons close to the scalp, and the measured electrical activity is small (typically in the range of 20 to 100 microvolts). In experimental settings, EEG is often used to detect changes in the neuronal activity in response to certain events or stimuli (Cohen, 2014a). A common way to extract this information from the signal is by processing the EEG data and examining changes in the power of the signal in certain frequency bands using time-frequency analyses (Fig. 1.3B) (Cohen, 2014b). These changes in the power are due to synchronization and desynchronization of the activity of groups of neurons in the brain. Frequency bands that are often distinguished are the delta band (2 to 4 Hz), theta band (5 to 7 Hz), alpha band (8 to 12 Hz), beta band (13 to 30 Hz), and gamma band (above 30 Hz).

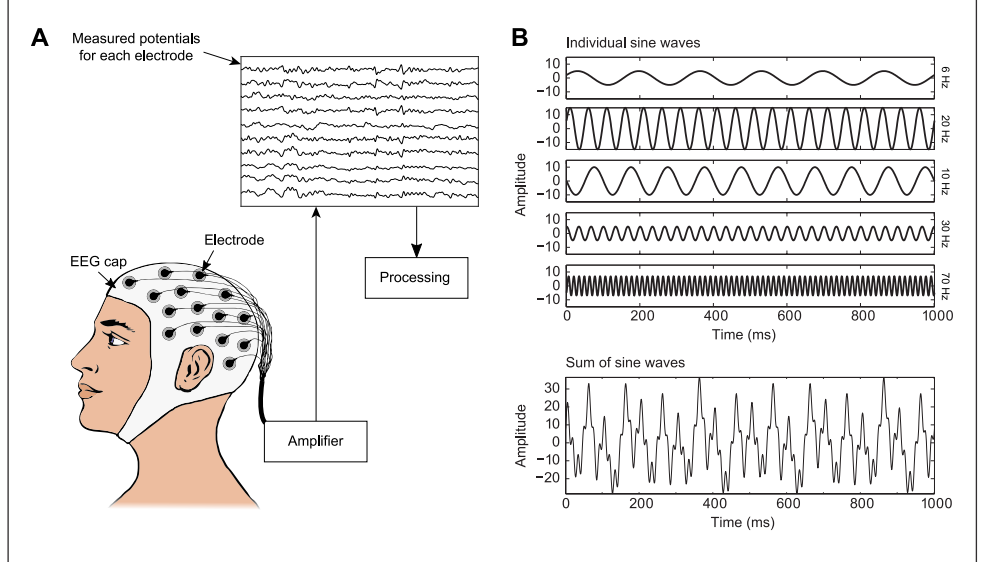


Figure 1.3. Electroencephalography (EEG) setup and signal. A) Illustration of an EEG setup. Electrodes are attached to an EEG cap to measure the electrical activity in the brain. The measurements are usually processed to be able to analyze specific patterns in the neuronal activity. Adapted from Nagel (2019). B) The neuronal activity measured at the level of the EEG electrodes reflects the sum (lower panel) of multiple sine waves with different amplitudes and frequencies (upper panels). EEG analyses often focus on fluctuations in the power of the signal in specific frequency bands, as these fluctuations have been linked to changes in specific cognitive processes. Adapted from Cohen (2014c).

# Online control of movement, motor learning and adaptation

#### 1.2.1 Online control of movement

To execute a movement, action plans need to be transformed into motor commands that are sent to the muscles to generate the required forces (Kim, Avraham, & Ivry, 2021). However, movements are frequently perturbed during execution due to motor noise and external forces. For example, a gust of wind might push the hand away from the reach target during a reaching movement. How does our body correct for such unexpected disturbances of the movement?

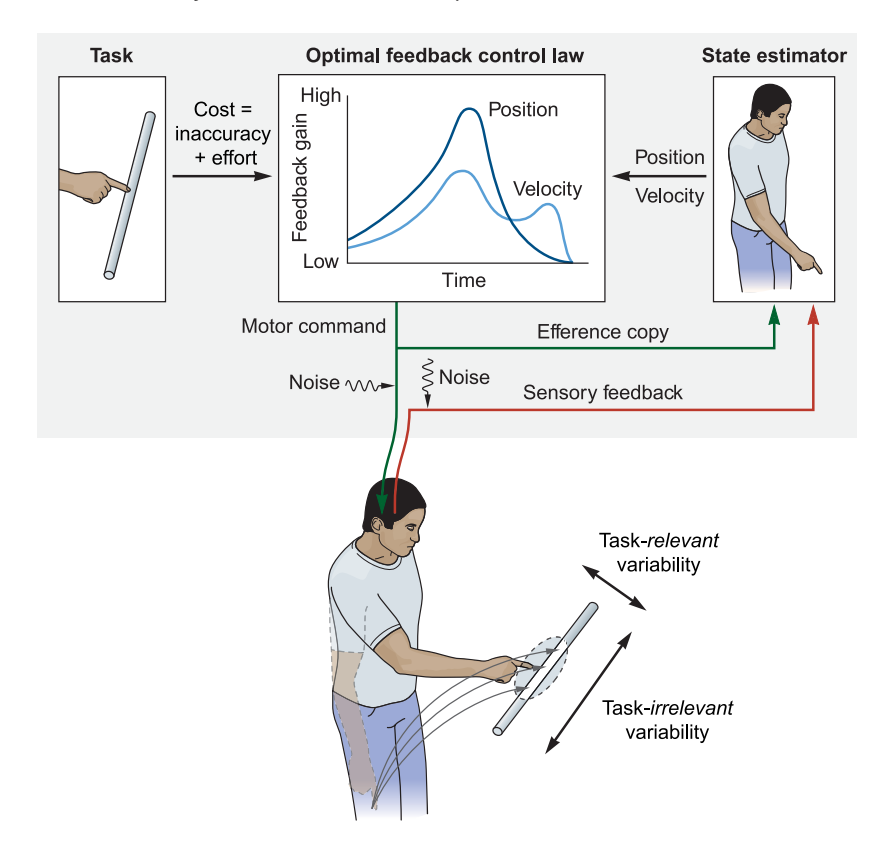


Figure 1.4. Optimal feedback control (adapted from Wolpert & Bastian, 2021). Optimal feedback control theory describes the online control of movements and proposes that the brain specifies a control policy with time-varying gains based on the movement goals and costs. The feedback gains determine how the motor command should be changed based on the state of the body and the environment. These states are estimated and depend on both sensory feedback and predictions from an internal forward model based on the efference copy of the motor command. In general, optimal control policies allow for movement variability in dimensions that are irrelevant for reaching the movement goal.

Optimal feedback control theory, proposed by Todorov and Jordan in 2002, describes the online control of movements (Fig. 1.4). It is a general framework that applies to different types of movement, such as walking, reaching and eye movements. According to this theory, the state of the system can be estimated at any point during the movement with a forward internal model that predicts the sensory feedback based on an efference copy of the motor commands (Scott, 2004; Todorov & Jordan, 2002). These predictions are integrated with the actual, noisy, sensory feedback to compute an optimal estimate of the state of the body and the environment. The brain is thought to formulate a control policy based on the specific movement goals and to correct for perturbations only if these goals might not be reached, allowing for movement variability in dimensions that are irrelevant for reaching the movement goal.

#### 1.2.2 Motor learning and adaptation

Differences between predictions of the sensory feedback and the actual sensory feedback can be due to noise. For example, due to motor noise it is impossible to execute a movement in the exact same way twice (van Beers, Haggard, & Wolpert, 2004). However, consistent differences between the predictions and the feedback may also be due to changes in the mapping between the control policy and the movement outcome or between the movement outcome and the sensory feedback (e.g., experimentally introduced by a force field perturbation or a visuomotor rotation, respectively, Kim et al., 2021).

Such differences between the predicted and the actual sensory feedback, also called sensory prediction errors, drive sensorimotor adaptation (Kim et al., 2021). Based on sensory prediction errors, the internal models and the control policy can be updated. Models of motor adaptation describe how this is done. Trial-to-trial changes in the internal model predictions can for example be described by mathematical models with a learning and a retention rate (see for example Smith, Ghazizadeh, & Shadmehr, 2006). The learning rate represents the proportion of the error that the system corrects for from one trial to the next, while the retention rate represents the proportion of the current estimate of the perturbation that is retained. Sensory information is thus not only critical for perception in general, but also for updating the internal models and the control policy through motor learning.

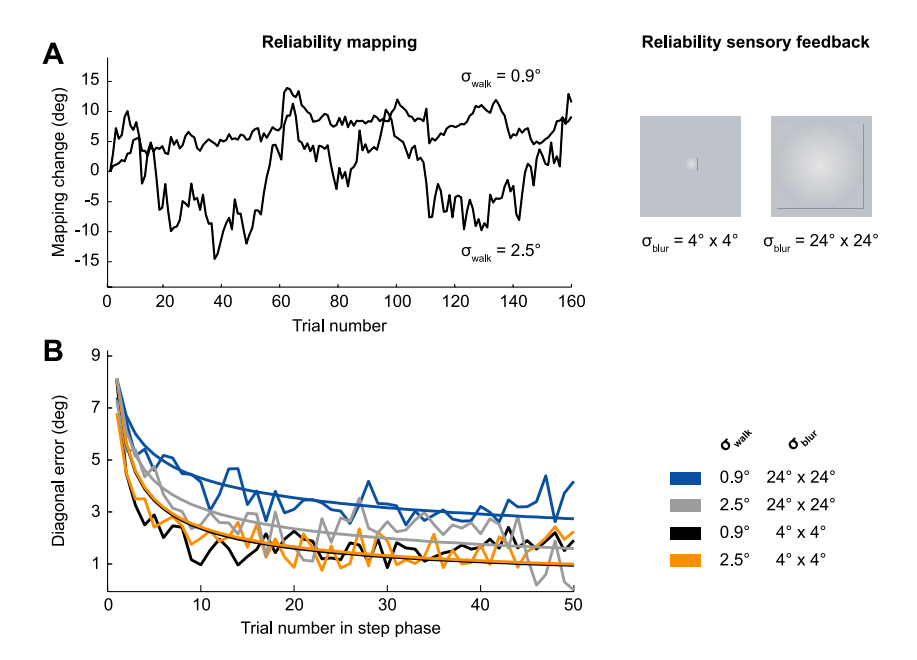


**Figure 1.5.** Reach adaptation studies dissociated the contribution of sensory feedback and sensory predictions (adapted from Burge et al., 2008). A) Participants made reaching movements towards a target while the reliability of the sensory feedback and the mapping between the control policy and the sensory feedback was experimentally manipulated. The reliability of the mapping between the movement and the visual feedback depended on the predictability and standard deviation ( $\sigma_{walk}$ ) of trial-to-trial changes in the mapping between the position of the hand and the visual feedback. Here, two autocorrelated random walks (same predictability) with different standard deviations (0.9 and 2.5°) were used. The reliability of the sensory feedback was manipulated by varying the blur of the visual feedback ( $\sigma_{blur}$ , 4° x 4° and 24° x 24°). B) During the step phase of the experiment, participants adapted to a large shift in the visual feedback of 8.2°. The average adaptation profiles across subjects are shown, along with the curves of the best-fitting power laws. The speed of adaptation, or the decrease in the error, depended on both the reliability of the mapping and the reliability of the visual feedback.

Studies in reach adaptation have experimentally manipulated the reliability of the sensory feedback and the mapping between the control policy and the sensory feedback to dissociate the contribution of sensory feedback and sensory predictions in motor adaptation (Burge, Ernst, & Banks, 2008; Wei & Körding, 2010). Participants made reaching movements towards a target while the visual feedback about the position of their hand was perturbed. The authors found that participants adapted faster to these perturbations when the mapping between the control policy and the visual feedback was less reliable (i.e., the perturbations were more variable and less predictable) and adapted slower when the visual feedback was less reliable (i.e., blurred)

(Fig. 1.5). These findings suggest that motor adaptation follows the predictions of Bayesian models in that systems adapt faster to perturbations when the estimate of the mapping is more uncertain because the estimate could be incorrect, and adapt slower when the sensory feedback is more noisy as if the observed perturbation is a measurement error.

## 1.2.3 Artificial signals

If a sensory system breaks down, estimates of the state of the body and the environment might be deteriorated and cannot be adequately updated. In such a situation, a clear benefit may be obtained by reinstating the missing information through an artificial sensory channel. Based on models of motor learning, in principle, any consistent mapping between a movement and feedback can be learned. For example, Dadarlat et al. (2015) showed that monkeys can learn to use the information from a prosthetic device, stimulating the primary somatosensory cortex, to make accurate reaching movements. The artificial feedback signal provided information about the relative position of the hand and the reach target. This signal was completely novel to the monkeys but was required to be able to complete the task. Similarly, Schumann and O'Regan (2017) showed that healthy human participants can learn to use an "extra sense" providing information about their head orientation relative to the magnetic north through auditory stimuli. Also, steps have been taken to use vibrations on the skin to substitute hearing in people with deafness or hearing problems (Perrotta, Asgeirsdottir & Eagleman, 2021).

Another example of an artificial mapping between a movement and the sensory feedback is steering (Danz, 2021). The term "artificial" refers here to the indirect relationship between the neural control mechanism and the resulting steering action, which relies on the interaction between the driver and the steering wheel system. During driving, steering motor commands are generated to control a steering wheel which in turn controls the motion of the vehicle and the body. Even though the steering motor commands are cognitively mediated and the mapping between the steering movement and the sensory feedback is indirect, in principle, people could build an internal model of this mapping. In **Chapter 3 and 4** of this thesis, I will examine whether people can learn this mapping to accurately estimate and control their self-motion.

#### 1.2.4 Self-motion estimation

To interact with our environment, we require an accurate percept of our selfmotion relative to the world. To successfully reach for a drink while your body is in motion, for example, you need to anticipate and account for the movement of your body. In general, self-motion estimation depends on the integration of sensory information, primarily vestibular, visual, and somatosensory signals, and motor information (Angelaki & Cullen, 2008; Britten, 2008).

Vestibular signals are generated in the vestibular system, located in the inner ear (Goldberg, Walker, & Hudspeth, 2000). The vestibular system consists of the semicircular canals and the otoliths (Fig. 1.6A). The semicircular canals sense rotational movements of the head, and the otoliths sense linear motion of the head as well as the orientation of the head relative to gravity. Both the semicircular canals and otoliths contain hair cells that convert head motion into vestibular signals. When the head accelerates, such as during self-motion. the hair bundles of the hair cells deflect. Depending on the direction of the deflection, the cell depolarizes or hyperpolarizes, which affects the firing rate of the afferent nerve fibers.

During self-motion, the visual system detects the changes in the image on our retina that result from the motion, also called optic flow (Fig. 1.6B) (Britten, 2008). The pattern of the optic flow depends on the heading direction. The center of expansion in the image aligns with the heading direction, and other points in the image move with different velocities depending on the speed of the self-motion and the depth of the visual scene. Neurons in the medial superior temporal area of the brain are known to be sensitive to optic flow (Gu, Watkins, Angelaki, & DeAngelis, 2006), and are therefore thought to play an important role in heading and self-motion estimation.

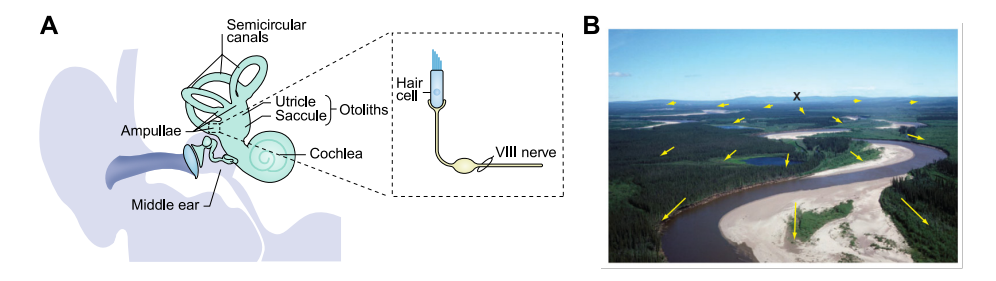


Figure 1.6. Sensory information used for self-motion estimation. A) The vestibular system is located in the inner ear and consists of the semicircular canals and the otoliths. Hair cells in the semicircular canals and the otoliths convert head acceleration into vestibular signals. Adapted from Cullen (2019). B) During self-motion, the visual system detects optic flow. The center of expansion in the image on the retina (black X) aligns with the heading direction, whereas other points in the image move with different velocities (yellow arrows). From Britten (2008).

In addition to vestibular and visual information, somatosensory cues can be used to estimate self-motion. Proprioceptors in the neck and body sense the orientation of the head on the body and of the body in space, respectively (Alberts et al., 2016; Clemens, De Vrijer, Selen, Van Gisbergen, & Medendorp, 2011). Additionally, cues provided by the wind, vibrations and changes in pressure give information about the self-motion (Campos & Bülthoff, 2012).

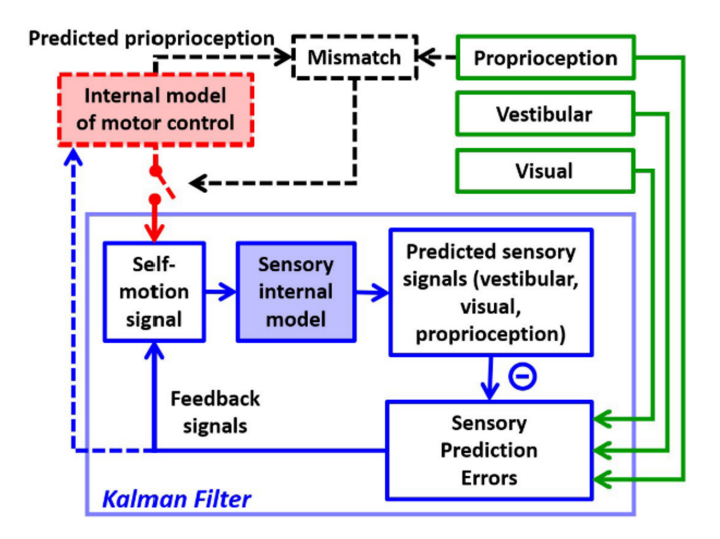


Figure 1.7. Estimation of active and passive self-motion (from Laurens and Angelaki, 2017). During active self-motion, an internal forward model (sensory internal model) predicts the sensory feedback based on an efference copy of the motor commands used to generate the self-motion (self-motion signal). If an accurate internal forward model is available, the sensory prediction error will be small, and the self-motion estimate will depend mainly on the predicted sensory feedback. During passive self-motion, the sensory feedback cannot be predicted, and the self-motion estimate will be driven by the sensory prediction errors. Laurens and Angelaki (2017) have described a model that uses a Kalman filter to compute optimal self-motion estimates during both active and passive self-motion. The computations additionally rely on a gating mechanism, which is thought to scale the response sensitivity of neurons in the vestibular processing pathway based on the size of the prediction error (i.e., after the introduction of a large prediction error, the neurons robustly encode the prediction error, whereas the response decreases during motor learning) (Brooks, Carriot, & Cullen, 2015).

Also in self-motion estimation, motor information and sensory predictions are known to play an important role (Brooks & Cullen, 2019). When the selfmotion is actively generated, the sensory feedback can be predicted based on an efference copy of the motor commands used to generate the motion. During passive self-motion, however, such predictions about the self-motion cannot be made. This distinction between active and passive movements was already made in the 19th century by Helmholtz (1867). Recent modeling work has led to a unified theory for active and passive self-motion estimation (Cullen, 2019; Laurens & Angelaki, 2017), in which the self-motion estimate is computed using the sensory prediction error (Fig. 1.7). This sensory prediction error is small during active self-motion, and the self-motion estimate will therefore depend mainly on the sensory predictions. During passive self-motion, on the other hand, the sensory prediction error will drive the self-motion estimate.

In the central nervous system, neural correlates of components of this unified theoretical framework have been found. In monkeys, neurons in the vestibular nuclei, which receive input from the vestibular nerve and output to higher neural structures that compute self-motion estimates, are active during passive self-motion (for a review, see Cullen, 2012). However, the activity is attenuated during active self-motion. The activity in these neurons is therefore thought to reflect the sensory prediction error. Additionally, because of its projections to the vestibular nuclei, the forward internal model that is used to compute the sensory predictions is thought to be located in the cerebellum (Brooks et al., 2015).

## 1.2.5 Closed-loop steering experiments

The unified theoretical framework for the estimation of passive and active self-motion assigns an important role to the efference copy, but the model is agnostic as to the nature of the motor signal. Building on the observation that we can learn consistent mappings between a movement and the sensory feedback, such as in sensory prosthetics, this opens up the possibility that also motor signals that have an indirect, or artificial, relationship with selfmotion cues can be used to predict the sensory feedback during self-motion estimation. Such motor signals are of efferent nature, but the movement is indirectly linked to another action and this relationship has to be learned. As described above, the steering motor commands that are generated during driving are an example of motor signals that have an indirect relationship with the sensory feedback. Closed-loop steering experiments have been used to study the integration of sensory feedback and sensory predictions based on such motor signals in self-motion estimation.

Roy and Cullen (2001) examined closed-loop steering in monkeys (Fig. 1.8). Monkeys were seated on a turntable and were trained to control the speed of their rotational self-motion with a steering wheel. Neural activity in the vestibular nuclei, which is thought to reflect the sensory prediction error, was

similar during active steering and passive rotations of the body. This suggests that the steering motor commands are not used to predict the sensory feedback, at least not at this level of the vestibular processing pathway. However, during visual self-motion, neurons in the medial superior temporal area in monkeys showed different responses to optic flow patterns generated during active steering compared to when the same optic flow patterns were passively viewed (Jacob & Duffy, 2015; Page & Duffy, 2008; but see also Egger & Britten, 2013).

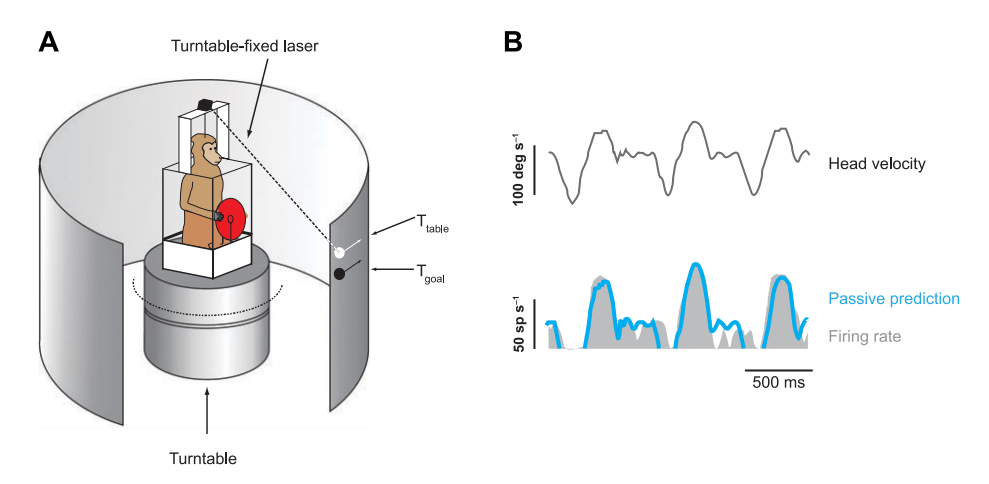


Figure 1.8. Closed-loop steering experiment with rotational self-motion in monkeys (adapted from Angelaki and Cullen, 2008). A) Monkeys used a steering wheel to control the rotation of a turntable to align a laser target attached to the turntable  $(T_{table})$  with a moving target  $(T_{goal})$ . B) Neurons in the vestibular nuclei reliably encoded the self-motion. The activity of these neurons is thought to reflect the sensory prediction error, and these results therefore suggest that the vestibular sensory feedback was not predicted by a forward internal model based on the steering motor commands.

More recently, closed-loop steering has also been studied in human participants (Alefantis et al., 2022; Lakshminarasimhan et al., 2018; Stavropoulos, Lakshminarasimhan, Laurens, Pitkow, & Angelaki, 2022). Alefantis et al. (2022) showed that, after training with optic flow cues, humans can navigate a virtual environment using a joystick without any online sensory feedback. This suggests that participants formed an internal model of the steering dynamics with training. Stavropoulos et al. (2022) used a similar experiment but varied the steering dynamics slightly from trial to trial. They found that participants could accurately navigate the environment with online optic flow cues, but performed worse when only vestibular cues were available, as if their estimate of the self-motion was biased by an incorrect internal model of the steering dynamics.

#### Box 2: Linear motion platform

To examine the role of sensory feedback and sensory predictions in self-motion estimation we use a linear motion platform, also called the sled (Fig. 1.9). During an experiment, participants are seated on the sled and control the lateral sled motion by rotating a steering wheel mounted in front of them. The angle of the steering wheel relative to the start angle encodes the velocity of the sled. If participants for example rotate the steering wheel to the left, the sled moves to the left, and the further they rotate the steering wheel, the faster the sled moves. The exact mapping between the steering wheel angle and the sled velocity is adjustable. To be able to test the role of vestibular feedback, experiments are done in darkness, excluding visual feedback. Additionally, participants wear headphones to mask auditory cues from the moving sled with white noise sounds.



Figure 1.9. Linear motion platform used for closed-loop steering experiments. During the experiment, participants are seated with their interaural axis aligned with the motion axis of the platform, such that they are laterally translated, and rotate a steering wheel to control the sled velocity. Experiments are done in darkness, and participants wear headphones to mask any auditory cues.

In Chapter 3 of this thesis, I will further examine whether the brain can build an accurate internal model of the steering dynamics in a closed-loop steering experiment with online vestibular feedback. Participants control a linear motion platform, also called the sled (see Box 2), with a steering wheel and learn to align their body with a memorized visual target. We examine their responses to abrupt changes in the steering dynamics during the experiment, and compare their steering behavior to that of participants who do not receive any online sensory feedback. If the brain builds an internal model of the steering dynamics, we expect participants who do receive online sensory feedback to respond to the abrupt changes in the steering dynamics while the steering movement is ongoing.

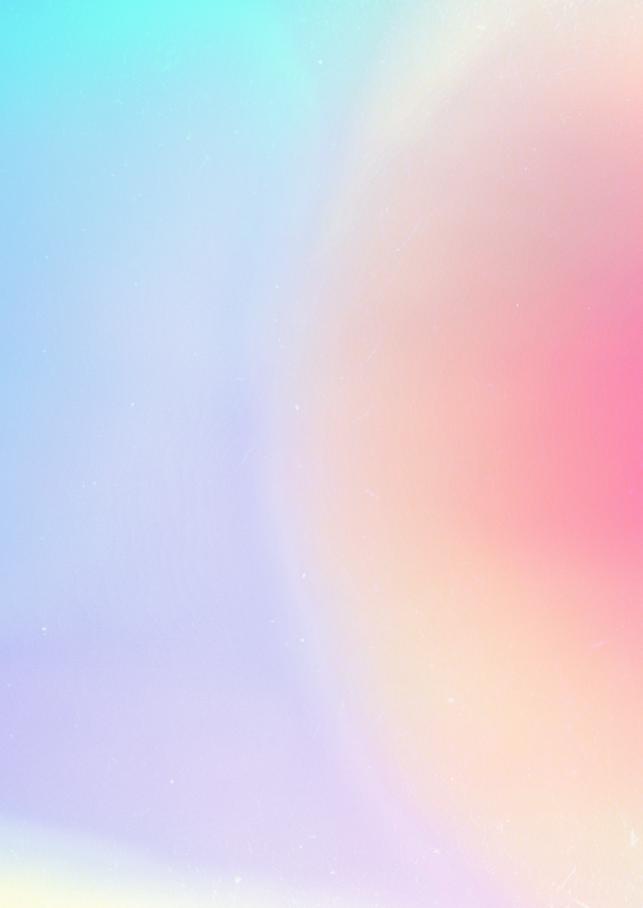
#### 1.2.6 Reweighting sensory and motor information

Based on the unified theoretical framework for passive and active self-motion, self-motion estimates are thought to be most accurate when they are based on both sensory predictions and sensory feedback (Laurens & Angelaki, 2017). However, participants should in principle be able to fairly accurately estimate their self-motion based on sensory feedback alone as well. This has also been observed in path integration studies, in which participants estimate their passive self-motion by integrating the online sensory feedback over time (Grasso, Glasauer, Georges-François, & Israël, 1999; Lappe, Jenkin, & Harris, 2007; Petzschner & Glasauer, 2011). As described above, studies in reach adaptation have tried to dissociate the contribution of sensory feedback and sensory predictions by experimentally manipulating the reliability of the sensory feedback and the mapping between the reaching movement and the sensory feedback (Burge et al., 2008; Wei & Körding, 2010).

In **Chapter 4**, I will use an experimental design that is inspired by these reach adaptation studies to examine the contributions of internal model predictions and sensory feedback during closed-loop steering in more detail, building on the experiment described in **Chapter 3**. Next to the abrupt changes in the steering dynamics, we vary the steering dynamics slightly from trial to trial as well. This way we intend to manipulate the weights on sensory predictions and online vestibular feedback. We examine the steering behavior for within-trial responses to the sensory feedback and predictions of the steering dynamics across trials. We expect participants to rely more on predictions of the steering dynamics and less on the online sensory feedback if the steering dynamics are more predictable.

#### 1.3 Thesis outline

In this thesis I will examine the processes that underlie the control of our movements in rich and dynamic environments. I will focus on two natural behaviors: reaching and steering. In Chapter 2, I will focus on reaching and will study the selection of actions and movement planning by looking at hand choice. More specifically, I will examine whether deciding between the left and right hand leads to the specification of parallel movement plans that compete for execution using EEG. In Chapter 3 and 4, I will focus on steering and will study the role of vestibular sensory feedback and sensory predictions during the control of self-motion. In Chapter 3, I will examine whether self-motion estimation during a closed-loop steering experiment depends on an internal model of the steering dynamics, or whether the self-motion estimate is primarily based on the online vestibular feedback. In Chapter 4, I will examine in more detail the role of internal model predictions and vestibular feedback in self-motion estimation during steering. By varying the steering dynamics from trial to trial, we aim to dissociate the contributions of sensory predictions and online feedback. In Chapter 5, I will summarize and discuss the findings. I will additionally consider their broader implications for sensorimotor control and will make suggestions for future research.



# Chapter 2

# Cortical beta-band power modulates with uncertainty in effector selection during motor planning

This chapter has been adapted from:

van Helvert, M.J.L., Oostwoud Wijdenes, L., Geerligs, L., & Medendorp, W.P. (2021). Cortical beta-band power modulates with uncertainty in effector selection during motor planning.

Journal of Neurophysiology, 126, 1891-1902.

## Abstract

While beta-band activity during motor planning is known to be modulated by uncertainty about where to act, less is known about its modulations to uncertainty about how to act. To investigate this issue, we recorded oscillatory brain activity with EEG while human participants (n = 17) performed a hand choice reaching task. The reaching hand was either predetermined or of participants' choice, and the target was close to one of the two hands or at about equal distance from both. To measure neural activity in a motion-artifact-free time window, the location of the upcoming target was cued 1000-1500 ms before the presentation of the target, whereby the cue was valid in 50% of trials. As evidence for motor planning during the cueing phase, behavioral observations showed that the cue affected later hand choice. Furthermore, reaction times were longer in the choice than in the predetermined trials, supporting the notion of a competitive process for hand selection. Modulations of beta-band power over central cortical regions, but not alpha-band or theta-band power, were in line with these observations. During the cueing period, reaches in predetermined trials were preceded by larger decreases in beta-band power than reaches in choice trials. Cue direction did not affect reaction times or beta-band power, which may be due to the cue being invalid in 50% of trials, retaining effector uncertainty during motor planning. Our findings suggest that effector uncertainty modulates beta-band power during motor planning.

#### 2.1 Introduction

At a picnic with many delicacies, there are numerous opportunities for action. We can look at one of several treats, or reach for it, and when we reach, we could use the left or right hand. How is this decision process being solved? Computational theories suggest that the brain chooses the action that maximizes utility, which depends on the cost associated with performing the action and the desirability of the outcome, i.e., the reward (Haggard, 2008; Shadmehr et al., 2016; Wolpert & Landy, 2012). In neural terms, it follows that the circuits involved in deciding between actions based on utility are strongly coupled to the circuits responsible for generating an action. Indeed, neurophysiological studies have suggested that multiple potential motor plans can be encoded in parallel and compete for selection within the brain's sensorimotor regions (Cisek, 2006).

In non-human primates, most of the evidence for this process of embodied decision making comes from experiments that manipulated the number or location of potential targets (Basso & Wurtz, 1997; Cisek & Kalaska, 2005; Glaser, Perich, Ramkumar, Miller, & Kording, 2018; Klaes, Westendorff, Chakrabarti, & Gail, 2011). For example, in a unimanual reaching task with two potential targets, neural activity in dorsal premotor cortex represents both options simultaneously and reflects the selection of one over the other when the choice is made (Cisek & Kalaska, 2005; but see Dekleva, Kording, & Miller, 2018, for an alternative interpretation). Analogous results have also been observed in humans. For instance, Tzagarakis et al. (2010, 2015) reported that cortical beta-band desynchronization, associated with motor planning (Jasper & Penfield, 1949; Pfurtscheller, 1992), depends on the number of potential targets and their directional uncertainty. Grent-'t-Jong et al. (2014, 2015) reported that the proximity of two potential reach goals has a direct influence on motor cortex activity, as measured by oscillatory power (see also Tzagarakis et al., 2015).

Utility of a movement does not only depend on the location of the target, it is also determined by the effector that needs to be moved. Within this notion, target and effector selection can be considered as part of an integrated computation in movement planning, in which the expected utility of each potential movement is defined by the distance and direction of the respective target relative to the respective effector (Bakker, Selen, & Medendorp, 2018; Dancause & Schieber, 2010; Schweighofer et al., 2015). Accordingly, if multiple potential targets evoke multiple concurrent movement plans of a single effector, deciding between multiple effectors to move to a single target may also lead to the specification of parallel movement plans. This has been indeed observed when selecting between eye versus arm movements; cortical areas involved in these movements are simultaneously activated until the effector is selected, as observed both in monkeys (Cui & Andersen, 2011) and humans (see Medendorp & Heed, 2019, for review). However, it is important to realize that eye and hand movements serve different purposes and, in natural situations, are typically used in combination (Heed, Beurze, Toni, Röder, & Medendorp, 2011), which could explain their simultaneous specification.

It is less clear whether the brain simultaneously specifies motor plans for the two arms. Using a combined EEG-fMRI study, Bernier et al. (Bernier et al., 2012) tested participants in an arm choice experiment with a fixed target location, and found activity in parietal and premotor cortex only contralateral to the reaching arm after target onset. This could be interpreted as if effector selection precedes movement planning, i.e. that hand selection is not associated with the simultaneous specification of two motor plans. This would be in line with findings of monkey area 5, showing that neurons only become activated after the hand of the reach is specified, but not if a target is presented without the hand being specified (Cui & Andersen, 2011). However, it could also be possible that the substantial differences in expected utility between contralateral and ipsilateral arm movements, due to the eccentric location of the target, biased the competition for selection to the contralateral motor plan in Bernier et al.'s study (2012).

Other studies do suggest competition between motor plans of the two hands. Reaction times are longer for reaches towards the target direction that leads to equiprobable right/left hand choices (point of subjective equality, PSE), resembling a more competitive hand selection process for this direction compared to other, lateral target directions (Bakker et al., 2018; Oliveira et al., 2010). Also, preparing reaches with two hands simultaneously results in more movement variability than preparing a single reach, suggesting that reach plans of the two hands share a common neural resource (Oostwoud Wijdenes, Ivry, & Bays, 2016). Using transcranial magnetic stimulation over left posterior parietal cortex, Oliveira et al. (2010) demonstrated that the competition between hands can be biased towards the ipsilateral, left hand. Fitzpatrick et al. (2019) reported greater BOLD activity in parietal cortex at the PSE than away, consistent with competition between the hands. Finally, using

EEG, Hamel-Thibault et al. (2018) presented evidence that hand selection at the PSE depended upon the phase of delta-band oscillations at target onset in contralateral motor regions, as if excitability of motor regions acts as a modulatory factor for hand choice.

While there is ample evidence about the involvement of beta-band oscillations in response selection (van Wijk, Daffertshofer, Roach, & Praamstra, 2009), the specific role in hand selection processing during movement planning is less clear. Beta-band power over sensorimotor regions decreases during instructed delayed-reach tasks, most pronounced over the hemisphere contralateral to the hand (for a review, see Kilavik, Zaepffel, Brovelli, MacKay, & Riehle, 2013). This is typically seen as a small phasic decrease after the initial cue, followed by a more sustained decrease until the execution of the movement. This sustained decrease is modulated by the participants' readiness hazard and followed by a post-movement rebound (Schoffelen, Oostenveld, & Fries, 2005; Tzagarakis et al., 2010). It has also been reported that fluctuations in betaband activity over contralateral and ipsilateral hemispheres during movement planning are predictive of upcoming actions (Pape & Siegel, 2016).

Given the importance of beta-band synchronization in movement planning, here we examine the role of these oscillations in coding multiple movement plans during hand choice. Participants performed a hand choice reaching task whereby the target location was cued 1000-1500 ms before it was presented. This allowed us to analyze the oscillatory activity within a clearly defined and motion-artifact-free time window just prior to movement onset. We hypothesized that if beta-band power reflects effector uncertainty, the power would decrease less if there was more uncertainty about which hand to move, similar to the effect of target direction uncertainty (Tzagarakis et al., 2010). We further reasoned that there would be more competition, and thus more uncertainty about which hand to move, if the target was in a direction close to PSE than if the target was close to either of the two hands (Oliveira et al., 2010).

#### 22 Methods

#### 2.2.1 **Participants**

Twenty participants took part in the study (5 males and 15 females, mean age 21 years, age range 19-26 years). All participants were right-handed, confirmed using the Edinburgh Handedness Inventory (Laterality Quotient, M = 86.92, SD = 13.54) (Oldfield, 1971). Participants had normal or correctedto-normal vision and reported no history of neurological or psychiatric diseases, or use of psychoactive medication or substances in the month prior to participation. The ethics committee of the Faculty of Social Sciences of Radboud University Nijmegen, the Netherlands, approved the study. All participants gave written informed consent prior to the start of the study, and were reimbursed for their time with a fixed amount of course credit.

## 2.2.2 **Setup**

Participants were seated in front of a touch screen (ProLite TF4237MSC-B3AG; liyama, Tokyo, Japan), positioned in the horizontal plane at the level of their thoracic diaphragm. The screen had a resolution of 1920 x 1080 pixels (pixel pitch 0.4845 mm) and a refresh rate of 60 Hz. As illustrated in Figure 2.1A, two starting positions for the left and right index finger were presented as gray discs of 3.5 cm diameter, approximately 20 cm away from the participant's sternum and 9 cm on either side of the body midline. A white fixation cross with a width of 2.5 cm was presented along the body midline, 12 cm in front of the two start positions. Cues and targets were presented as light orange and blue 3.5 cm discs, respectively, at 30 cm distance from the point midway between the two start positions, in five different directions: -40°, -10°, 0°, 10°, 40°. A 64-channel active electrode EEG system was used to record brain activity (Brain Products, Gilching, Germany). The onset of visual stimuli on the touch screen was determined using a photodiode and was used to identify and align epochs in the EEG recording. Horizontal and vertical electrooculograms (EOGs) were recorded by placing electrodes at the supraorbital and infraorbital ridges of the left eye and the outer canthi of the left and right eye. Impedance values for all electrodes were kept below 20 k $\Omega$  and the signal was referenced against the signal on left mastoid electrode TP9. The data were filtered online with a low cutoff value of 0.016 Hz and a high cutoff value of 200 Hz and digitized with a sampling frequency of 500 Hz and a resolution of  $0.1 \mu V$ . The experiment was controlled using custom-written software in Python, based on the Kivy library for multi-touch applications.

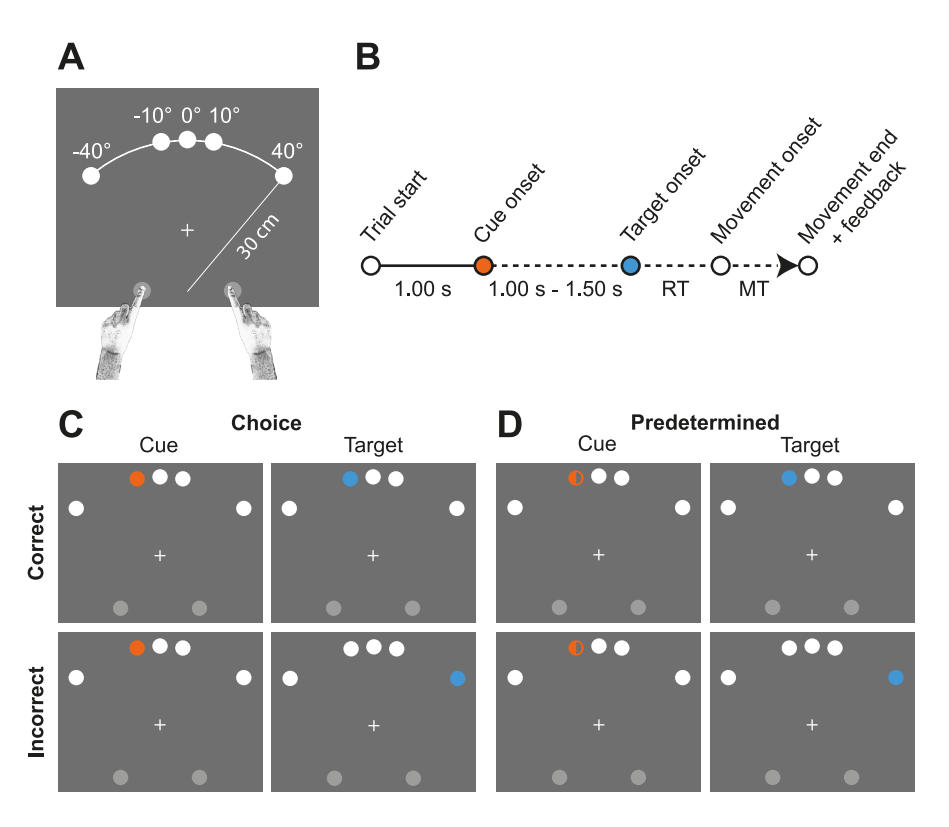


Figure 2.1. Illustration of the experimental setup, procedure, and paradigm. A) Schematic illustration of the experimental setup. Start positions (gray disks), gaze fixation cross, and the five potential cue and target directions (white disks) are shown. B) Order of events in a single trial. C) Choice trials; the upper panels show a correctly cued trial, during which the cue (orange) appeared at the same position as the target (blue), the lower panels show an incorrectly cued trial, during which the target appeared at a different position than the cue. Note that the other potential cue and target directions were not shown during the experiment. D) Predetermined trials; same as in C), but here the cue stimulus instructed which hand to use (here: left hand).

#### 2.2.3 Paradigm

The experiment took place in a completely darkened room, except for the light of the touch screen. Participants performed a unimanual reaching task in which they were free to use either hand (choice trials) or in which the response hand was instructed on the screen (predetermined trials). All trials were initiated by asking participants to place the tips of their left and right index fingers on the starting positions, which then turned white, and look at the fixation cross. After a delay of 1 s one of the five target directions was cued for either 1.00, 1.25, or 1.50 s (Fig 2.1B). Presented as a full orange disk, the cue instructed a choice trial (Fig 2.1C); if the color filled half of the disc, it signaled a predetermined trial (Fig 2.1D), with the filled side (left or right) instructing which hand to use.

Participants were informed about the types of cues prior to the experiment and practiced this before the start of the experiment. Furthermore, the cue was either valid in terms of the upcoming target direction (i.e., correctly cued the target, Fig 2.1C and 2.1D, upper panels) or invalid (Fig 2.1C and 2.1D, lower panels). At target presentation the cue disappeared and a short beep was played. Participants were asked to touch the target as fast as possible while the eyes were free to move. To ensure that participants were motivated to reach toward the target quickly, they received a feedback message and a score after each response. If participants adequately touched the target within 0.7 s (i.e., reaction + movement time) the message read, 'Well done! +1 point', followed by the total earned score across trials. If this duration was beyond 0.7 s, the feedback message was 'Too slow', and no points were obtained. Participants did not receive a reward based on their scores, but were incentivized to move as fast as possible by showing them the scores of the best performing participants before the start of the experiment. If the movement was initiated prior to the onset of the target, the trial was restarted. The incorrectly cued trials serve to verify that motor planning occurred during the cueing phase rather than participants waiting for the target to start preparing their movement.

Each participant completed 900 trials in total, which took about one hour. These comprised of 450 correctly cued trials (90 repetitions of each of the five locations) and 450 incorrectly cued trials (22 or 23 repetitions of each of the 20 cue x target combinations). There were 800 choice trials and 100 predetermined trials, of which 50 left hand and 50 right hand trials (25 correctly cued trials and 25 incorrectly cued trials each). The number of predetermined trials was lower than the number of choice trials, as the predetermined trials were added as intervening catch trials. During these trials, no choice had to be made about the hand to use. For each participant, trials were presented in a random order in six blocks of 150 trials, separated by short breaks. Prior to the main experiment, participants performed 30 practice trials, including all trial types.

#### 2.2.4 Data analysis

#### 2.2.4.1 Behavioral analysis

Behavioral data were processed in MATLAB R2017a. Statistical analyses were done in R 4.0.1 and the alpha level was set to 0.05. Choice data were based on the touch screen measurements. Movement onset was defined as the moment the first hand released contact with the touch screen after the target was presented. Hand choice was determined as the hand that departed from the touch screen first. Trials during which the participant released both hands and predetermined trials during which the participant did not use the instructed hand were not taken into account in further analyses. On average, this was the case in 8 trials per participant (SD = 3.22). Hand choice preferences were quantified as the proportion of right hand choices for each target direction.

Although there were only five cue and target directions, we summarized the psychometric data for the correctly cued choice trials by fitting a cumulative Gaussian distribution per participant using a maximum likelihood approach (Wichmann & Hill, 2001):

$$P(x) = \lambda + (1 - 2\lambda) \frac{1}{\sigma \sqrt{(2\pi)}} \int_{-\infty}^{x} e^{-\frac{(t-\mu)^2}{2\sigma^2}} dt$$
 (eq. 2.1)

in which P (x) represents the proportion of right hand choices for cue and target direction x. The mean of the curve,  $\mu$ , represents the participant's PSE, i.e. the direction at which the right and left hand were chosen equally often. Parameter  $\sigma$  is the standard deviation of the Gaussian, and reflects the variation in choice behavior. Parameter  $\lambda$  represents the lapse rate, accounting for errors caused by participant lapses or mistakes, e.g. unduly reaching with the right hand to the most leftward target. Its value was restricted to small values (< 0.1). We equated the cue direction closest to the PSE direction as the direction that evoked the highest effector competition. Note that the fitted cue direction corresponds to the direction for which the proportion of right hand choices is closest to 0.5 for all participants. Data from three participants were excluded as they showed such a strong preference to reach with their dominant right hand that it was not possible to fit a cumulative Gaussian function, and therefore to select a PSE cue. The extreme left and right directions induced the lowest effector competition. For plotting purposes we also fitted a cumulative Gaussian distribution to the proportion of right hand choices for the five different cue and target directions averaged across participants.

The incorrectly cued choice trials tested whether participants planned movements during the cueing phase. If participants instigated reach planning upon cue presentation, we expect that this would affect the reach upon target presentation. To test if cue direction affected hand choice a cue direction (-40°, -10°, 0°, 10°, 40°) x target direction (-40°, -10°, 0°, 10°, 40°) repeatedmeasures ANOVA was performed on the proportion of right hand responses for all choice trials (ez package in R). F statistic values were adjusted for violations of sphericity with Greenhouse-Geisser corrections.

Reaction time (RT) was defined as the time between target onset and movement onset. Trials with reaction times <100 ms or >1000 ms were excluded from further analyses. On average, this was the case in 1 trial per participant (SD = 1.19). Movement time (MT) was defined as the time between movement onset and the time when the finger first touched the target. Trials with movement times >1000 ms were excluded from further analyses since these typically involved corrective movements. On average, this was the case in 9 trials per participant (SD = 17.92). To test if effector competition was reflected in reaction times, a linear mixed-effects model with participant number as a random factor with random intercept and fixed factors instruction (predetermined, choice), cue direction (PSE, extreme), cue validity (correct, incorrect), and cue time (1.00, 1.25, 1.50 s), as well as the interaction effects, was fitted to the reaction times of all trials using maximum likelihood estimation (nlme package in R). Model fits were assessed with a likelihood ratio test. Bonferroni corrected pairwise t-tests were used to further analyze significant interaction effects post hoc.

# 2.2.4.2 EEG analysis

EEG data were processed offline using the MATLAB software toolbox FieldTrip, version 20171130 (Oostenveld, Fries, Maris, & Schoffelen, 2011). Data were split into epochs aligned to the onset of the cue (t = 0 s) and the signal was rereferenced against the average signal of the EEG electrodes. Slow drifts in the signal were eliminated by applying a high-pass filter with a cutoff frequency of 1 Hz. Eye blinks were semi-automatically identified based on the difference signal between the two vertical EOG electrodes following the FieldTrip procedure for rejection of eye blink artifacts. Trials with eye blinks around the onset of the cue (time window from 75 ms prior to cue onset to 25 ms after cue onset) were removed from further analyses. On average, this resulted in removal of 18 trials per participant (SD = 16.89). Ocular artifacts during the remainder of the trial were removed from the signal by running an independent component analysis. Rejection of components with an evident ocular origin was done according to the criteria described by McMenamin et al. (2010). After removal of these components, trials with excessive muscle activity in the time window from 200 ms prior to cue onset until target onset were semi-automatically identified and removed from further analyses following the FieldTrip procedure for rejection of muscle artifacts (for further details, see Gonzalez-Moreno et al., 2014). On average, this resulted in removal of 102 trials per participant (SD = 50.76). Bad channels were identified by visually inspecting the preprocessed data and were repaired by replacing the data with the plain average signal of neighboring channels based on triangulation

(two channels repaired in total). Data were low-pass filtered with a cutoff frequency of 40 Hz and down-sampled to 200 Hz.

Time-frequency representations of the data were computed with a Hanning taper with variable window length (5 cycles of the frequency of interest per time window), 10 ms steps and a 1 Hz resolution. The procedure was repeated with the epochs realigned to the onset of the movement (t = 0 s). Power values were corrected relative to a baseline computed per participant, trial group, frequency bin and channel. This baseline was defined as the average power in the time window from 200 ms before cue onset until cue onset, and was computed after averaging across trials in a trial group. Results were similar with a baseline from 500 to 200 ms before cue onset. Baseline-corrected power values were expressed in decibels.

First, we sought to identify clusters of channels that showed activity related to movement preparation. More specifically, we performed a nonparametric cluster-based permutation test to find clusters of channels that showed a decrease in power in the beta-band frequency range (13 to 30 Hz) prior to either left or right hand responses. Trials for which the hand to use was predetermined were grouped based on the hand used (left or right hand). Both correctly and incorrectly cued trials were included, as we did not expect cue direction to affect which hand was prepared for these predetermined trials. We used a nonparametric cluster-based permutation test to find clusters of channels that showed contrasting activity prior to left and right hand movements. This cluster-based permutation test is based on the calculation of cluster-level statistics, connecting samples that are adjacent in space and time (Maris & Oostenveld, 2007). To contrast left and right hand trials, power values in the right hand trial group were subtracted from the power values in the left hand trial group. The remainder was averaged along the frequency dimension within the beta-band range (13 to 30 Hz). The permutation test was applied for the channels in the left and right hemisphere separately, and channels were spatially clustered using triangulation of the sensor positions. Clusters in time were restricted to occur in the time window from 500 ms before movement onset until movement onset, mainly overlapping with the reaction time window. Both the cluster alpha level and the alpha level to reject the null hypothesis of no clusters in the data were set to 0.05. Mirror-symmetric channels that could be found in a significant cluster in the left hemisphere as well as a significant cluster in the right hemisphere were selected for further analyses, and data were averaged across the channels within a channel cluster.

Second, we were interested in whether effector competition was reflected in beta-band power during motor planning. Trials were grouped based on instruction (predetermined, choice), cue direction (extreme, PSE) and hand used (left, right). For the predetermined trials, both correctly and incorrectly cued trials were included. For the choice trials, only the correctly cued trials were included, as participants might have chosen to switch hands after the presentation of an incorrectly cued target, making it inappropriate to group trials based on the hand used. For reaches towards the extreme cues, only left hand trials were included for the leftmost cue (-40°) and only right hand trials were included for the rightmost cue (40°). Power values were computed for the sensor clusters ipsilateral and contralateral to the hand used, and were collapsed across hands, resulting in trial groups based on instruction (predetermined, choice), cue direction (extreme, PSE) and sensor cluster (contralateral, ipsilateral). Power values were averaged along the frequency dimension in the beta-band range (13 to 30 Hz).

To test if beta-band power was modulated by instruction, cue direction and sensor cluster, we performed a repeated-measures ANOVA on the average beta-band power during the time window from cue onset until 1000 ms after cue onset (cue-locked) as well as the time window from 1000 ms before response onset until response onset (response-locked), with instruction (predetermined, choice), cue location (extreme, PSE), and sensor cluster (ipsilateral, contralateral) as factors. A Bayesian ANOVA was used to compute Bayes factors for all main and interaction effects (BayesFactor package in R, see also Rouder, Morey, Speckman, & Province, 2012). To examine whether the effects were limited to the power in the beta-band frequency range, the procedure was repeated for the power in the theta-band (5 to 7 Hz) and alphaband frequency range (8 to 12 Hz).

### 2.3 Results

To examine if cortical power reflects uncertainty in hand choice, participants performed a cued hand choice reaching experiment, whereby the hand to use was chosen by the participant, based on a cue and target, or instructed by the cue. Figure 2.2A shows the proportion of right hand choices for the five different target directions when correctly cued averaged across participants (black circles) and their psychometric fit (black line), superimposed on the fits of individual participants (gray lines) with the direction at which the right and left hand were chosen equally often (point of subjective equality, PSE; gray circles). Confirming previous literature (Bryden et al., 2000; Gabbard & Rabb, 2000), the ipsilateral hand was typically selected to reach for peripheral targets, i.e. the left hand reached to the -40° target, the right hand reached to the 40° target. Most participants had a negative PSE, indicating an overall bias to selecting the right hand, which is consistent with the right hand preference of our participants. The direction closest to the participants' PSE was selected as the high competition direction:  $-10^{\circ}$  (n = 13),  $0^{\circ}$  (n = 3), or  $10^{\circ}$  (n = 1). We will refer to this direction as the participant's PSE cue or target.

We used the incorrectly cued choice trials to find behavioral evidence for motor planning during the cueing phase. We reasoned that if participants simply postponed motor planning until the presentation of the target, the cueing phase should not affect response behavior. Alternatively, if motor planning occurs in the cueing phase, it should bias hand choice. Figure 2.2B shows that cue location affects hand choice. For example, for a -40° cue and target (lowerleft circle), participants almost invariably use the left hand, while for the -40° target in combination with other cue locations the subsequent hand choice is more ambiguous. Similar effects can be seen across all invalid cue-target combinations. Thus motor planning during the cueing phase affected later hand choice. In support, across all choice trials, a repeated-measures ANOVA showed significant main effects of cue (F(1.68, 26.83) = 27.02, p < 0.001) and target direction (F(1.66, 26.57) = 102.18, p < 0.001) on hand choice, as well as a significant interaction (F(7.04, 112.60) = 7.60, p < 0.001). This confirms that the cue affects the eventual response, justifying our choice to study movement preparation during the cue period.

To test whether the paradigm evokes competitive processes in which both hands compete for movement execution we performed a reaction time analysis. Figure 2.2C shows the reaction times for the different conditions. A linear mixed-effects model fitted on the reaction times with fixed effects instruction (predetermined, choice), cue direction (PSE, extreme), cue validity (correct, incorrect) and cue time (1.00, 1.25, 1.50 s) showed a main effect of instruction, illustrating longer reaction times for choice trials than for predetermined trials  $(\chi^2(1) = 31.56, p < 0.0001)$ . There was also a main effect of cue time  $(\chi^2(2) =$ 45.02, p < 0.0001). Post hoc tests revealed that reaction times were longest for the shortest cue period (M = 349 ms) and shortest for the longest cue period (M = 332 ms) (p < 0.0001).

Based on Oliveira et al. (2010) we hypothesized that reaction times would be longer for the PSE cue, where the effector uncertainty is highest, than for the extreme cues, but there was no main effect of cue direction on reaction time. However, there were two significant interaction effects with the factor cue direction: the two-way interaction between instruction and cue direction  $(\chi^2(1) = 5.37, p = 0.021)$  and the three-way interaction between instruction, cue direction and cue validity ( $\chi^2(1) = 12.20$ , p < 0.001). The two-way interaction seems to be driven by longer reaction times for choice trials than predetermined trials if the cue was in an extreme direction (p = 0.16), rather than if the cue was in the PSE direction (p = 0.66). The three-way interaction suggests that this effect was driven by the incorrectly cued trials. Overall, reaction times were not longer for the PSE cue than for the extreme cues. However, for incorrectly cued choice trials, reaction times were longer for the extreme cues than for the PSE cue.

Finally, there was a significant interaction effect of instruction and cue validity on reaction time ( $\chi^2(1) = 15.36$ , p < 0.0001), demonstrating that incorrect cues only prolonged reaction times for choice trials (p < 0.0001), but not for predetermined trials (p = 0.064). Most likely participants did switch hands from cue to target in choice trials, while switching was not allowed in predetermined trials.

We next turned to examining the cortical mechanisms, studying whether power changes in motor planning regions reflect uncertainty about the upcoming effector. Our focus is on the role of beta-band oscillations, known to be involved in motor planning, and implicated in the coding of multiple target-specific motor plans. We used the predetermined trials to select the cortical regions that show beta-band activity during left and right hand motor planning around movement onset. As shown in Figure 2.3, we found two clusters of sensors that showed a significant selectivity in the beta band for the contralateral hand, one in the left (p = 0.039) and one in the right (p = 0.021) hemisphere. The mirror-symmetric channels that could be found in both significant clusters mostly covered central areas of the brain. Across the left hemisphere these channels were FC1, C1, C3, C5, T7, CP1 and CP5, and across the right hemisphere these channels were FC2, C2, C4, C6, T8, CP2 and CP6. These clusters are centered around central channels C3 and C4, known to be involved in movement planning (Pfurtscheller, 1992).

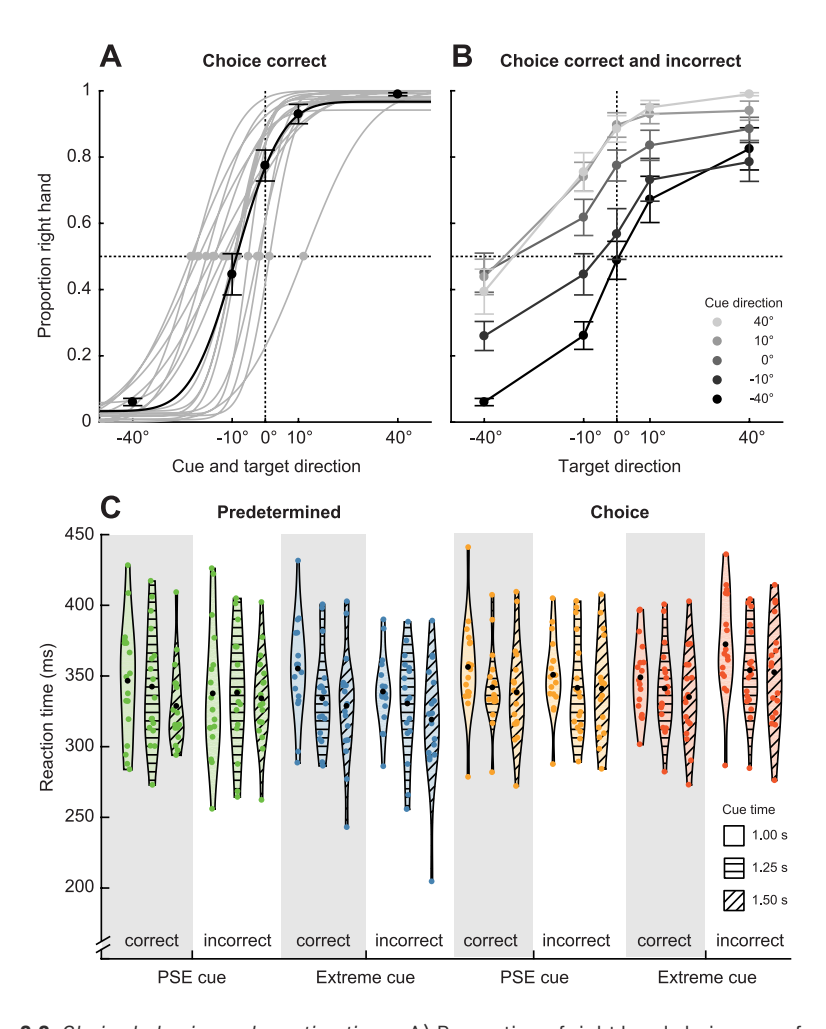


**Figure 2.2.** Choice behavior and reaction times. A) Proportion of right hand choices as a function of cue and target direction for correctly cued choice trials (black circles) fitted with a cumulative Gaussian distribution for all participants (black line). Points of subjective equality (gray circles) and cumulative Gaussian fits for individual participants (gray lines). Error bars represent SEM. On average, 79 trials (SD = 1.87) were included for each direction per participant. B) Proportion of right hand choices as a function of cue (gray lines) and target direction (abscissa) for correctly and incorrectly cued choice trials for all participants. A repeated-measures ANOVA revealed significant main effects of cue and target direction, as well as an interaction effect, on hand choice (n = 17). On average, 20 trials (SD = 0.83) were included for each combination per participant. Error bars represent SEM. C) Reaction times as a function of instruction, cue direction, cue validity and cue time for all participants. Violin shape outlines show the kernel density estimates of the individual participant data points (colored dots). Black dots show the mean across participants. A linear-mixed effects model revealed significant main effects of instruction and cue time on reaction times, as well as three interaction effects involving the factors instruction, cue direction and cue validity (n = 17).

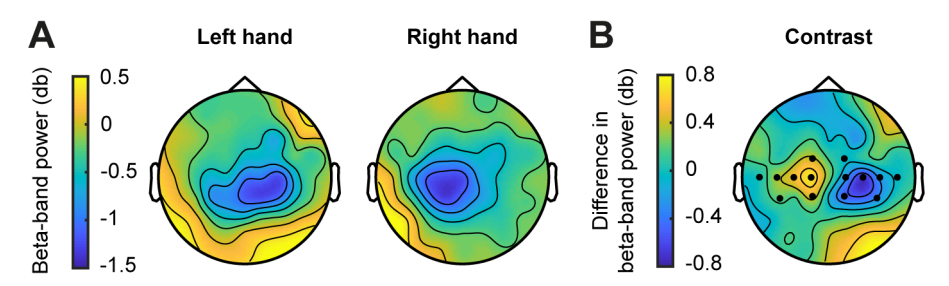


Figure 2.3. Topographic map of beta-band power preceding left and right hand movements. A) Mean beta-band power for the predetermined trials (correctly and incorrectly cued) preceding left and right hand movements (time-locked to movement onset, averaged across the 500 ms preceding movement onset). On average, 40 left hand trials (SD = 4.25) and 42 right hand trials (SD = 3.78) were included per participant. B) Mean difference in beta-band power between the hands (left minus right hand). Channel clusters (black dots) were identified with a nonparametric cluster-based permutation test (n = 17).

We examined whether beta-band power within these channels during the cueing phase reflects a hand selection process. Figure 2.4 illustrates relative beta-band power as a function of time, aligned to cue onset (left panels) and response onset (right panels), for both the choice and predetermined trials at the PSE and extreme cues, separately for sensor clusters ipsilateral and contralateral to the selected hand. While there appears a clear difference after cue presentation between choice and predetermined trials in the contralateral cluster, this effect is less pronounced in the ipsilateral cluster. In the contralateral cluster, the power in the beta-band after onset of the cue decreased more in predetermined than choice trials; this difference is sustained until response onset, and appears slightly larger for cues at PSE than at an extreme location. An instruction (predetermined, choice) x cue direction (PSE, extreme) x sensor cluster (ipsilateral, contralateral) repeated measures ANOVA with beta-band power aligned to cue onset revealed significant main effects of sensor cluster (F(1, 16) = 40.61, p < 0.0001), consistent with the contralateral selectivity, and instruction (F(1, 16) = 20.14, p < 0.001), consistent with a smaller decrease in beta-band power in choice trials than in predetermined trials. Similar results were found for the signal aligned to response onset, with significant main effects of sensor cluster (F(1, 16) = 83.77,p < 0.0001) and instruction (F(1, 16) = 20.42, p < 0.001).

There was no main effect of cue direction on beta-band power aligned to cue onset (F(1, 16) = 2.30, p = 0.149) or aligned to response onset (F(1, 16) = 1.31, p = 1.31)p = 0.269), nor were there any significant interaction effects. One could expect that in the contralateral hemisphere, for choice trials but not predetermined

trials, there would be more competition between the hands, and thus more uncertainty, for PSE than for extreme cues. However, an instruction (choice, predetermined) x cue direction (PSE, extreme) repeated measures ANOVA on beta-band power aligned to cue onset in the contralateral cluster only showed a significant main effect of instruction (F(1, 16) = 29.67, p < 0.0001). The interaction between instruction and cue direction was not significant (F(1, 16) = 0.64, p = 0.436). Also a Bayesian ANOVA revealed a Bayes factor for the interaction between instruction and cue direction of 0.423, which can be interpreted as inconclusive evidence (Jeffreys, 1961). Similar results were found when the signal was aligned to response onset.

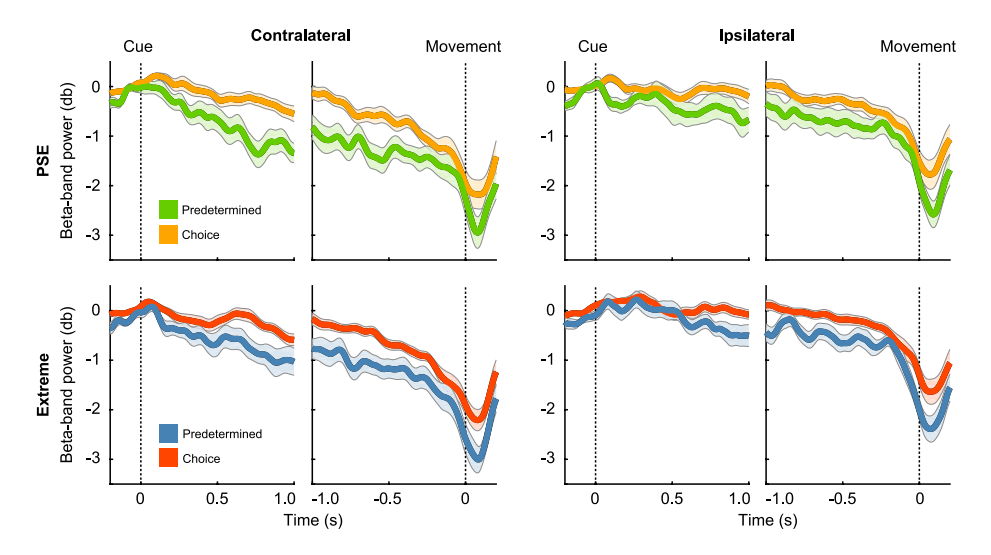
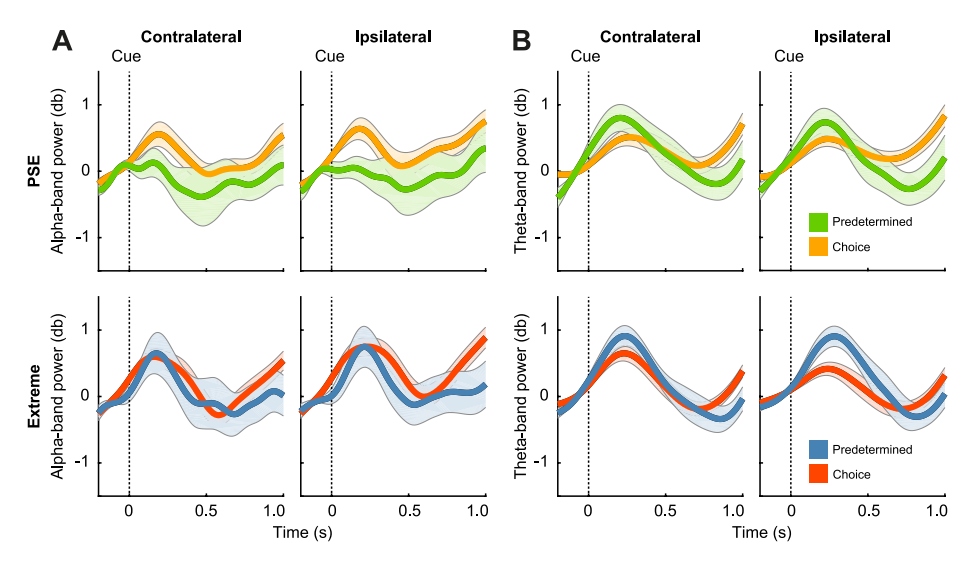


Figure 2.4. Beta-band power. Relative beta-band power as a function of time in the contralateral (left columns) and ipsilateral (right columns) sensor cluster for the PSE (upper row) and the extreme cue (bottom row). Left and right subpanels show the signal aligned to cue and movement onset, respectively. Shaded areas represent SEM. Repeated-measures ANOVAs with the average beta-band power during the time window from cue onset until 1 s after cue onset and the time window from 1 s before response onset until response onset revealed significant main effects of instruction and sensor cluster (n = 17). The number of trials included per participant was higher in the choice condition (PSE cue: M = 69, SD = 7.01; extreme cue: M = 132, SD = 10.53) than in the predetermined condition (PSE cue: M = 17, SD = 2.09; extreme cue: M = 16, SD = 2.15).

To examine whether the effect of effector uncertainty is specific to the signal in the beta-band, we performed the same analysis in the alpha (8 to 12 Hz) and thetaband (5 to 7 Hz) frequency range. Power in the alpha-band is known to show a similar reduction to beta-band power prior to movement onset (Pfurtscheller, 1992). However, alpha-band power does not modulate with directional uncertainty about the upcoming movement (Tzagarakis et al., 2015). Figure 2.5A shows the power in the alpha-band as a function of time, grouped based on instruction (predetermined, choice), cue direction (extreme, PSE), and sensor cluster (ipsilateral, contralateral). A repeated-measures ANOVA on the average alpha-band power during the cue phase did not reveal any significant main effects of instruction (F(1, 16) = 2.77, p = 0.116), cue direction (F(1, 16) = 0.77, p = 0.393), or sensor cluster (F(1, 16) = 4.46, p = 0.051), or any significant interaction effects.

Finally, we examined the effect of effector uncertainty on the oscillations in the theta-band, which have been implicated in motor planning and anticipation (Dufour, Thénault, & Bernier, 2018; Perfetti et al., 2011). Figure 2.5B shows the power in the theta-band as a function of time during the cueing phase. A repeated-measures ANOVA did not reveal significant main effects of instruction (F(1, 16) = 0.00, p = 0.967), cue direction (F(1, 16) = 0.85, p = 0.371), or sensor cluster (F(1, 16) = 0.45, p = 0.514), or any interactions.



**Figure 2.5.** Alpha-band and theta-band power. A) Relative alpha-band power as a function of time aligned to cue onset in the contralateral (left columns) and ipsilateral (right columns) sensor cluster for the PSE (upper row) and extreme cue (bottom row). Shaded areas represent SEM. B) Relative theta-band power as a function of time. Configurations the same as panel A. Repeated-measures ANOVAs with the average alpha-band and theta-band power during the time window from cue onset until 1 s after cue onset did not reveal any significant effects of instruction, cue location and sensor cluster (n = 17). These analyses included the same trials as reported in Figure 2.4.

### 24 Discussion

To investigate the effect of effector uncertainty on beta-band oscillatory activity during motor preparation, participants performed a hand reaching task whereby the effector to use was either predetermined or free of choice. We hypothesized that competition between the left and right hand would be low, independent of the cue direction, if the hand to be used was predetermined. If participants were free to choose a hand, we expected greater competition and hence a smaller decrease in beta-band power. Additionally, we expected more competition during hand choice for the PSE cue, where the right and left hand were chosen equally often, than for eccentric cues. Results indicate that effector competition indeed affects beta-band power during motor planning: when participants were free to choose the hand to use beta-band power decreased less than when the hand to use was predetermined. We did not observe a significant effect of cue direction on beta-band power.

The strength of the present study is the use of a cueing paradigm in a hand choice experiment, which allowed to validate that participants prepared the movement in a clearly defined and motion-artifact-free analysis interval. Our results demonstrate that effector uncertainty induced by instruction affected betaband power over central brain areas during motor planning. More specifically, beta-band power decreased less when participants were free to choose the hand to use than when the hand was predetermined. Lower levels of betaband power are thought to be associated with a readiness to move (Khanna & Carmena, 2017). This idea is in line with our expectations, as the instruction to use a specific hand should diminish competition between left and right-hand motor plans, and therefore ease motor planning. This is further underlined by the observation that instruction also affected reaction times: reaction times were longer when participants were free to choose the hand to use than when the hand was predetermined. This reaction time pattern has been previously observed by Oliveira et al. (2010) and is thought to show that hand selection comes with a cost. All in all, our results suggest that beta-band power was affected by effector uncertainty induced by instruction, with a smaller decrease in power when participants chose the hand for the ensuing reach.

Contrary to our expectations, our results do not show an effect of cue direction, neither on beta-band power, nor on reaction times. We expected that reaches towards the PSE would elicit more competition between the left and right hand than reaches towards targets in the periphery, for which one hand is usually clearly preferred over the other (Bakker et al., 2018; Oliveira et al., 2010; Stoloff et al., 2011). Indeed, Oliveira et al. (2010) reported that a reaction time difference disappeared by restricting reaches to only one hand, as we do in the predetermined condition. Our experimental cueing paradigm did not elicit a difference in effector competition for the PSE and extreme targets. A potential reason can be found in the introduction of incorrect cues, which could have unintendedly increased uncertainty about the effector to use. For every presented cue, there was only 50% chance that the target would be presented in the same direction. The incorrect cues were included to be able to show that participants prepared their movement during the cueing phase, rather than waiting for the target. Without this experimental manipulation, it remains questionable whether participants in fact prepared a movement during the cueing phase. As a disadvantage, the presence of invalid cues may have resulted in too much uncertainty about which hand to use and therefore participants did not yet fully commit to preparing a single hand. It would be interesting for future studies to develop a paradigm that can control for movement preparation, as in the present paradigm, while incentivizing participants to commit to the movement. The effect of cue validity on effector uncertainty should be limited to the choice trials, as competition is thought to be low for reaches with a predetermined hand, regardless of the direction of the cue and target. Indeed, our results show that incorrect cues prolong reaction times for choice trials, but not for predetermined trials. Thus, the introduction of the incorrect cues might have resulted in a lack of a difference in effector uncertainty for the PSE and extreme targets for the choice trials, explaining why no effect of cue direction was observed here.

The absence of an effect of cue direction for the choice trials cannot be explained by an overall lack of movement preparation during the cue period. Not only do our results show that incorrect cues prolong reaction times for choice trials, but hand choice was also biased by the direction of the (incorrect) cue. Additionally, we found that reaction times were shorter with longer cue times. These findings suggest that participants prepared the movement based on the cue. This is in line with findings from previous delayed response cueing experiments; Tzagarakis et al. (2010, 2015) found that reaction times were longer if the cue was less informative in terms of the direction of the upcoming target, and Oostwoud Wijdenes et al. (2016) showed that movement variability during a reaching movement was larger if the preceding cue did not specify the hand to use.

In our analysis, the effect of effector uncertainty induced by instruction on brain oscillatory activity over central areas of the brain was limited to the

power in the beta-band. Even though oscillations in the alpha-band are known to show a similar decrease in power during motor planning to oscillations in the beta-band (Pfurtscheller, 1992), we did not observe a modulation of alpha-band power based on effector uncertainty. This is in line with findings for directional uncertainty where beta-band but not alpha-band power decreases more if target direction is more certain (Grent-'t-Jong et al., 2014; Tzagarakis et al., 2015). Additionally, Rhodes et al. (2018) found that alphaband power during a cue period only decreases (followed by an increase) if the direction of the upcoming target is unambiguous, suggesting the activity to be related to movement execution processes rather than motor planning. It thus seems as if alpha-band and beta-band power over central areas of the brain reflect complementary but distinct processes, with alpha-band power being insensitive to uncertainty about the upcoming movement.

Theta-band power is known to increase during motor planning (Perfetti et al., 2011), and has been shown to modulate with the anticipation of visual feedback (Dufour et al., 2018). Here, we did not observe a modulation of theta-band power based on effector uncertainty induced by instruction. Thus, the effect of effector uncertainty on oscillatory power during motor planning seems to be reflected in beta-band power specifically, with the reservation that we did not analyze power changes in the gamma band. Van Der Werf et al. (2010) have reported direction-selective synchronization in the 70 to 90 Hz gammafrequency band, originating from the medial aspect of the posterior parietal cortex, when planning a reaching movement. Future work should address whether gamma-band synchronization also modulates with hand choice.

How the modulation of beta-band power over central areas of the brain coincides with other changes in neural activity observed during effector selection remains to be answered. Here, we focused on beta-band activity from channels positioned along the central coronal plane of the head, covering central areas of the brain. Localizing the exact neural source of this activity, however, was not one of the main objectives of this study. Previous studies have attempted to find the source of neural activity related to effector uncertainty. Hand choice has, for instance, been shown to be related to the phase of deltaband oscillations at the onset of the reach target in the dorsal premotor cortex and primary motor cortex contralateral to the hand used (Hamel-Thibault et al., 2018). Additionally, BOLD activity appears to be modulated by effector uncertainty in parietal cortex (Fitzpatrick et al., 2019), which is in line with the finding that TMS over the posterior parietal cortex biases hand choice (Oliveira et al., 2010). It remains unknown whether these phenomena, distinct in the type of neural activity and source location, are linked, and for example arise from activity in the same neuronal ensembles, or whether these findings arise from independent processes.

In general, motor decisions are thought to be biased by the expected utility of potential movements. This utility depends on the costs and benefits of a certain movement and is based on the location of the movement target relative to the effector. However, also other factors might be taken into account, such as the task or trial instruction. Neural activity related to motor decision making based on utility is thought to intertwine with the activity related to motor planning (Cisek, 2006). Evidence for this has been found in both human (Grent-'t-Jong et al., 2014, 2015; Tzagarakis et al., 2010, 2015) and non-human primates (Basso & Wurtz, 1997; Cisek & Kalaska, 2005; Glaser et al., 2018; Klaes et al., 2011). In line with this, we observe an effect of motor decision making on beta-band power - a neural marker of motor planning (Jasper & Penfield, 1949; Pfurtscheller, 1992).

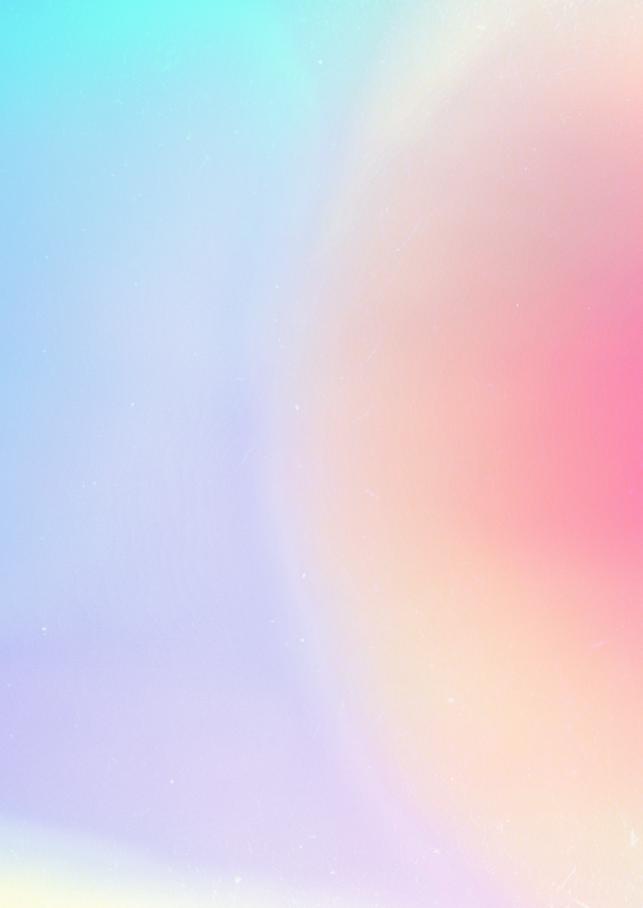
Our results are in line with the idea that motor plans for the two arms are prepared in parallel and compete for execution. We found that beta-band power during movement preparation decreased less with higher effector uncertainty, and thus more competition between the two hands, suggesting less commitment to a single motor plan. The idea of parallel processing of motor plans has however been a topic of debate. Bernier et al. (2012) suggested that effector selection actually precedes motor planning. In their experiment, they found activity in the parietal and premotor cortex contralateral to the hand used, but this was only observed after target onset, and thus after the hand was thought to be selected. However, their hand choice experiment differed from the paradigm used here. Bernier et al. (2012) asked participants to reach to two eccentric targets. Additionally, participants never actually chose the hand to use themselves, but were either instructed early on in the trial (based on the cue) or at target onset. Both the location of the targets and the instruction of the hand might have diminished possible competition between left and right hand movement plans, similar as to the predetermined reaches towards an extreme target direction here. It is important to point out though that Bernier et al.'s (2012) findings are in line with results from monkey studies that show that neuronal activity only encodes selected reach plans, instead of potential reach plans, in area 5 (Cui & Andersen, 2011) and dorsal premotor cortex (Dekleva et al., 2018). Based on these results, Dekleva et al. (2018) challenge the idea of the parallel specification of motor plans for potential reaching

actions (Cisek & Kalaska, 2005), and suggest that evidence for the encoding of multiple motor plans is simply a result of trial averaging. Unfortunately, we lack the signal-to-noise ratio to address this issue at the single trial level, but this would be an interesting issue for further research.

The difference in beta-band power between predetermined and choice trials observed here fits with the idea that effector uncertainty modulates oscillatory activity. However, factors other than effector uncertainty may have affected beta-band power during the experiment as well. For example, muscle co-contractions during control of arm posture have been shown to modulate beta-band power (Snyder, Beardsley, & Schmit, 2019). Here, most trials in which participants moved both hands were choice trials (76 out of the 85 trials in total with two-hand movements that were removed from the analysis). Even though this supports the notion of higher effector uncertainty for the choice trials, this could also indicate that muscle activity in the two arms was higher for choice than predetermined trials. In line with this, for the predetermined trials, muscle activity during the delay period could be increased in the instructed arm only as a result of response inhibition. Future work should address whether the differences observed in beta-band power correlate with muscle contraction forces.

It could also be asked whether the unbalanced number of trials in the predetermined and choice conditions biased our conclusions. While participants completed 100 predetermined trials versus 800 choice trials, we do not believe that participants perceived the predetermined cue stimulus as a deviant. The effect of instruction on beta-band power did not show up just shortly after the presentation of the cue, which might reflect the processing of a surprising visual stimulus, but appeared to be sustained and to even increase throughout the cue period. In support, although the data for the predetermined trials had slightly larger variability than the data for the choice trials, the main effect of instruction on beta-band power was highly significant (p < 0.001).

In conclusion, the results of this study suggest that effector competition during motor planning is reflected in beta-band, but not alpha or theta-band, power over central regions. More specifically, beta-band power decreased less with more competition between the left and right hand. Alpha and theta band power lacked these modulations. Our findings support the more general idea that the brain specifies multiple possible effector-specific actions in parallel up to the level of motor preparation.



# Chapter 3

# Predictive steering: integration of artificial motor signals in self-motion estimation

This chapter has been adapted from:

van Helvert, M.J.L., Selen, L.P.J., van Beers, R.J., & Medendorp, W.P. (2022). Predictive steering: integration of artificial motor signals in self-motion estimation.

Journal of Neurophysiology, 128, 1395-1408.

# Abstract

The brain's computations for active and passive self-motion estimation can be unified with a single model that optimally combines vestibular and visual signals with sensory predictions based on efference copies. It is unknown whether this theoretical framework also applies to the integration of artificial motor signals, like those that occur when driving a car, or whether self-motion estimation in this situation relies on sole feedback control. Here, we examined if training humans to control a self-motion platform leads to the construction of an accurate internal model of the mapping between the steering movement and the vestibular reafference. Participants (n = 15) sat on a linear motion platform and actively controlled the platform's velocity using a steering wheel to translate their body to a memorized visual target (Motion condition). We compared their steering behavior to that of participants (n = 15) who remained stationary and instead aligned a non-visible line with the target (Stationary condition). To probe learning, the gain between the steering wheel angle and the platform or line velocity changed abruptly twice during the experiment. These gain changes were virtually undetectable in the displacement error in the Motion condition, whereas clear deviations were observed in the Stationary condition, showing that participants in the Motion condition made within-trial changes to their steering behavior. We conclude that vestibular feedback allows not only the online control of steering, but also a rapid adaptation to the gain changes in order to update the brain's internal model of the mapping between the steering movement and the vestibular reafference.

### Introduction 3.1

Self-motion estimation depends on the integration of sensory and motor information. During passively generated motion (e.g., a passenger in a moving car), perception of self-motion comes primarily from the visual system, which provides optic flow cues (Britten, 2008), and the vestibular system (Angelaki & Cullen, 2008; Medendorp & Selen, 2017). Because sensory signals may be ambiguous (e.g., the otoliths cannot distinguish between translational motion and gravitational acceleration), the brain is thought to use an internal sensory integration model that combines sensory information from different modalities to form a final self-motion percept (Angelaki, Shaikh, Green, & Dickman, 2004; Clemens et al., 2011; Merfeld, Zupan, & Peterka, 1999).

When the motion is generated actively, the brain can also integrate information related to the motor command to estimate self-motion (for a review, see Brooks & Cullen, 2019). In fact, self-motion is judged better when it is actively generated than passively imposed (Carriot, Brooks, & Cullen, 2013; Genzel, Firzlaff, Wiegrebe, & MacNeilage, 2016; Medendorp, 2011; Sanders, Chang, Hiss, Uchanski, & Hullar, 2011). Also, patients with vestibular deficits perceive self-motion significantly better when self-generated (Glasauer, Amorim, Viaud-Delmon, & Berthoz, 2002; Kaski et al., 2016; Medendorp, Alberts, Verhagen, Koppen, & Selen, 2018; Worchel, 1952).

While these findings could be interpreted as evidence that vestibular signals (and sensory signals more generally) are functionally less important in actively moving subjects, recent modeling work has provided a unified theory for how active and passive motion can be estimated (Cullen, 2019; Laurens & Angelaki, 2017), with a fundamental role for both sensory signals and the efference copy. According to this theory, a multisensory self-motion estimate is computed using sensory prediction errors, i.e., the difference between actual and predicted sensory signals. During active motion, motor commands can be used to anticipate the corresponding sensory reafference, such that the sensory prediction error is minimal. In contrast, sensory activity cannot be anticipated during passive motion, resulting in non-zero sensory prediction errors, which then drive the self-motion estimate.

Under both active and passive motion, vestibular signals (as well as other sensory signals like vision) are continuously monitored to update the internal prediction. Thus, without intact sensory organs, the sensory prediction errors cannot be corrected, and the self-motion estimate may no longer be accurate during either active or passive motion. Because sensory information and motor commands, as well as the neural processing itself, are endowed with intrinsic random noise, Laurens and Angelaki (2017) modelled the computations using a Kalman filter to determine the optimal (Bayesian) estimate of self-motion. Given uncertainty in the moment-to-moment sensory information, such a Bayesian computation also relies on a priori expectations about incoming sensory signals (Clemens et al., 2011; Laurens & Droulez, 2007; MacNeilage, Ganesan, & Angelaki, 2008; Prsa, Jimenez-Rezende, & Blanke, 2015).

While this framework suggests that not only sensory signals but also efference copies of motor commands are critical in self-motion perception, it is agnostic as to the nature of the motor signal. This opens up the possibility that also artificial (or indirect) motor signals can be used for self-motion perception, as long as they are associated with an accurate internal model for predicting the sensory reafference. Such artificial motor signals are for example generated when driving a car; the steering is cognitively mediated and of efferent nature. The use of such artificial motor signals for self-motion perception is the topic of the present study.

Data on this issue are sparse and contradictory. For example, Roy and Cullen (2001) taught monkeys to drive themselves using a steering wheel that controlled the speed of the turntable on which they were seated. They compared neural activity between an active steering condition and voluntary head rotation conditions. While neuronal activity was suppressed at early sensory levels during active head rotations, reflecting a near-zero prediction error, this was not observed during self-generated driving, during which neurons responded as if the motion was externally applied. These findings suggest that an artificial motor signal, here a cognitive steering signal, is not used to predict the sensory afference at early sensory levels. In contrast, other work (Jacob & Duffy, 2015; Page & Duffy, 2008) has reported that neurons in the dorsal stream (medial superior temporal area) show altered responses to visual self-motion when monkeys steer to move in a certain direction compared to when they passively view the same optic flow pattern (but see also Egger & Britten, 2013), as if the brain not only relied on sensory self-motion information but also made an internal model prediction based on steering-related signals.

In the present study we address this issue in humans, testing whether and how steering-related signals are used in self-motion perception. Recent virtual reality experiments examined how humans (and monkeys) virtually navigated to a memorized location by integrating optic flow generated by their own joystick movements (Alefantis et al., 2022; Lakshminarasimhan et al., 2018; Stavropoulos et al., 2022). Biases in their steering depended on optic flow density, as a marker of the reliability of sensory evidence, and the control gain of the joystick, as a measure of the internal model prediction of the optic flow, suggesting that the brain combined both signals in the percept of nonvestibular self-motion. However, the authors mainly focused on the processing of visual information, and the role of the vestibular sense was only studied under continuously changing control dynamics of the joystick (Stavropoulos et al., 2022). It remains unknown if the brain formed an internal model to predict the vestibular self-motion signal or whether it solved the task primarily using vestibular feedback control, without relying on the control dynamics. In support of the latter, vestibular feedback control models have previously been suggested for goal-directed path integration, in which the distance of a traveled path is computed from the sole inertial sensory input (Glasauer, Schneider, Grasso, & Ivanenko, 2007).

We created a motor signal of cognitive nature (an artificial efference copy) and test how it is used in combination with vestibular-derived self-motion signals. This outflow signal was generated by training subjects to drive their own body, by handling a steering wheel that controlled the lateral motion velocity of a vestibular platform, to a memorized visual target (Motion condition). We examined how vestibular feedback is used in the online control of steering and studied the dynamics by which the mapping between steering movement and resulting vestibular feedback - the internal model is learned by abruptly changing the gain between the steering wheel angle and the velocity of the platform twice during the experiment. If participants construct an internal model of the mapping between the steering movement and the vestibular reafference, we expect rapid, within-trial, changes to their steering behavior after these gain changes in order to align their body with the memorized target. We compared their behavior to that of participants who did not have vestibular feedback about their motion, and could thus only employ a feedforward strategy, as they handled the steering wheel to control a line cursor (Stationary condition).

### 3.2 Methods

### 3.2.1 **Participants**

Thirty participants were randomly assigned to one of two experimental conditions. The Motion group included 15 participants (five men and ten women) ranging in age from 18 to 35 years, and the Stationary group included 15 participants (six men and nine women) ranging in age from 18 to 29 years. All participants were naïve to the purpose of the experiment and reported to have normal or corrected-to-normal vision and no history of motion sickness. The ethics committee of the Faculty of Social Sciences of Radboud University Nijmegen, the Netherlands, approved the study and all participants gave written informed consent prior to the start of the study. Participants were reimbursed for their time with course credit or €12,50. The experimental session took around 75 minutes per participant.

# 3.2.2 **Setup**

The experiment took place in a dark room. Participants were seated on a custom-built linear motion platform, also called the sled, with their interaural axis aligned with the motion axis of the sled (Fig. 3.1A). The track of the sled was approximately 95 cm long. The sled was powered by a linear motor (TB15N; Tecnotion, Almelo, The Netherlands) and controlled by a servo drive (Kollmorgen S700; Danaher, Washington, DC, United States). Participants were restrained by a five-point seat belt and could stop the motion of the sled at any time by pressing one of the emergency buttons on either side of the sled chair. A steering wheel (G27 Racing Wheel; Logitech, Lausanne, Switzerland) with a range of rotation from 450 to +450 deg and a resolution of 0.0549 deg was mounted in front of the participants at chest level. The steering wheel was placed at a comfortable handling distance from the body for each individual participant. The angle of the steering wheel encoded the linear velocity of the sled (Motion condition) or a vertical line cursor (Stationary condition). Visual stimuli were presented on a 55 inch OLED screen (55EA8809-ZC; LG, Seoul, South Korea) with a resolution of 1920 x 1080 pixels and a refresh rate of 60 Hz, positioned centrally in front of the sled track at a viewing distance of approximately 170 cm. Participants wore headphones during the entire experiment to mask the noise of the moving sled with white noise sounds. The experiment was controlled using custom-written software in Python (version 3.6.9; Python Software Foundation).

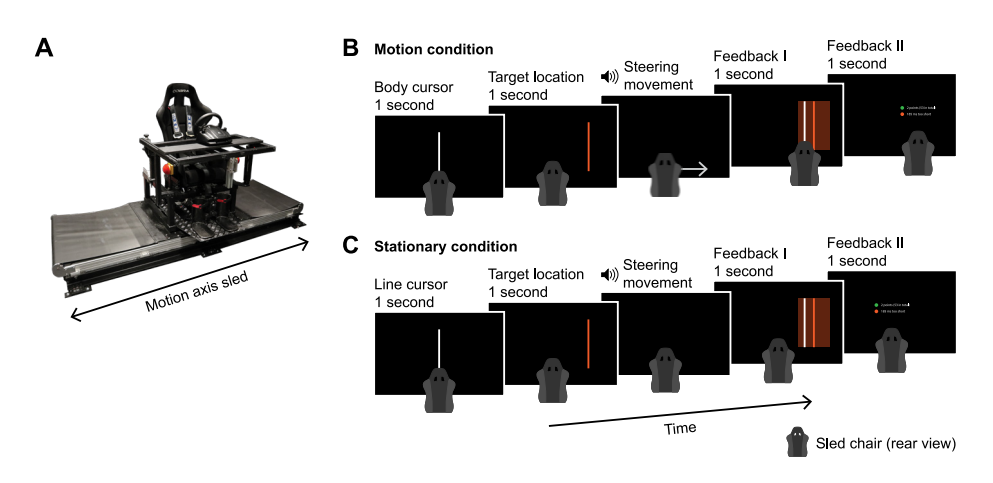


Figure 3.1. Experimental setup and paradigm. A) Experimental setup. Participants were seated with their interaural axis aliqned with the motion axis of the sled and turned a steering wheel. B) Motion condition paradigm. Participants were first shown the body cursor (white line), followed by the target (orange line). After the disappearance of the target, a beep instructed participants to turn the steering wheel to translate their body in alignment with the memorized target location. After the motion, visual feedback about the distance from the reappearing body cursor to the target location (Feedback I) and the movement duration (Feedback II) was provided. C) Stationary condition paradigm. Participants were first shown the line cursor (white line), followed by the target (orange line). After the disappearance of the target, a beep instructed participants to turn the steering wheel to translate the memorized line cursor in alignment with the memorized target location. Participants remained stationary and did not receive any visual feedback during the steering movement. After the movement, visual feedback about the distance from the reappearing line cursor to the target location (Feedback I) and the movement duration (Feedback II) was provided.

### 3.2.3 **Paradigm**

### 3.2.3.1 Motion condition

In the Motion condition, participants turned the steering wheel to laterally translate their body to align with a memorized visual target. The angle of the steering wheel encoded the linear velocity of the sled. The experimental session started with a two-minute familiarization with visual feedback to become acquainted with the initial gain between the angle of the steering wheel and the velocity of the sled (1.4 cm/s per deg, see below). After the familiarization, the main experiment started.

Figure 3.1B shows the sequence of events during an experimental trial. At the start of the trial, the position of the body midline was presented on the screen as a vertical white line with a length of 25.4 cm for 1 s. We will refer to this

line as the body cursor. Next, the target, represented by a vertical orange line with the same length, was presented for 1 s. The target distance, defined as the distance from the body cursor to the target location, was 20, 30 or 40 cm. The target could appear to the left or to the right of the body midline. After disappearance of the target, a beep was played via the headphones to inform the participant to start the steering movement to align their body midline with the memorized target location.

The motion started when the participant turned the steering wheel 0.0549 deg (one "click") away from the steering wheel angle at trial start. Participants received no visual information during the motion. As described above, the initial gain between the angle of the steering wheel and the velocity of the sled was 1.4 cm/s per deg. To probe learning, the gain changed abruptly twice during the experiment (trial 1-90: 1.4 cm/s per deg; trial 91-162: 0.8 cm/s per deg; trial 163-234: 1.4 cm/s per deg). Participants were not informed about the initial gain or the gain changes, and were instructed to make a smooth steering movement. The latency between the rotation of the steering wheel and the translation of the sled was typically lower than 10 ms. The maximum absolute velocity of the sled was set to 100 cm/s. If the steering wheel angle encoded a higher sled velocity, it was capped at this maximum velocity (< 1 trial per participant). During the motion, white noise was played through the headphones to mask any auditory cues. When the absolute velocity encoded by the steering wheel angle fell below 2 cm/s the sled stopped, and the white noise sound ended.

After the motion, participants received feedback about the accuracy of their displacement and the duration of the steering movement. First, both the body cursor and the target were presented on the screen for 1 s. This informed participants about how far they ended from the target location, and whether they undershot or overshot the target location with their self-generated motion. To incentivize participants to adequately perform the task they also received a score. Two points were awarded if the undershoot or overshoot was smaller than 0.15 times the target distance, represented on the screen by a translucent orange rectangular area centered on the target stimulus. One point or zero points were awarded if the undershoot or overshoot was between 0.15 and 0.30 times or larger than 0.30 times the target distance, respectively. Subsequently, a line of text reiterating the score and the total score so far and a line of text with the movement duration were presented on the screen for 1 s. Participants were encouraged to finish their steering movement within 900 to

1300 ms from movement start to ensure suprathreshold vestibular stimulation while remaining below the maximal sled velocity. The line of text read: "Timing perfect" if the movement ended after 900 to 1300 ms, and "n ms too short/long" if the movement took shorter or longer. The lines of text were preceded by colored circles, with the color quickly informing the participants about their performance (displacement accuracy: green, orange and red for two, one and zero points, respectively; movement duration: green, orange and red for a perfect timing, 300 ms too short or long and more than 300 ms too short or long, respectively).

Trials were presented in blocks of six trials with the target presented at different locations: 20, 30 and 40 cm to the left and right of the body cursor at trial start. Target distances within a trial block were presented in a semirandom order, with leftward and rightward displacements alternating, and each distance presented once in either direction. The sled started a trial at the location where the previous trial ended. However, if the position of the sled at the end of a trial was restricting its motion on the next trial (because of the limited sled track length of ~95 cm) to less than 1.5 times the target distance, the sled was first passively moved to a position 30 cm away from the middle of the sled track in the direction opposite that of the upcoming displacement, leaving ~80 cm for the motion. The main experiment started with 18 practice trials, during which the experimenter was present for task instructions. The practice trials were followed by the 234 experimental trials, of which the first always tested a rightward displacement. The experimental trials were separated by short breaks (< 2 minutes) after every 36 trials, during which the lights in the experimental room were turned on to prevent dark adaptation.

# 3.2.3.2 Stationary condition

In the Stationary condition, participants turned the steering wheel to laterally translate a non-visible line cursor in alignment with a memorized visual target, while the sled (and thus the body) remained stationary. The experimental session started with a two-minute familiarization with visual feedback to become acquainted with the initial gain between the angle of the steering wheel and the velocity of the line cursor (1.4 cm/s per deg, see below). After the familiarization, the main experiment started.

During the main experiment, targets were presented as in the Motion condition (Fig. 3.1C). However, instead of the body cursor, participants controlled a nonvisible line cursor that moved independently of the stationary body. At the start of the trial, the line cursor was presented on the screen in front of the participant, aligned with the body midline, as a vertical white line with a length of 25.4 cm for 1 s. After the subsequent presentation of the target, a beep was played via the headphones to inform the participant to start the steering movement to align the line cursor with the memorized target. Note that neither the line cursor nor the target was visible during the steering movement. White noise was played through the headphones during the steering movement to keep conditions similar.

The gain between the steering wheel angle from trial start and the velocity of the line cursor changed over trials in the same way as in the Motion condition (trial 1-90: 1.4 cm/s per deg; trial 91-162: 0.8 cm/s per deg; trial 163-234: 1.4 cm/s per deg). During the steering movement, the position of the line cursor was updated in the background by adding up the products of the encoded velocities and the time between steering wheel samples. Contrary to the Motion condition, no maximum absolute velocity was set. When the absolute velocity encoded by the steering wheel angle fell below 2 cm/s the white noise sound ended and participants received feedback and a score as in the Motion condition (the updated position of the line cursor, in contrast to the body cursor, was shown along with the target).

Trials were presented in blocks of six trials as in the Motion condition. The main experiment started with 18 practice trials, during which the experimenter was present for task instructions. The practice trials were followed by the 234 experimental trials, of which the first always tested a rightward displacement. The experimental trials were separated by short breaks (< 2 minutes) after every 36 trials, during which the lights in the experimental room were turned on to prevent dark adaptation.

# 3.2.4 Data analysis

Data were processed offline in MATLAB (version R2017a; The MathWorks, Inc., Natick, Massachusetts, United States). Trials during which participants displaced the sled (Motion condition) or the line cursor (Stationary condition) in the direction opposite of the target or during which participants rotated the steering wheel less than 7.5 deg from the angle at trial start were excluded from the analysis. Additionally, for the Motion condition, trials during which the absolute velocity encoded by the steering wheel angle reached the set maximum of 100 cm/s or during which the sled reached one of the ends of the sled track were excluded. On average, one trial was excluded per participant (mean  $\pm$  SD; Motion condition: 1.40  $\pm$  1.45 trials per participant; Stationary condition:  $0.67 \pm 0.82$  trials per participant).

For all included trials movement onset was defined as the first time point the steering wheel rotated more than 2.5 deg away from the angle at trial start. Movement end was defined as the first time point after movement onset the steering wheel angle fell below 2.5 deg from the angle at trial start. Participants failed to bring the steering wheel angle back within this range (i.e., stopped steering prematurely) on average on five trials per participant (Motion condition:  $4.60 \pm 4.17$  trials; Stationary condition:  $5.20 \pm 6.70$  trials). For these trials, movement end was defined as the time point the steering wheel angle remained constant for at least 100 ms or reached a local minimum while encoding a low velocity (i.e., rotated less than 7.5 deg away from the angle at trial start). Movement duration was defined as the time between movement onset and movement end. Displacement error was defined as the distance between the body cursor (Motion condition) or the line cursor (Stationary condition) at movement end and the target. Negative errors represent undershoots; positive errors represent overshoots. Relative displacement errors were computed as the ratio of the displacement error and the target distance.

# 3.2.4.1 Normalized steering behavior and encoded velocity

To be able to depict changes in steering behavior and the encoded velocity of the sled or the line cursor in response to the two gain changes across participants, we first normalized the time traces of the steering wheel angle and the encoded velocity. For each participant, we first calculated the mean movement duration, the mean maximum absolute steering wheel angle and the mean maximum absolute encoded velocity (speed) of the baseline trials (trials 73-90, the last three trial blocks before the first gain change), grouped based on target distance and direction. We subsequently normalized the movement duration, steering wheel angle and encoded velocity samples on each trial by dividing them by the mean movement duration, the mean maximum absolute steering wheel angle and the mean maximum speed, respectively, of the three baseline trials with a corresponding target distance and direction. Normalized steering wheel angles and normalized encoded velocities were resampled to 1000 samples per trial using linear interpolation and were averaged across participants. We then created a corresponding linearly spaced time vector of 1000 samples for each trial running from zero, representing movement onset, to the mean normalized movement duration across participants for plotting purposes.

## 3.2.4.2 Scale factors and skewness

To quantify changes in steering kinematics in response to the two gain changes, we scaled both the raw time and raw steering wheel angle samples on each trial relative to the baseline trials with a corresponding target distance and direction. This linear transformation from baseline trial b to trial of interest i can be described by:

$$\begin{bmatrix} \mathbf{t}_{i} \\ \mathbf{\alpha}_{i} \end{bmatrix} = \begin{bmatrix} S_{t_{i,b}} & 0 \\ 0 & S_{\alpha_{i,b}} \end{bmatrix} \times \begin{bmatrix} \mathbf{t}_{b} \\ \mathbf{\alpha}_{b} \end{bmatrix}$$
 (eq. 3.1)

where  $t_i$  and  $t_h$  represent the time vectors,  $a_i$  and  $a_h$  the vectors with steering wheel angles, and  $s_{\alpha}$  and  $s_{\alpha}$  the scale factors for the time vector and the vector with steering wheel angles, respectively. To fit the scale factors, the data from the baseline trial and the trial of interest were first resampled to have matching lengths (i.e., the trial with the least samples was resampled using linear interpolation to have as many samples as the longer trial). Subsequently, scale factors were fitted by minimizing the combined sum of squared errors using the fminsearch function in MATLAB. For each trial, the fitted scale factors relative to the three baseline trials with a corresponding target distance and direction were averaged. This approach is similar to a baseline normalization of the movement duration and the maximum absolute steering wheel angle of the respective trial, but because it takes all samples of the trial into account it is more robust to changes in the shape of the steering profiles (e.g., less biased by long tails).

We additionally assessed skewness of the time traces of the steering wheel angle as a function of time by calculating Bowley's coefficient of skewness for each trial i:

$$B_i = \frac{Q_{3_i} - 2Q_{2_i} + Q_{1_i}}{Q_{3_i} - Q_{1_i}}$$
 (eq. 3.2)

where B represents the skewness coefficient, and  $Q_1$ ,  $Q_2$ , and  $Q_3$  represent the times at which 25%, 50%, and 75% of the total distance travelled during the trial was covered, respectively. The skewness coefficients were baseline corrected by subtracting the average of the baseline trials with a corresponding target distance and direction. Negative skewness coefficients represent leftskewed steering profiles relative to baseline; positive skewness coefficients represent right-skewed steering profiles relative to baseline.

### 3.2.4.3 Statistics

Statistical analyses were done in R (version 4.0.1; see R Core Team, 2017) using the package ez (version 4.4-0; see Lawrence, 2016). Results were considered significant if the p-value was smaller than 0.05. To characterize baseline performance, we examined the average displacement error, movement duration and the maximum absolute steering wheel angle across the baseline trials (trials 73-90) with a mixed factorial ANOVA with condition (Motion and Stationary) as between-subject factor and target distance (20, 30 and 40 cm) and target direction (leftward and rightward) as within-subject factors. The results were adjusted according to the Greenhouse-Geisser correction in case of violations of sphericity. We report the generalized eta squared  $(\eta_G^2)$  as a measure of the effect size (Bakeman, 2005).

To assess differences in changes in steering behavior in response to the two gain changes, we compared the behavior on trial 90 and trial 91 (high-to-low gain change) and on trial 162 and trial 163 (low-to-high gain change). We examined the change in the relative displacement error, the two scale factors and the skewness coefficient using a mixed factorial ANOVA with condition (Motion and Stationary) as between-subject factor and gain change (high-tolow and low-to-high) as within-subject factor. Data from one participant in the Stationary condition were excluded from the analyses due to a trial rejection around the low-to-high gain change. We additionally assessed whether the change in the relative displacement error was significantly different from zero in the Motion condition using a one-sample t-test for each gain change. We report Cohen's d as a measure of the effect size (Cohen, 1988).

### 3.3 Results

We created a closed-loop steering experiment, in which the participant's motor signal, enacted through a steering movement, directly influenced the ensuing body motion, and hence the feedback from the vestibular system. We examined how vestibular feedback is used in the online control of steering and studied the time course by which the mapping between steering movement and the whole-body translation is updated to changes in the control dynamics (Motion condition). We compared this to the steering of an external object (a line cursor) in a body-stationary condition (Stationary condition).

Figure 3.2A shows the mean displacement error across participants as a function of the trial block per target distance and condition, pooled across target directions. Displacement errors across the baseline trials (trial blocks 13-15) were similar across conditions ( $F_{1.28} = 1.83$ , p = .187,  $\eta_G^2 = .02$ ) and target directions ( $F_{1.28} = 1.97$ , p = .172,  $\eta_G^2 = .02$ ), but varied across target distances  $(F_{1.62.45.41} = 33.95, p < .001, \eta_G^2 = .28)$ . Participants were most accurate on baseline trials with an intermediate target distance (mean  $\pm$  SD; 30 cm: 0.60  $\pm$  3.94 cm), overshot the target location on trials with a small target distance (20 cm:  $2.81 \pm$ 3.07 cm), and undershot the target location on trials with a large target distance (40 cm:  $-3.18 \pm 5.34$  cm). Displacement errors across the baseline trials thus showed a range effect (Petzschner & Glasauer, 2011; Poulton, 1975). In the Stationary condition, participants undershot and overshot the target location shortly after the high-to-low and low-to-high gain change, respectively, irrespective of the target distance. However, the gain changes did not seem to influence the displacement error in the Motion condition. As this apparent lack of an effect of the gain changes in the Motion condition might be due to the low temporal resolution (trials were averaged across all six trials composing a trial block), we will refrain from statistics here. We will zoom in on the effect of the gain changes on the level of single trials later on.

The apparent lack of an effect of the gain changes on the displacement error in the Motion condition could also suggest that participants used the online vestibular feedback to make within-trial adjustments to their steering movement. These within-trial adjustments are likely to be reflected in the duration of the movement, the angle of the steering wheel and the velocity of the sled encoded by the angle of the steering wheel. The velocity of the sled is directly affected by the gain changes, and both the movement duration and the steering wheel angle can be adjusted in response to this error.

Figure 3.2B shows the mean movement duration across participants as a function of the trial block per target distance and condition, pooled across target directions. Movement duration across the baseline trials was similar across conditions ( $F_{1.28} = 0.58$ , p = .454,  $\eta_G^2 = .01$ ) and target directions ( $F_{1.28} = 0.96$ , p = .337,  $\eta_G^2 = .005$ ), but varied across target distances ( $F_{1.53.42.71} = 46.57$ , p <.001,  $\eta_G^2$  =.22). Participants took more time for the movement the longer the target distance (20 cm:  $859 \pm 125$  ms; 30 cm:  $947 \pm 112$  ms; 40 cm: 1006 $\pm$  111 ms). Overall, the baseline movement duration was at the lower end of the imposed window from 900 to 1300 ms (Motion condition:  $925 \pm 147$  ms; Stationary condition: 949 ± 111 ms). In the trial block after the high-to-low gain

change, the movement duration increased immediately in the Motion condition across all target distances, followed shortly by the Stationary condition. Movement duration remained elevated, with a larger overall increase for the Stationary condition. In the trial block after the low-to-high gain change, movement duration immediately returned to baseline values in the Motion condition, whereas movement duration decreased a little more gradually in the Stationary condition.

Figure 3.2C shows the mean maximum absolute steering wheel angle across participants as a function of the trial block per target distance and condition, pooled across target directions. The maximum absolute steering wheel angle across the baseline trials was similar across conditions ( $F_{1.28}$  = 0.43, p = .520,  $\eta_G^2$ =.01) and target directions ( $F_{1.28}$ =1.57, p=.221,  $\eta_G^2$ =.004), but varied across target distances ( $F_{2.56}$  = 117.34, p < .001,  $\eta_G^2$  = .36). Participants increased the maximum angle with increasing target distances (20 cm:  $28.74 \pm 5.23$  deg; 30 cm: 34.49 $\pm$  5.60 deg; 40 cm: 39.09  $\pm$  6.55 deg). We additionally found a small but significant interaction effect between target direction and condition ( $F_{1,20} = 5.55$ , p = .026,  $\eta_G^2 = .01$ ). This interaction effect seems to be driven by a higher mean maximum absolute steering wheel angle for leftward than rightward displacements across the baseline trials in the Stationary condition (leftward:  $35.75 \pm 6.92$  deg; rightward:  $33.62 \pm 6.54$  deg), whereas the angle was similar across directions in the Motion condition (leftward:  $33.19 \pm 7.20$  deg; rightward:  $33.84 \pm 7.95 \text{ deg}$ ).

In the trial block after the high-to-low gain change, the maximum absolute steering wheel angle increased in the Motion condition across all target distances. The maximum absolute steering wheel angle remained relatively high until the low-to-high gain change, after which it decreased rapidly. In the Stationary condition, the maximum absolute steering wheel angle also increased and decreased after the high-to-low and low-to-high gain change, respectively, but more gradually.

Figure 3.2D shows the mean maximum speed of the sled or the line cursor encoded by the steering wheel angle as a function of the trial block per target distance and condition, pooled across target directions. Due to the rapid changes in the steering wheel angle in the Motion condition in response to the gain changes, the maximum speed of the sled remained rather constant across the experiment. In the Stationary condition, the maximum speed of the line cursor returned to baseline values more gradually.

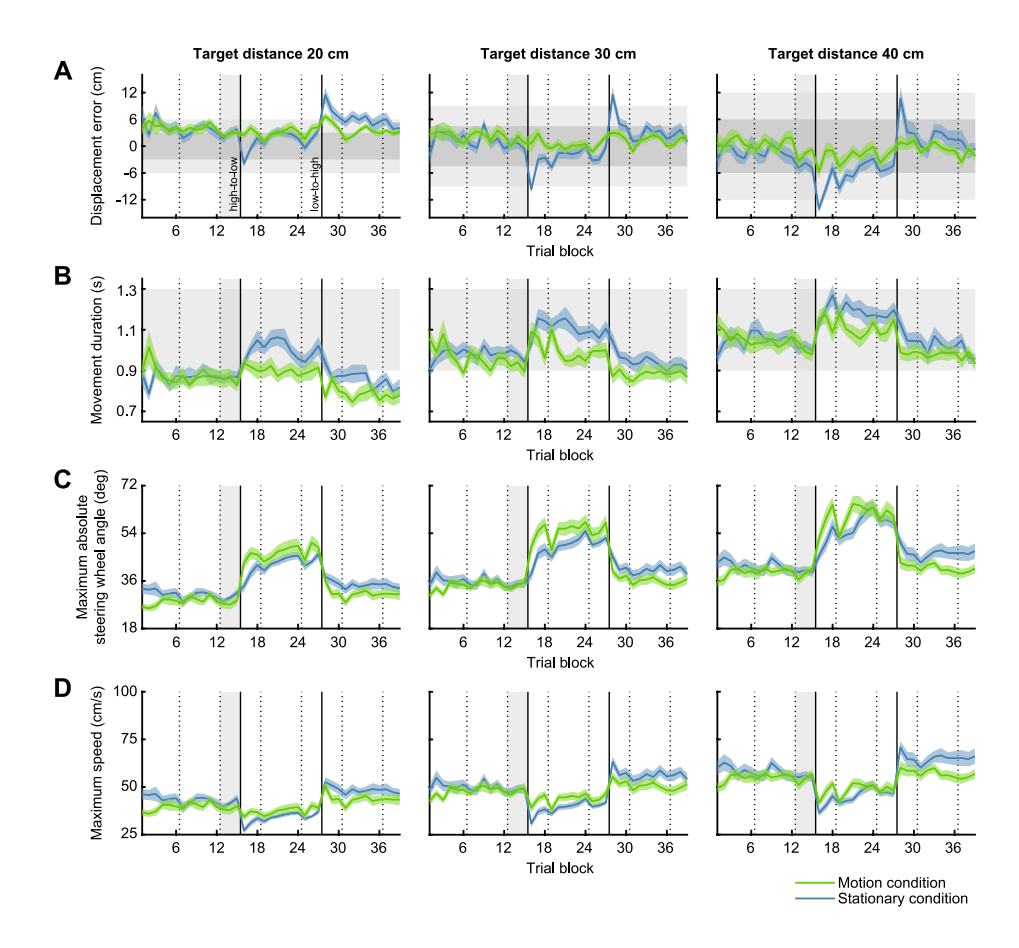


Figure 3.2. Displacement error, movement duration, maximum absolute steering wheel angle and maximum speed. A) Mean displacement error across participants as a function of trial block grouped based on target distance (panels) and experimental condition (colored lines). Displacement errors have been averaged across leftward and rightward displacements within a trial block. Negative numbers represent undershoots; positive numbers represent overshoots. Colored shaded areas represent between-subjects SEM. Horizontal dark and light gray bands show the range of displacement errors for which participants received 2 points and 1 point, respectively. Dashed vertical lines represent breaks, and solid vertical lines represent changes in the gain between the steering wheel angle and the velocity of the sled (Motion condition) or the line cursor (Stationary condition). Vertical light gray bands show the baseline trial blocks (trial blocks 13-15). A mixed factorial ANOVA revealed a significant main effect of target distance on the baseline displacement error (p < .001; Motion condition: n = 15; Stationary condition: n = 15). B) Same configuration as in A, but with the mean movement duration across participants. Horizontal light gray bands show the 900 to 1300 ms window within which participants were encouraged to finish their movement. A mixed factorial ANOVA revealed a significant main effect of target distance on the baseline movement duration (p < .001). C) Same configuration as in A, but with the mean maximum absolute steering wheel angle across participants. A mixed factorial ANOVA revealed a significant main effect of target distance on the baseline maximum absolute steering wheel angle (p < .001), as well as a significant interaction effect between target

direction and experimental condition (p = .026, not visible in the figure). D) Same configuration as in A, but with the mean maximum speed across participants. The speed is directly related to the steering wheel angle shown in C, with a gain of 1.4 cm/s per deg (trial block 1-15 and trial block 28-39) or 0.8 cm/s per deg (trial block 16-27).

To be able to inspect the effect of the gain changes at a high temporal resolution of single trials, while taking the semi-random trial order into account, we computed the relative displacement error as the ratio of the displacement error and the target distance. Figure 3.3A shows the relative displacement error across all trials, separately for the Motion condition and the Stationary condition. While the relative displacement error straddled closely around zero in the Motion condition, also after the gain changes, this was not the case in the Stationary condition, where there are clear deviations following the gain changes. Figure 3.3B illustrates the difference in the relative displacement error between the first trial after and the last trial before the gain changes, showing larger changes in the relative displacement error in the Stationary condition (high-to-low:  $-0.53 \pm 0.28$ ; low-to-high:  $0.85 \pm 0.52$ ) than in the Motion condition (high-to-low:  $-0.11 \pm 0.32$ ; low-to-high:  $0.18 \pm 0.50$ ). A mixed factorial ANOVA revealed a significant main effect of the gain change ( $F_{127}$  = 57.54, p < .001,  $\eta_G^2 = .51$ ) and a significant interaction effect between the gain change and the condition ( $F_{1.27}$  = 23.89, p <.001,  $\eta_G^2$  =.30) on the change in the relative displacement error. This interaction effect indicates that the gain changes indeed affected the relative displacement error differently across conditions. Two one-sample t-tests revealed that the changes in the relative displacement error in the Motion condition were not significantly different from zero (high-to-low: t(14) = -1.34, p = .202, d = -0.35; low-to-high: t(14) = -1.39, p = .186, d = 0.36).

The observation that the relative displacement error was virtually constant across gain changes in the Motion condition, also on the level of single trials, suggests that participants indeed used the online vestibular feedback to make within-trial adjustments to their steering movement, as described above. Figure 3.4 illustrates these within-trial adjustments in response to the two gain changes. Participants in the Motion condition increased the duration and the absolute steering wheel angle of their steering movement within the first trial after the high-to-low gain change (trial 91) relative to the previous baseline trial (trial 90) to compensate for the lower gain (Fig. 3.4A). In the Stationary condition, no online feedback was available, and participants could thus not have been aware of the gain changes during the trials immediately after. This is also reflected in their behavior: the duration and the absolute steering wheel

angle of their steering movement remained similar from the trial before the gain change (trial 90) to the trial after (trial 91), resulting in a substantial decrease in the encoded velocity and an undershoot of the target location (see also Fig. 3.3A). In both conditions, however, participants increased the absolute steering wheel angle in later trials with the low gain, leading to a restoration of the encoded velocity close to baseline values, as shown in Figure 3.4B (trial 162). After the low-to-high gain change, participants in the Motion condition decreased the duration and the absolute steering wheel angle again within the first trial (trial 163) to compensate for the higher gain. In the Stationary condition, steering behavior remained the same from the trial before the gain change (trial 162) to the trial after (trial 163). This resulted in a substantial increase in the encoded velocity and an overshoot of the target location (see also Fig. 3.3A).

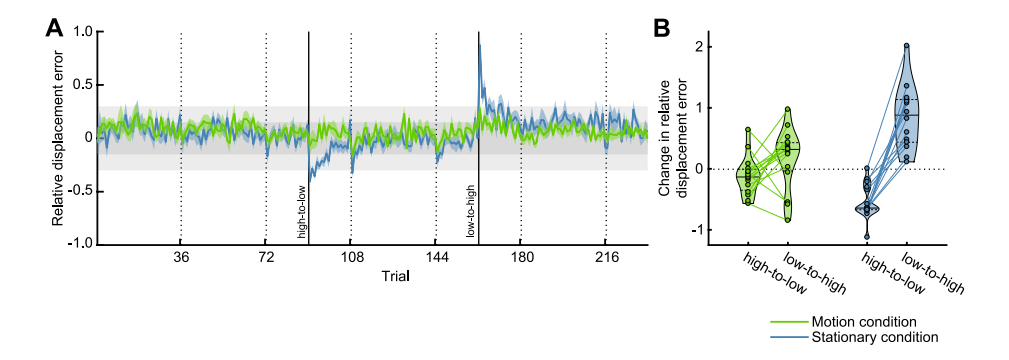


Figure 3.3. Relative displacement error. A) Mean relative displacement error across participants as a function of trial grouped based on experimental condition (colored lines). Relative displacement error was computed as the ratio of the displacement error and the target distance. Colored shaded areas represent between-subjects SEM. Dark and light gray bands show the range of displacement errors for which participants received 2 points and 1 point, respectively. Dashed vertical lines represent breaks, and solid vertical lines represent changes in the gain between the steering wheel angle and the velocity of the sled (Motion condition) or the line cursor (Stationary condition). B) Mean difference in relative displacement error between the first trial after and the last trial before the gain changes (high-to-low: trial 91 - trial 90; low-to-high: trial 163 - trial 162) across participants. Violin shape outlines show the kernel density estimates of the individual participant data points (colored dots connected by colored lines). Solid and dashed horizontal lines within the violin shapes represent the median and interquartile range, respectively. A mixed factorial ANOVA revealed a significant interaction effect between the gain change and the experimental condition (p < .001; Motion condition: n = 15; Stationary condition: n = 14), as well as a significant main effect of the gain change (p < .001).

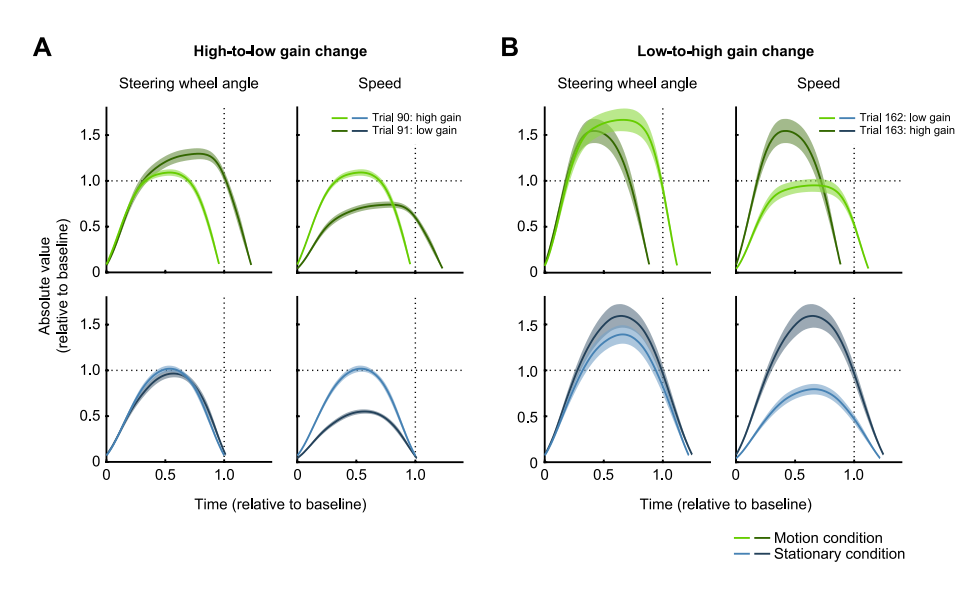


Figure 3.4. Steering behavior around the gain changes. A) Average absolute steering wheel angle (left panels) and average speed (right panels) as a function of time across participants for the trial before and after the high-to-low gain change (trial 90 and 91, respectively), in the Motion (green colors) and Stationary condition (blue colors). Values were normalized relative to baseline. Colored shaded areas represent between-subjects SEM. B) Same configuration as in A, but with the trial before and after the low-to-high gain change (trial 162 and 163, respectively).

We next quantified the within-trial adjustments in response to the gain changes in both conditions at a high temporal resolution of single trials by scaling of the time-axis and steering wheel angle-axis relative to the baseline (trials 73-90). With this linear transformation, the axes of the trial of interest are independently stretched and compressed to match the baseline trial. Figures 3.5A and 3.5B show the fitted scale factors for the time-axis, describing the movement duration, and the steering wheel angle-axis, respectively, across all trials. In line with Figure 3.4, both the movement duration and steering wheel angle increased relative to baseline immediately after the high-to-low gain change and decreased immediately after the lowto-high gain change in the Motion condition. Similar patterns were observed for the Stationary condition, albeit with a one-trial delay and slower changes in behavior. Participants in both conditions continued to adjust their steering behavior in response to the gain changes across trials. This is most clearly visible after the high-to-low gain change: after the immediate increase in movement duration and steering wheel angle, participants continued to increase the steering wheel angle across trials while decreasing the movement duration. The latter is not surprising, as we encouraged participants to finish their steering movement within a time window from 900 to 1300 ms, and thereby indirectly encouraged them to adjust the steering wheel angle instead of the movement duration.

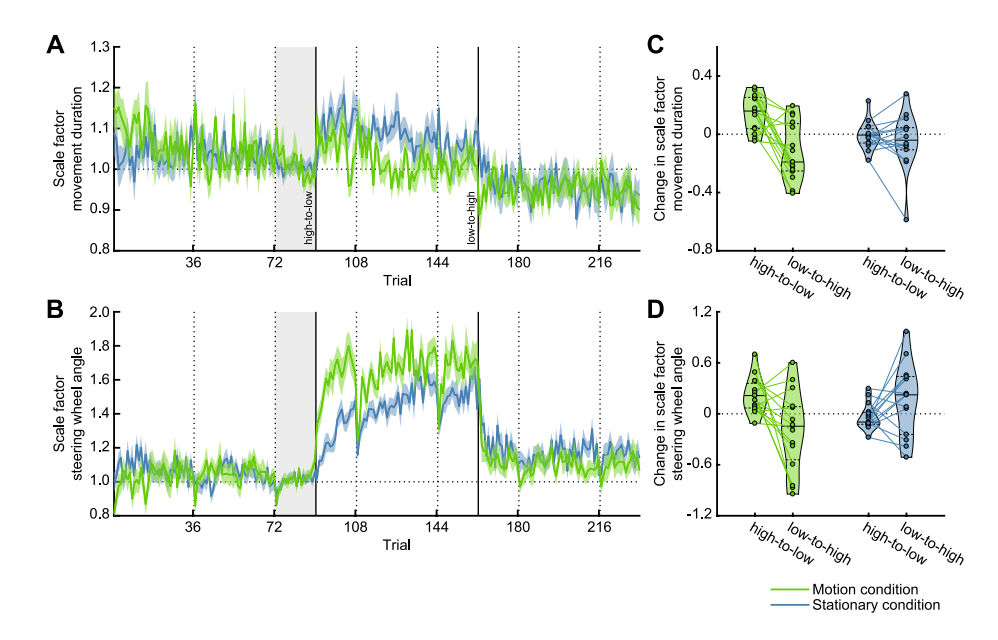


Figure 3.5. Scale factors movement duration and steering wheel angle. A) Mean movement duration scale factor across participants as a function of trial grouped based on experimental condition (colored lines). Scale factors were fitted relative to the baseline trials (trials 73-90, vertical light gray band) with a corresponding target distance and direction. Colored shaded areas represent between-subjects SEM. Dashed vertical lines represent breaks, and solid vertical lines represent changes in the gain between the steering wheel angle and the velocity of the sled (Motion condition) or the line cursor (Stationary condition). B) Same as in A, but with the steering wheel angle scale factor. C) Mean difference in the movement duration scale factor between the first trial after and the last trial before the gain changes (high-to-low: trial 91 - trial 90; low-to-high: trial 163 - trial 162) across participants. Violin shape outlines show the kernel density estimates of the individual participant data points (colored dots connected by colored lines). Solid and dashed horizontal lines within the violin shapes represent the median and interquartile range, respectively. A mixed factorial ANOVA revealed a significant interaction effect between the gain change and the experimental condition (p = .003; Motion condition: n = 15; Stationary condition: n = 14), as well as a significant main effect of the gain change (p < .001). D) Same as in C, but with the steering wheel angle scale factor. A mixed factorial ANOVA revealed a significant interaction effect between the gain change and the experimental condition (p = .003).

Figure 3.5C illustrates the difference in the movement duration scale factor between the first trial after and last trial before the gain changes, showing a significant main effect of the gain change ( $F_{127} = 14.56$ , p < .001,  $\eta_G^2 = .19$ ) and

a significant interaction effect between the gain change and the condition  $(F_{137} = 10.34, p = .003, \eta_G^2 = .14)$ . Figure 3.5D illustrates the difference in the steering wheel angle scale factor across the trials just before and after the gain changes, showing no significant main effect of the gain change ( $F_{1,27}$  = 1.39, p=.249,  $\eta_G^2$  =.03), but a significant interaction effect between the gain change and the condition ( $F_{1.27} = 10.66$ , p = .003,  $\eta_G^2 = .18$ ). These significant interaction effects indicate that the gain changes affected the scale factors differently across conditions. Participants in the Motion condition increased both the movement duration and the steering wheel angle from one trial to the next after the high-to-low gain change to compensate for the lower gain, illustrated by the positive changes in the scale factors (movement duration:  $0.15 \pm 0.12$ ; steering wheel angle:  $0.22 \pm 0.21$ ). After the low-to-high gain change, these participants decreased the movement duration and the steering wheel angle to compensate for the higher gain, illustrated by the negative changes in the scale factors (movement duration:  $-0.12 \pm 0.20$ ; steering wheel angle: -0.20± 0.47). As expected, participants in the Stationary condition kept their behavior constant across the high-to-low gain change (movement duration:  $-0.01 \pm 0.09$ ; steering wheel angle:  $0.04 \pm 0.15$ ) and the low-to-high gain change (movement duration:  $-0.05 \pm 0.20$ ; steering wheel angle:  $0.17 \pm 0.42$ ).

These results show that participants in the Motion condition used the online vestibular feedback to change their steering behavior within the first trial after the gain changes. We therefore examined the skewness of the observed steering profiles. If participants in the Motion condition rapidly correct their steering movement after a gain change, early in the motion, we expect a skew of the steering profile. We computed Bowley's skewness coefficient for each trial. This skewness coefficient provides information about how the distance travelled is distributed across the trial duration. Figure 3.6A shows the mean skewness coefficient across participants as a function of trial number, separately for the Motion and the Stationary condition. In the Motion condition, the skewness coefficient decreased after the high-to-low gain change, indicating a left-skewed steering profile (i.e., the increase of the absolute steering wheel angle was slower than the decrease, see also trial 91 in Fig. 3.4A). After the low-to-high gain change, the skewness coefficient increased, indicating a right-skewed steering profile (i.e., the increase of the absolute steering wheel angle was faster than the decrease, see also trial 163 in Fig. 3.4B). Both changes in the skewness coefficient were short-lasting and did not persist across the trials following the first trial after the gain changes. In the Stationary condition, skewness coefficients remained rather constant across trials and gain changes. Figure 3.6B illustrates the difference in the skewness coefficient across the trials just before and after the gain changes, showing a small but significant interaction effect between the gain change and the condition ( $F_{1,\,27}=5.54$ , p=.026,  $\eta_G^2=.11$ ). This indicates that the gain changes affected the skewness coefficient differently across conditions, with more skewed steering profiles in the Motion condition (high-to-low: -0.017  $\pm$  0.033; low-to-high: 0.020  $\pm$  0.034) than in the Stationary condition (high-to-low: -0.001  $\pm$  0.015; low-to-high: -0.005  $\pm$  0.033). No significant main effect of the gain change was found ( $F_{1,\,27}=3.83$ , p=.061,  $\eta_G^2=.08$ ).

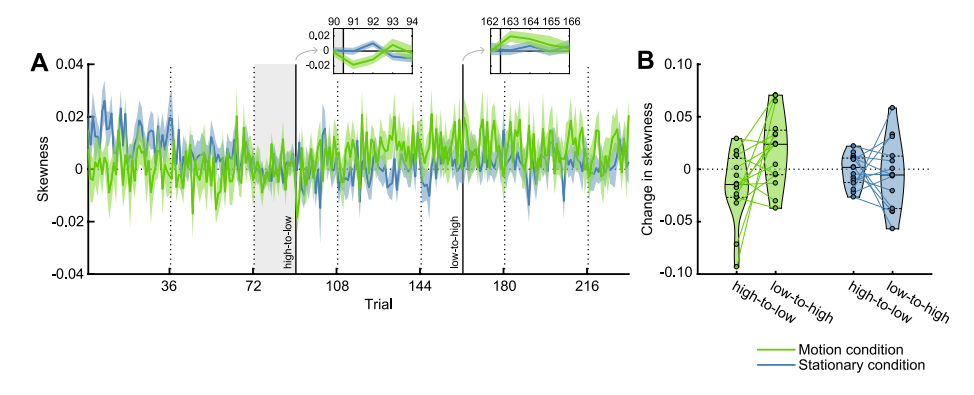


Figure 3.6. Skewness. A) Mean skewness coefficient across participants as a function of trial grouped based on experimental condition (colored lines). Skewness coefficients were baseline corrected by subtracting the average across the baseline trials (trials 73-90, vertical light gray bands) with a corresponding target distance and direction. Negative skewness coefficients represent left-skewed steering profiles; positive skewness coefficients represent right-skewed steering profiles. Colored shaded areas represent between-subjects SEM. Dashed vertical lines represent breaks, and solid vertical lines represent changes in the gain between the steering wheel angle and the velocity of the sled (Motion condition) or the line cursor (Stationary condition). Insets show the zoomed views of the trials before and after the gain changes. B) Mean difference in the skewness coefficient between the first trial after and the last trial before the gain changes (high-to-low: trial 91 - trial 90; low-to-high: trial 163 - trial 162) across participants. Violin shape outlines show the kernel density estimates of the individual participant data points (colored dots connected by colored lines). Solid and dashed horizontal lines within the violin shapes represent the median and interquartile range, respectively. A mixed factorial ANOVA revealed a significant interaction effect between the gain change and the experimental condition (p = .026; Motion condition: n = 15; Stationary condition: n = 14).

#### **Discussion** 3.4

Participants were tested in a naturalistic self-motion task in which they actively controlled their own body motion on a motion sled, while traversing to a remembered target location in darkness (Motion condition). The goal was to examine whether participants estimated their self-motion based on the vestibular signals resulting from their body motion and developed an internal model about the mapping of the steering movement and the vestibular reafference. To find signatures of this internal model construction we unexpectedly changed the gain between the steering movement and the sled motion twice during the experiment and recorded participants' changes in steering behavior. We compared their steering behavior with that of participants who controlled a line cursor instead of their own body motion, and thus did not have access to online vestibular feedback (Stationary condition).

In the Motion condition, the sudden gain changes did not result in systematic changes in displacement errors (Fig. 3.2 and 3.3). Instead, we observed within-trial changes in steering behavior immediately after the gain changes; participants increased and decreased the movement duration and the steering wheel angle to compensate for the high-to-low and the low-to-high gain changes, respectively (Fig. 3.4 and 3.5). These within-trial adjustments, resulting in skewed steering profiles (Fig. 3.6), suggest that participants continuously monitored and integrated the available vestibular feedback to keep track of their self-motion when aligning their body with the memorized target. Additionally, participants continued to revise the movement duration and steering wheel angle in subsequent trials with the new gain, gradually improving their adaptation to the new control dynamics (i.e., revise the movement duration and the steering wheel angle to be able to adhere to the imposed movement duration). This shift from fast and reactive changes in behavior to more tactful and planned changes suggests that participants built and updated an internal model of the steering signal and the associated selfmotion based on the online vestibular feedback.

In contrast, in the Stationary condition, the gain changes resulted in substantially increased displacement errors (Fig. 3.2 and 3.3). This is not surprising; participants assigned to this condition found out about the gain changes at the earliest at the end of the first trial after the gain changes, based on the visual feedback about their displacement error. Across trials, however, these participants adjusted their steering behavior based on this feedback to compensate for the gain changes; after the gain changes they gradually changed the movement duration and the steering wheel angle, without changing the skewness of their steering movement (Fig. 3.4, 3.5 and 3.6), causing the displacement error to decrease. Overall, the results suggest that also the participants in the Stationary condition built an internal model, illustrated by their overall ability to perform the task (i.e., the displacement error at the end of the baseline did not differ from the Motion condition), and employed a feedforward control strategy to gradually improve their performance across trials after the gain changes based on the visual feedback at the end of the trial.

Could participants in the Motion condition have performed the task without forming an internal model (and thus without online predictions of the self-motion. i.e., the vestibular reafference)? By integrating the vestibular information relating to the velocity of the sled over time - as in models of path integration (Lappe et al., 2007) - participants could have kept track of the position of the sled in space, and stopped the sled when the required travel distance, specified by the target, was reached. However, the fast changes in steering behavior in response to the gain changes, as also shown by the changes in the scale factors and skewness coefficient describing the steering profiles (Fig. 3.4, 3.5 and 3.6), suggest that participants had some expectations relating to the velocity of the sled. So, the tentative explanation of our results is that participants are able to generate predictions about the vestibular feedback based on artificial motor signals (i.e., the steering movement) and compare these predictions to the actual online vestibular feedback in order to estimate their self-motion (Cullen, 2019; Laurens & Angelaki, 2017). These computations are similar to those underlying the perception of true active self-motion, and our results therefore suggest that artificial signals, such as the steering motor signal, can serve as an efference copy that can be integrated in self-motion perception.

Importantly, we do not want to claim that sensory feedback strategies play no role in this steering behavior. For example, the steering profiles differ slightly between the Motion and Stationary condition when the adaptation is complete - the former showing a plateaued phase in steering wheel angle midway the motion as well as in the associated velocity (as generated by our platform) while the latter showing a symmetric bell-shaped steering profile. If a bellshaped steering profile reflects optimal adaptation, our participants may not have adapted optimally to the control dynamics, but also may not have ignored these dynamics. Since the vestibular system, specifically the otolith, is mainly sensitive to acceleration, a phase of constant velocity sacrifices the reliability

of vestibular feedback about the motion. To maintain task performance, this would require the participants to rely on an internal representation of the control dynamics and an adjusted control policy.

The present study builds on experiments in both self-motion perception and motor learning. Motor learning experiments, such as force field experiments during which reaching movements are perturbed by forces applied to the arm, have shown that participants adapt to new but sustained environments faster if online (visual) feedback is available (Batcho, Gagné, Bouyer, Roy, & Mercier, 2016; Franklin, So, Burdet, & Kawato, 2007). Additionally, even when the environment is completely unpredictable and changes from trial to trial, participants have been shown to be able to use online feedback to adapt by adjusting their behavior (Crevecoeur, Thonnard, & Lefèvre, 2020). Our results are in line with these observations; after the unexpected gain changes, participants in the Motion condition, who had online vestibular feedback, adjusted their steering behavior faster than participants in the Stationary condition. Of note, reaching movements are often ballistic, with movement durations around 600 ms, and are therefore likely to depend to a large extent on feedforward processes. The steering movements in the current experiment were slower, with movement durations around 900 ms, and there might therefore have been even more time for online adjustments, making continuous reliance on sensory feedback certainly a key aspect of the control strategy. Follow-up studies are required to further investigate the nature of the efference copy and the corresponding internal model representation based on artificial motor signals.

Our study is one among the few recent studies that tested self-motion perception under a direct coupling between the actions of the participants and the sensory feedback (Alefantis et al., 2022; Lakshminarasimhan et al., 2018; Stavropoulos et al., 2022). These recent experiments imposed fewer artificial constraints than the traditional open-loop psychophysical paradigms on self-motion perception (e.g., de Winkel et al., 2013; Dokka, MacNeilage, DeAngelis, & Angelaki, 2011; Fetsch, Turner, DeAngelis, & Angelaki, 2009; ter Horst, Koppen, Selen, & Medendorp, 2015; Tramper & Medendorp, 2015). In the previous psychophysical experiments, the perception of self-motion was assessed by responses on a two-alternative forced choice task, allowing to estimate how the brain weighs and adapts to sensory cues during the motion in the absence of changing motor cues (Tramper & Medendorp, 2015; Zaidel, Turner, & Angelaki, 2011). While these experiments have led to important advances in the self-motion perception field, they cannot inform us how cues with time-varying noise levels are integrated over longer periods of time or which utility functions and task dependencies guide the naturalistic closedloop navigation behavior.

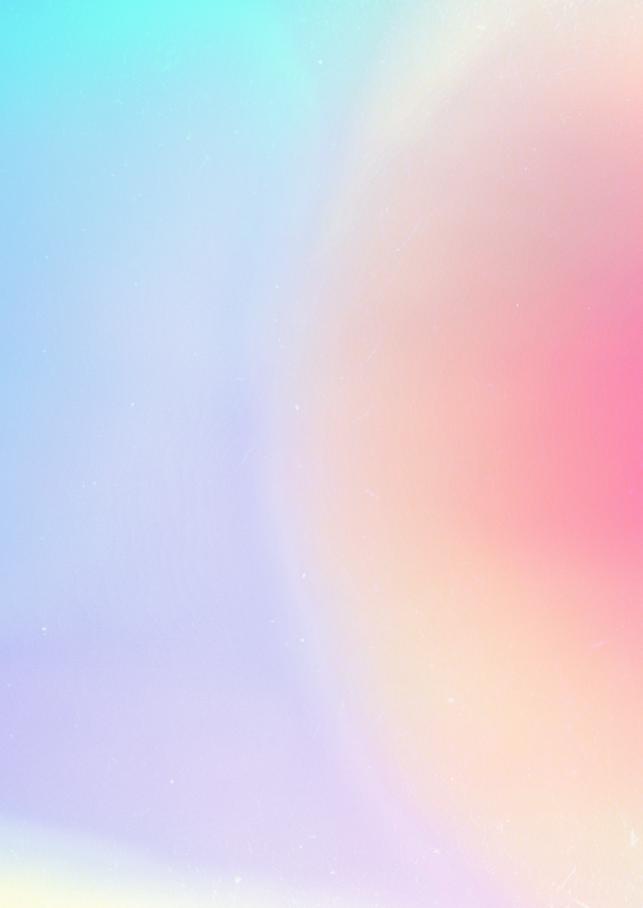
In a recent study by Stavropoulos et al. (2022), human participants controlled their self-displacement on a motion platform to navigate to a target with and without the presence of concurrent optic flow. They found that steering behavior in darkness was biased (i.e., participants undershot the target location), and therefore concluded that participants could not accurately estimate their selfmotion and update their internal model based on the vestibular cues alone. This conclusion differs from the present results, but could be explained by differences in the experimental design. More specifically, their participants did not receive any performance-related feedback, and the control dynamics of the motion platform changed from trial to trial, both of which may have kept participants from building an accurate internal model of the mapping between the steering movement and the vestibular feedback.

The rapid changes in steering behavior in response to the gain changes suggest that our participants quickly updated their internal models to anticipate the ensuing self-motion. Further support for this notion comes from previous studies showing that, during passive but predictable self-motion, the effects of the self-motion are anticipated. For example, during passivelyinduced angular (for a review, see Blouin, Bresciani, Guillaud, & Simoneau, 2015) and linear whole-body displacements (Sarwary, Selen, & Medendorp, 2013), participants were able to anticipate and counteract the inertial forces exerted on the arm, resulting in accurate goal-directed reaching movements. Also Prsa et al. (2015) showed that passive angular displacement estimates in human participants were biased towards the average over a block of random displacement magnitudes, suggesting that participants built up some expectations about the vestibular input.

Roy and Cullen (2001) have shown that neurons in the vestibular nuclei (VN) of monkeys respond similarly during steering-controlled and passively-induced self-motion. Under the assumption that the firing rates of neurons in the VN reflect sensory prediction errors (Brooks et al., 2015; Laurens & Angelaki, 2017), this suggests that no steering-related predictions about the vestibular reafference are made in the VN. Even though the vestibular cerebellum is often suggested to house the internal model for self-motion estimation because of its projections to the vestibular nuclei (Cullen, Brooks, Jamali, Carriot, & Massot,

2011), the internal model of the mapping between steering movements and self-motion seems located on a more downstream level within the vestibular processing pathway (Alefantis et al., 2022). This is in line with observations during the processing of the visual reafference of steering movements; Page and Duffy (2008) reported that neurons in the medial superior temporal area in monkeys responded differently to optic flow cues resulting from steering movements compared to passive viewing of the same optic flow cues.

The use of artificial signals in self-motion perception is currently exploited in the development of vestibular implants for patients with a vestibular deficit (Guyot et al., 2016; van de Berg et al., 2017). These vestibular implants electrically stimulate the vestibular nerve in a biomimetic way and provide patients with artificial vestibular feedback. Similarly, these patients have been shown to benefit from tactile and auditory cues that provide information about the vestibular input through an arbitrary mapping (for a review, see Guyot et al., 2016). This mapping has to be learned, similar to the gain in the present study, and the learning of such a mapping has even been extended to augmenting perception in healthy human subjects by adding an extra "vestibular" sense (i.e., head orientation relative to the geomagnetic North) (Schumann & O'Regan, 2017). Altogether, these experiments show that participants can learn the mapping between an artificial sensory feedback signal and their selfmotion, similar to the artificial motor signal used in the current study.



# Chapter 4

# Vestibular-derived internal models in active self-motion estimation

This chapter has been adapted from:

van Helvert, M.J.L., Selen, L.P.J., van Beers, R.J., & Medendorp, W.P. (2024). Vestibular-derived internal models in active self-motion estimation.

Journal of Neurophysiology, in revision.

## **Abstract**

Self-motion estimation is thought to depend on sensory information as well as on sensory predictions derived from motor feedback. In driving, the vestibular afference can in principle be predicted based on the steering motor commands if an accurate internal model of the steering dynamics is available. Here, we used a closed-loop steering experiment to examine whether participants can build such an internal model of the steering dynamics. Participants steered a motion platform on which they were seated to align their body with a memorized visual target. We varied the gain between the steering wheel angle and the velocity of the motion platform across trials in three different ways: unpredictable (white noise), moderately predictable (random walk), or highly predictable (constant gain). We examined whether participants took the across-trial predictability of the gain into account to control their steering (internal model hypothesis), or whether they simply integrated the vestibular feedback over time to estimate their travelled distance (path integration hypothesis). Results from a trial series regression analysis show that participants took the gain of the previous trial into account more when it followed a random walk across trials than when it varied unpredictably across trials. Furthermore, on interleaved trials with a large jump in the gain, they made fast corrective responses, irrespective of gain predictability. These findings suggest that the brain can construct an internal model of the steering dynamics to predict the vestibular reafference in driving and self-motion estimation.

#### 4.1 Introduction

Sensory feedback, especially visual and vestibular, is important in self-motion estimation. People can estimate their self-motion from visual (Britten, 2008) or vestibular (Cheng & Gu, 2018) information alone, but are more precise when feedback from both is available and integrated (Britton & Arshad, 2019; DeAngelis & Angelaki, 2011; Keshavarzi, Velez-Fort, & Margrie, 2023; Medendorp & Selen, 2017; ter Horst et al., 2015).

When the motion is generated actively, self-motion estimates also depend on predictions from internal models of sensory and body dynamics that transform motor commands into predicted sensory consequences (Brooks & Cullen, 2019; Laurens & Angelaki, 2017). In combination with actual sensory feedback, these predictions lead to better estimates of self-motion (Campos, Butler, & Bülthoff, 2012; Carriot et al., 2013; Genzel et al., 2016; Medendorp, 2011; Sanders et al., 2011), also in patients with vestibular deficits (Glasauer et al., 2002; Kaski et al., 2016; Medendorp et al., 2018; Worchel, 1952). Both during passive and active self-motion, the sensory feedback is thought to be continuously monitored in order to update the self-motion estimate and adjust the internal model if necessary (Brooks et al., 2015; Prsa et al., 2015).

The role of sensory feedback and predictions in self-motion estimation has been studied with closed-loop steering experiments in both monkeys (Egger & Britten, 2013; Jacob & Duffy, 2015; Page & Duffy, 2008; Roy & Cullen, 2001) and humans (Alefantis et al., 2022; Lakshminarasimhan et al., 2018; Stavropoulos et al., 2022; van Helvert, Selen, van Beers, & Medendorp, 2022). In these experiments, the self-motion is controlled by a joystick or steering wheel, and the sensory feedback can in principle be predicted based on the steering motor command if an accurate internal model of the steering dynamics is available. Alefantis et al. (2022) studied human steering behavior in a virtual environment and found that participants were able to navigate the environment on trials with optic flow cues, but also on interleaved trials without any sensory feedback, suggesting that participants had formed an internal model of the steering dynamics with training. Similarly, Stavropoulos et al. (2022) studied navigation with optic flow and vestibular cues while the steering dynamics varied from trial to trial according to a random walk (i.e., the dynamics on the previous trial are predictive of the dynamics on the current trial), from responsive to sluggish steering control. Their participants could steer accurately whenever optic flow cues were provided, but less so when only vestibular cues were available and steering control was responsive. It is thus not evident that vestibular cues alone can be used to build an internal model by which the generated self-motion can be predicted based on the steering motor command under changing steering dynamics. This is the topic of the present study.

We have previously examined the role of predictions and sensory feedback, in particular vestibular feedback, in self-motion estimation in a steering experiment in which the steering dynamics changed only twice during the experiment (van Helvert et al., 2022). Seated on a linear motion sled, participants were instructed to align their body with a memorized visual target using a steering wheel that controlled their lateral body motion. We found that participants responded rapidly (i.e., made within-trial adjustments to their steering movement) to the sudden step changes in the steering dynamics (i.e., the gain between the steering wheel angle and their body velocity). Across trials, participants' performance gradually improved further by adjusting to the new steering dynamics. One explanation of these findings is that participants built an internal model of the steering dynamics, which transforms the steering motor commands into predicted vestibular feedback, that they continued to update throughout the experiment based on the vestibular feedback (Brooks et al., 2015; van Helvert et al., 2022). Another explanation is that participants simply relied on path integration mechanisms (Lappe et al., 2007; Loomis et al., 1993; Zhou & Gu, 2023), estimating their location relative to the target by integrating the vestibular information over time without building an internal model of the steering dynamics. In the present study we aim to distinguish between these two explanations (internal model versus path integration), taking inspiration from studies on the adaptation of reaching movements.

Burge et al. (2008) and Wei and Körding (2010) studied visuomotor adaptation of reaching movements while the uncertainty of the visual feedback about the reach endpoint and the uncertainty of the spatial mapping between the reach endpoint and the visual feedback was varied. It was found that adaptation proceeded slower with higher visual feedback uncertainty and faster with higher spatial mapping uncertainty. Gonzalez Castro et al. (2014) compared adaptation to a force field that varied in strength unpredictably across trials or to a force field that followed a random walk across trials. They found that participants relied more on sensory feedback in the unpredictable condition, while trusting sensory predictions more in the random walk condition.

In the present study, we used a similar experimental design to dissociate the contribution of vestibular feedback and vestibular predictions in self-motion

estimation during driving. Participants steered a linear sled on which they were seated to translate their body to a memorized visual target. We varied the gain between the steering wheel angle and the velocity of the sled across trials in three different ways: a white noise condition (unpredictable gain), a random walk condition (moderately predictable gain) and a constant gain condition (highly predictable).

We examined the steering behavior for within-trial responses to the vestibular feedback and vestibular predictions based on an internal model of the steering dynamics. Furthermore, we assessed the participants' responses to more extreme changes in the steering dynamics by introducing large jumps in the gain (i.e., step trials) near the end of each trial block. If participants simply integrated the vestibular information over time to estimate the travelled distance (path integration hypothesis), we would expect to see no differences in the steering behavior across the three conditions. In contrast, if participants did take the across-trial predictability of the gain into account (internal model hypothesis), we expect them to respond fastest to changes in the gain in the white noise condition, followed by the random walk condition and the constant gain condition.

#### 4.2 Methods

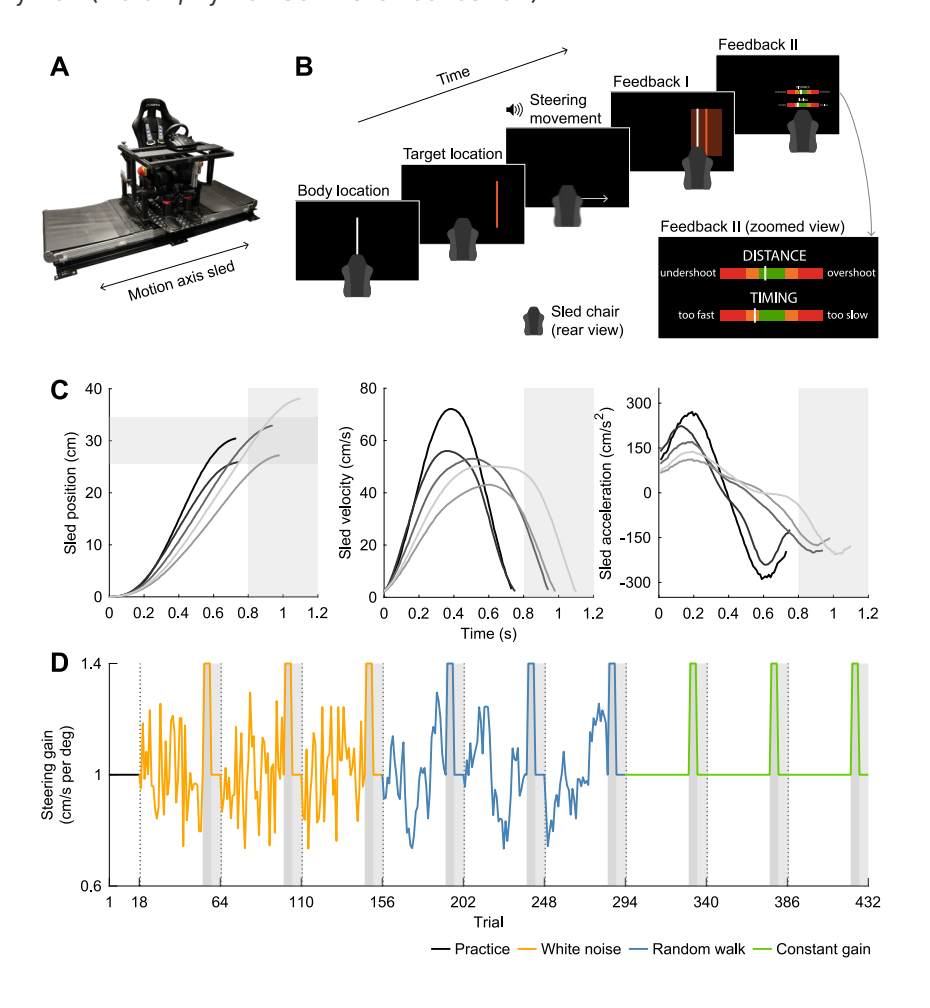
#### 4.2.1 **Participants**

The study was approved by the ethics committee of the Faculty of Social Sciences of Radboud University Nijmegen, the Netherlands. Twenty-six naïve participants took part in the study (7 men and 19 women; 18-30 years old) and gave their written informed consent before the start of the experiment. They reported to have normal or corrected-to-normal vision, normal hearing, and no history of motion sickness. The experiment took around 90 minutes per participant, and participants were compensated with course credit or €15,00.

# 4.2.2 **Setup**

Participants were seated on a custom-built linear motion platform, also called the sled, and used a steering wheel to control the sled speed (Fig. 4.1A). They sat with their interaural axis aligned with the motion axis of the sled, such that they were laterally translated. They were restrained by a five-point seat belt and could stop the sled motion at any time by pressing one of the emergency buttons on either side of the sled chair. The experiment was performed in

darkness. The sled was powered by a linear motor (TB15N; Tecnotion, Almelo, The Netherlands) and controlled by a servo drive (Kollmorgen S700; Danaher, Washington, DC, USA). The sled track was approximately 93 cm long. The steering wheel (G25 Racing Wheel; Logitech, Lausanne, Switzerland) was mounted at a comfortable handling distance in front of the participant at chest level and had a resolution of 0.0549° and a range of rotation from -450° to +450°. The steering wheel angle was recorded at 100 Hz. Participants viewed a 55-inch OLED screen (55EA8809-ZC; LG, Seoul, South Korea) with a resolution of 1920 x 1080 pixels and a refresh rate of 60 Hz, positioned centrally in front of the sled track at a viewing distance of approximately 170 cm, and wore noise-cancelling earphones to mask auditory cues induced by the sled motion with white noise sounds (QuietComfort 20; Bose Corporation, Framingham, MA, USA). The experiment was controlled using custom-written software in Python (v.3.6.9; Python Software Foundation).



< Figure 4.1. Experimental setup and paradigm. A) Experimental setup. Participants were seated with their interaural axis aligned with the motion axis of the sled and turned a steering wheel to control the sled velocity. B) Experimental paradigm. Participants were first shown their location as a white line, followed by the target location as an orange line. After the disappearance of the target location, a beep instructed participants to turn the steering wheel to translate their body and align it with the memorized target location. When the sled speed was again close to 0 cm/s, visual feedback about the displacement error (Feedback I and II) and the movement duration (Feedback II) was provided. Inset shows the zoomed view of the feedback bars in Feedback II. C) Sled position, velocity and acceleration as a function of time (aligned to movement onset) for five representative condition-specific trials in the constant gain condition (gray lines). For each trial, the measured absolute sled position relative to the start location, the absolute sled velocity encoded by the steering wheel angle, and the sled acceleration, computed by low-pass filtering the derivative of the encoded sled velocity using a moving average filter with a window length of nine samples, are shown. D) Example of the steering gain across trials, Each participant completed nine trial blocks. Each trial block started with 36 condition-specific trials, in which the gain varied from trial to trial (white noise and random walk condition) or remained the same (constant gain condition). Participants were exposed to the exact same gains in the white noise and random walk condition, but trials were organized such that their lag-1 autocorrelation was close to zero in the white noise condition and above 0.8 in the random walk condition. Each trial block was concluded with a baseline trial (gain of 1.0 cm/s per deg), followed by four step trials (high gain of 1.4 cm/s per deg; dark gray areas) and six washout trials (baseline gain of 1.0 cm/s per deg; light gray areas). Participants completed three trial blocks per condition, each followed by a short break (dashed vertical lines), and completed 18 practice trials before the experiment (baseline gain of 1.0 cm/s per deg).

# 4.2.3 Paradigm

Figure 4.1B shows the order of events during an experimental trial. At the start of a trial, a vertical white line aligned with the body midline (width 0.3 cm and height 25.4 cm) was presented on the screen for 1 second, which represented the start location of the body. After this, a vertical orange line (width 0.3 cm and height 25.4 cm) was presented on the screen for 1 second, representing the target location. The target location was alternately presented to the left and to the right of the start location of the body. The target distance, defined as the distance between the start location of the body and the target location, was always 30 cm. Participants were not informed about the fixed target distance.

After disappearance of the target, a short beep was played via the earphones to instruct the participant to rotate the steering wheel to align their body midline with the memorized target location. The sled motion started when the participant turned the steering wheel 0.0549 deg (the smallest detectable change) away from the steering wheel angle at trial start. The steering wheel angle at trial start was typically between -20 and 20 deg, with 0 deg representing the center of the range. The angle of the steering wheel relative to the angle at trial start encoded the velocity of the sled, but the exact

steering gain changed throughout the experiment (see below). The latency between the rotation of the steering wheel and the translation of the sled was approximately 25 ms. The maximum speed of the sled was set to 100 cm/s. If the steering wheel angle encoded a higher sled speed, it was capped at this maximum speed. The sled stopped when the steering wheel angle fell within -2 to 2 deg from the start angle, or when the steering wheel angle fell within -6 to 6 deg from the start angle and remained constant for 100 ms or started rising again (stopped steering prematurely or started a new steering movement). If the sled reached one of the ends of the track, it also stopped. Figure 4.1C shows the sled position, velocity and acceleration as a function of time for five representative trials. White noise was played via the earphones during the steering movement to mask auditory cues induced by the sled motion.

After the sled stopped, participants received feedback about their performance. First, both the current location of the body and the target location were presented on the screen for 1 s. This informed participants about how far they ended up from the target location and whether they undershot or overshot the target location. To encourage participants to be as accurate as possible, participants received "hit" feedback if the distance between the current location of the body and the target location was smaller than 4.5 cm. This "hit" area was represented on the screen by a translucent orange rectangular area (width 9 cm and height 25.4 cm) horizontally centered on the target location (Feedback I in Fig. 4.1B). After this, two horizontal feedback bars (width 15.2 cm and height 1 cm) were shown for 2 s (Feedback II in Fig. 4.1B). The center of the feedback bars was green, flanked by orange and red areas towards the edges. A white bar on the upper feedback bar reiterated the displacement error, with the center of the green area corresponding to the target location, and the left and right edges of the green area corresponding to an undershoot and overshoot of 4.5 cm, respectively (i.e., the "hit" window). A cheerful sound was played via the earphones if the participant "hit" the target. A white bar on the lower feedback bar showed the movement duration. Participants were encouraged to finish their steering movement within 800-1200 ms from movement start to ensure suprathreshold vestibular stimulation while remaining below the maximum sled speed. The center of the green area of the feedback bar corresponded to a movement duration of 1000 ms, and the left and right edges of the green area corresponded to a movement duration of 800 and 1200 ms, respectively. If the displacement error or the movement duration was out of bounds (i.e., actual location of the white bar was more extreme than the left and right outer edges of the red areas of the feedback bar, corresponding to movement durations of 200 ms and 1800 ms, respectively), the white bar was presented on the outer edge of the feedback bar closest to the true location.

The next trial started after the feedback had disappeared. If the location of the sled at the end of the trial restricted its motion on the next trial to less than 45 cm, the sled was first passively moved to a new starting location. This starting location was 15 cm away from the middle of the sled track in the direction opposite of the upcoming target location, leaving approximately 60 cm for the upcoming displacement.

As described above, the steering gain (i.e., the gain between the angle of the steering wheel and the velocity of the sled) changed throughout the experiment. All participants experienced three different conditions: a random walk condition, a white noise condition, and a constant gain condition (Fig. 4.1D). In total, the experiment consisted of nine trial blocks, with three trial blocks per condition. Each trial block started with 36 trials specific to the condition. On the last of these condition-specific trials, the steering gain was always 1.0 cm/s per deg (baseline trial), and this trial was always followed by four trials with a high gain of 1.4 cm/s per deg (step trials) and six trials with the baseline gain of 1.0 cm/s per deg (washout trials).

For the random walk condition, the gains of the other condition-specific trials were generated backwards, starting from the baseline trial, in the following way:

$$gain_i = gain_{i+1} + noise$$
 (eq. 4.1)

in which i is the trial number. Noise samples were drawn from a Gaussian distribution with a mean of 0 cm/s per deg and a standard deviation of 0.1 cm/s per deg. Random walks were drawn until a walk (excluding the baseline trial) met the following criteria: a mean gain between 0.99 and 1.01 cm/s per deg, a standard deviation between 0.139 and 0.141 cm/s per deg, and a lag-1 autocorrelation value higher than 0.8 (i.e., high predictability). Autocorrelation values were computed by dividing the autocovariance values by the variance of the gains, such that the autocorrelation values fell within -1 to 1. We controlled the standard deviation to ensure spread in the gains while avoiding gains more extreme than the gain on the step trials. The procedure was repeated three times per participant, yielding three random walks per participant.

For the white noise condition, the gains from the three random walks, except for the baseline trials, were shuffled. This was done 10,000 times per walk, and for each walk the instance with the lowest absolute lag-1 autocorrelation value was selected (all between 0.001 and -0.001). This way, the conditionspecific trials in the white noise trial blocks had the same means and standard deviations as the condition-specific trials in the random walk trial blocks. In the constant gain condition, all 36 condition-specific trials in the three trial blocks had a gain of 1.0 cm/s per deg (baseline gain).

The conditions were presented in a random order per participant. The number of repetitions of all six possible combinations was balanced across participants whose data was included in the analysis (see below). The three trial blocks per condition were presented consecutively but in random order. At the end of each trial block, the percentage of "hit" trials was presented on the screen, followed by a short break (> 45 seconds) during which the lights in the experimental room were turned on to prevent dark adaptation. Before the experiment, all participants completed 18 practice trials with a baseline gain of 1.0 cm/s per deg, during which the experimenter was present for task instructions. In total, each participant completed 432 trials.

# 4.2.4 Data analysis

Data were processed offline in MATLAB (v.R2017a; the MathWorks, Inc., Natick, MA). Data from two participants were excluded from the analysis because of their relatively low scores (average percentage of "hit" trials across trial blocks 48 and 58%; range included participants 66-90%). Trials during which participants rotated the steering wheel less than 7.5 deg or displaced the sled in the direction opposite of the target were excluded from the analysis. Additionally, trials during which the speed encoded by the steering wheel angle reached the set maximum of 100 cm/s or during which the sled reached one of the ends of the sled track were excluded. On average, one trial was excluded per participant (range 0-2 trials).

Movement onset was defined as the first time point that the steering wheel was rotated more than 2 deg. Movement end was defined as the first time point after movement onset that the steering wheel angle fell within -2 to 2 deg, or as the time point after which the steering wheel angle remained constant for at least 100 ms or reached a local minimum between -7.5 and 7.5 deg (i.e., failed to bring the steering wheel back to the start position or started a new steering movement). Movement duration was defined as the time between

movement onset and movement end. Displacement error was defined as the difference between the location of the body at movement end and the target location. Negative errors represent undershoots and positive errors represent overshoots.

#### 4.2.4.1 Trial series regression analysis

To examine whether the predictability of the gains affected the steering behavior on the condition-specific trials in the white noise and random walk condition, we performed a trial series regression analysis. For each time point t within trial i, we modelled the steering wheel angle a as a linear combination of a constant representing the average steering wheel angle at time point tacross trials, the gain on trial i (i.e., the current trial), the gain on trial i-1 (i.e., the previous trial), and residual error  $\epsilon$ :

$$a_i(t) = \beta_0(t) + \beta_1(t) \times gain_i + \beta_2(t) \times gain_{i-1} + \varepsilon_i(t)$$
 (eq. 4.2)

First, we selected the condition-specific trials (including the baseline trial but excluding the first trial of each trial block) and sampled the absolute steering wheel angle every 20 ms from 0 to 800 ms after movement onset for computational efficiency. Gains were z-scored based on the means and standard deviations of the gains on the included trials within the corresponding trial block. Trial blocks from the constant gain condition were not included in this analysis, because the gain was kept constant throughout the conditionspecific trials, making it impossible to use a regression analysis. The regression model was fitted per sampled time point within a trial, per trial block of the white noise and random walk condition, and per participant, yielding 5,904 runs in total (41 time points x 6 trial blocks x 24 participants).

To check whether the autocorrelation in the gains in the random walk condition could potentially lead to autocorrelated regression coefficients, we used simulations of the regression model in Equation 4.2. These simulations showed that the regression coefficients could be reliably estimated, both when the autocorrelation values of the predictors were high, similar to the random walk condition, and when the autocorrelation values were close to zero, similar to the white noise condition. This shows that the gains were distinct enough across trials to reliably estimate the regression coefficients described in Equation 4.2 in both the white noise and the random walk condition.

Based on the regression coefficients from the regression fits, we additionally predicted the absolute steering wheel angle as a function of time, as well as the separate effects of the current and the previous gain on the steering wheel angle, for the baseline and step trials. To compute the predictions, gains were z-scored based on the means and standard deviations of the gains from the included condition-specific trials within the corresponding trial block and were multiplied with the regression coefficients following Equation 4.2. Predictions were made per sampled time point within a trial, per trial block of the white noise and random walk condition, and per participant. If the predicted steering wheel angle fell below 2 deg, the steering movement ended.

#### 4.2.4.2 Statistics

Statistical analyses were done in MATLAB and R (v.4.0.1; see R Core Team, 2017). The alpha value for statistical significance was set to 0.05, and this value was Bonferroni-corrected in case of multiple comparisons (exact value of alpha specified with the results of the tests). To compare the overall performance across conditions and trial block repetitions, we examined the average displacement error, movement duration and maximum absolute steering wheel angle across trials within a block using a two-way repeated-measures ANOVA with condition (white noise, random walk, and constant gain) and trial block number (first, second, and third repetition) as within-subject factors using the ez-package in R (v.4.4-0; see Lawrence, 2016). The results were adjusted according to the Greenhouse-Geisser correction in case of violations of sphericity, and we report the generalized eta-squared  $(\eta_G^2)$  as a measure of the effect size. To examine the responses to the step changes in the gain across conditions, we averaged the displacement error, movement duration and maximum absolute steering wheel angle on the baseline trial and the step trials across trial blocks within a condition and examined differences between the trials and conditions using a two-way repeated-measures ANOVA with condition (white noise, random walk, and constant gain) and trial (baseline and first, second, third, and fourth step trial) as within-subject factors. We used paired-samples t-tests to directly compare the groups post hoc. To compare the results of the regression fits across the white noise and random walk condition, we averaged the regression coefficients across trial blocks within a condition and compared the values of the regression coefficients across the two conditions at each time point with a paired-samples t-test in MATLAB.

#### 4.3 **Results**

We used a closed-loop steering experiment in which participants steered a linear sled to align their body with a memorized visual target. We varied the steering gain in three different ways, and examined whether participants took the predictability of the gain into account in their steering behavior (internal model hypothesis) or whether participants simply integrated the vestibular information over time (path integration hypothesis).

#### 4.3.1 General observations

Figure 4.2A shows the average displacement error across participants as a function of trial number for each of the three conditions. Participants hit the target on average in 75% of trials (range 66-90%). The average displacement error was close to zero in all three conditions (white noise: M = 0.25 cm, SD = 1.12 cm; random walk: M = 0.03 cm, SD = 1.06 cm; constant gain: M = 0.30 cm, SD = 1.12 cm) and in all three trial blocks within a condition (first repetition: M = 0.18 cm, SD = 1.22 cm; second repetition: M = 0.32 cm, SD = 1.05 cm; third repetition: M = 0.09 cm, SD = 1.02 cm). In line, the overall displacement error did not differ significantly across the conditions ( $F_{246} = 1.23$ , p = .301,  $\eta_G^2 = .011$ ) or across the three trial blocks within a condition ( $F_{2.46} = 1.58$ , p = .218,  $\eta_G^2 = .008$ ). Additionally, there was no significant interaction effect between the condition and the trial block number ( $F_{4.92}$  = 1.02, p =.401,  $\eta_G^2$ =.011). The included participants were thus able to hit the target in most trials.

Figure 4.2B shows the average movement duration in the same format as in Figure 4.2A. On average, participants finished their steering movement within the imposed time window from 800 to 1200 ms in all three conditions (white noise: M = 970 ms, SD = 97 ms; random walk: M = 994 ms, SD = 108 ms; constant gain: M = 972 ms, SD = 86 ms) and in all three trial blocks (first repetition: M = 987 ms, SD = 101 ms; second repetition: M = 974 ms, SD = 99 ms; third repetition: M = 975 ms, SD = 93 ms). There was no significant difference in the overall movement duration across conditions ( $F_{1.61,36.95}$  = 1.78, p = .188,  $\eta_G^2 = .012$ ) or trial blocks ( $F_{266} = 1.32$ , p = .277,  $\eta_G^2 = .004$ ). Additionally, there was no significant interaction effect between the condition and the trial block number ( $F_{492} = 1.32, p = .268, \eta_G^2 = .004$ ).

Figure 4.2C shows the average maximum absolute steering wheel angle in the same format as in Figure 4.2A. The average maximum absolute steering wheel angle was similar across conditions (white noise: M = 46.7 deg, SD = 7.0 deg;

random walk: M=44.9 deg, SD=6.9 deg; constant gain: M=45.7 deg, SD=7.0 deg) and repetitions (first repetition: M=45.4 deg, SD=7.1 deg; second repetition: M=46.2 deg, SD=7.0 deg; third repetition: M=45.7 deg, SD=6.9 deg). In line, the maximum absolute steering wheel angle was not significantly affected by the condition ( $F_{2,46}=2.13$ , p=.130,  $\eta_G^2=.011$ ) or the trial block number ( $F_{1.48,33.96}=1.23$ , p=.294,  $\eta_G^2=.003$ ), nor was there an interaction effect ( $F_{2.93,67.38}=1.14$ , p=.338,  $\eta_G^2=.002$ ).

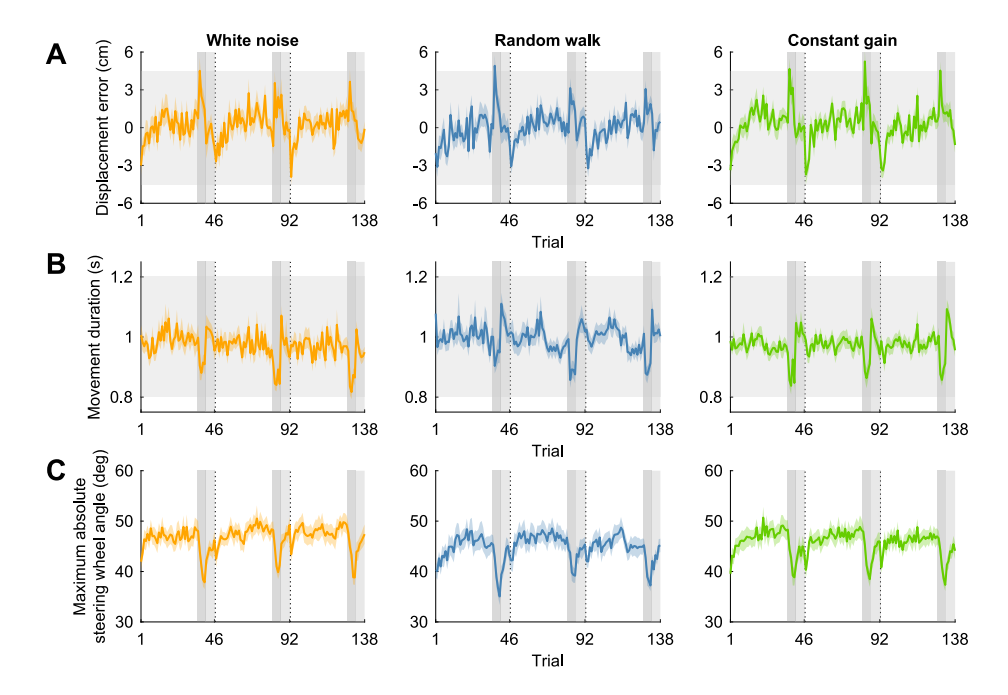
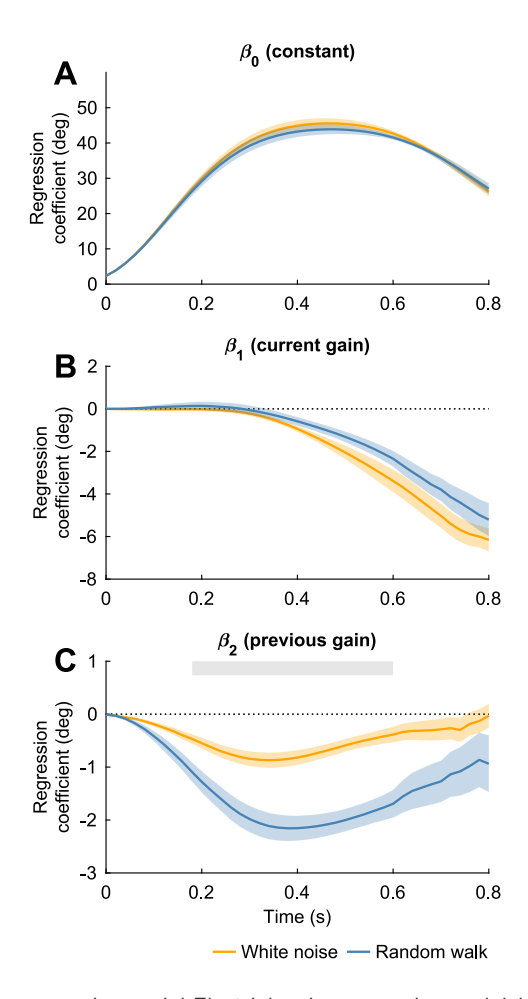


Figure 4.2. Displacement error, movement duration and maximum absolute steering wheel angle. A) Mean displacement error across participants as a function of trial number grouped based on the experimental condition (panels). Negative numbers represent undershoots; positive numbers represent overshoots. Colored shaded areas represent between-subjects means  $\pm$  SE. Participants completed three trial blocks per condition in sequence and the conditions were presented in a random order per participant. Each trial block was concluded with a baseline trial, followed by four step trials with a high gain (dark gray vertical areas) and six washout trials with the baseline gain (light gray vertical areas). Dashed vertical lines represent breaks and horizontal light gray bands show the range of displacement errors within which participants "hit" the target. B) Same configuration as in A, but with the mean movement duration across participants. Horizontal light gray bands show the time window within which participants were encouraged to finish their steering movement. C) Same configuration as in A, but with the mean maximum absolute steering wheel angle across participants.



**Figure 4.3.** Trial series regression model. The trial series regression model described the steering wheel angle as a function of a constant, the gain on the current trial, and the gain on the previous trial. A) Mean value of the regression coefficient representing the constant across trial blocks and participants as a function of time grouped based on experimental condition (colored lines). Values represent the average steering wheel angle as a function of time across the condition-specific trials within a trial block. Colored shaded areas represent between-subjects means  $\pm$  SE. B) Same configuration as in A, but with the mean value of the regression coefficient of the current gain across trial blocks and participants. Negative regression coefficients indicate that participants decreased and increased the steering wheel angle with an increase and decrease in the gain relative to the mean, respectively. C) Same configuration as in A, but with the mean value of the regression coefficient of the previous gain across trial blocks and participants. The regression coefficient differed significantly between the conditions from 180 to 600 ms after movement onset, as also indicated by the light gray shaded horizontal area (p < .0012).

## 4.3.2 Trial series regression analysis

These findings suggest that, overall, the steering behavior was similar across conditions and trial blocks. However, in the white noise and random walk condition, the steering gain varied from trial to trial and across participants. Averaging across trials within a trial block and across participants could therefore mask effects of the gain on the steering behavior at the single-trial level. To examine the relationship between the gain and the steering behavior at the single-trial level we fitted a trial series regression model (see Methods). Using this approach, we describe for each condition-specific trial of the white noise and random walk condition the steering wheel angle at a certain point in time as a function of the gain on the current trial, the gain on the previous trial, and a constant (or offset). Figure 4.3 shows the results of the regression model. The regression coefficient representing the constant as a function of time follows the average steering wheel profile (Fig. 4.3A). The constant did not differ significantly across the two conditions (smallest p-value: p = .113 at 560 ms after movement onset; Bonferroni-corrected  $\alpha = .0012$ ).

Figure 4.3B shows the regression coefficient for the current gain, which was zero at the beginning of the steering movement and started to decrease after approximately 300 ms in the white noise condition (significantly different from zero from 340 to 800 ms after movement onset; range p-values from p = .0008to p < .0001; Bonferroni-corrected  $\alpha$  = .0012) as well as in the random walk condition (significantly different from zero from 440 to 800 ms after movement onset; range p-values from p = .0004 to p < .0001; Bonferroni-corrected  $\alpha$  =.0012). Negative regression coefficients indicate that participants decreased the steering wheel angle with an increase in the gain relative to the mean gain and vice versa. Participants thus reacted adequately to changes in the gain from trial to trial by steering against the gain change midway the steering movement. The regression coefficient for the current gain did not differ across the two conditions (smallest p-value: p = .0074 at 540 ms after movement onset: Bonferroni-corrected  $\alpha = .0012$ ).

Figure 4.3C shows the regression coefficient for the previous gain, which decreased almost immediately after movement onset and started increasing again after approximately 400 ms in both conditions. The regression coefficient differed significantly from zero from 40 to 540 ms in the white noise condition (range p-values from p = .0011 to p < .0001; Bonferroni-corrected  $\alpha = .0012$ ), and from 80 to 660 ms in the random walk condition (range p-values from p = .0009 to p < .0001; Bonferroni-corrected  $\alpha = .0012$ ). The effect was small

in the white noise condition, as expected. The regression coefficient was significantly more negative in the random walk condition than in the white noise condition (significant from 180 to 600 ms after movement onset; range p-values from p = .0012 to p < .0001; Bonferroni-corrected  $\alpha = .0012$ ), indicating that the effect of the previous gain on the steering wheel angle was larger in the random walk condition. This is in line with the internal model hypothesis, as it is more advantageous to take the previous gain into account in the random walk condition because it is more predictive of the current gain due to the high autocorrelation.

## 4.3.3 Step trial analysis

To examine whether these differences in the steering strategy across the conditions were also directly visible in the steering behavior after larger jumps in the gain, we added four step trials with a high gain of 1.4 cm/s per deg to the end of each trial block. All step trials were preceded by a baseline trial and were followed by six washout trials, all with a gain of 1.0 cm/s per deg.

Figure 4.4 shows the displacement error, movement duration and maximum absolute steering wheel angle for the baseline and step trials, grouped based on the condition and averaged across trial blocks and participants. To examine participants' responses to the step changes in the gain, we compared the baseline trial and the step trials across conditions. In all conditions, the average displacement error on the first step trial was positive and larger than the average displacement error on the baseline trial (Fig. 4.4A). There was a significant main effect of the trial on the displacement error ( $F_{4.92} = 18.27$ , p < .001,  $\eta_G^2$  = .205), and post hoc paired-samples t-tests revealed that there was a significant difference between the baseline trial and all four step trials (range p-values from p = .002 to p < .0001; Bonferroni-corrected  $\alpha = .005$ ), and between the first step trial and the subsequent step trials (all p-values <.0001; Bonferroni-corrected  $\alpha$  =.005). There was no significant main effect of the condition on the displacement error ( $F_{2.46}$  = 0.83, p =.444,  $\eta_G^2$  =.006), or a significant interaction effect ( $F_{8.184} = 0.41$ , p = .912,  $\eta_G^2 = .007$ ). However, in all three conditions the overshoot of the target location on the first step trial was smaller than 12 cm, which is the displacement error that would be expected if participants did not respond to the increase in the gain (target distance of 30 cm and gain increase from 1.0 cm/s per deg to 1.4 cm/s per deg). This suggests that participants changed their steering movement online during the first step trial to compensate for the increase in the gain in all three conditions.

This is confirmed by changes in the movement duration (Fig. 4.4B) and maximum absolute steering wheel angle (Fig. 4.4C) from the baseline trial to the step trials. The movement duration differed significantly across trials in all conditions ( $F_{4.92}$  = 30.57, p <.001,  $\eta_G^2$  =.122), with significantly shorter movement durations on the step trials than on the baseline trial (all p-values <.0001; Bonferroni-corrected  $\alpha$  =.005). Interestingly, the movement duration increased again across the step trials, with significantly longer movement durations on the third step trial than on the first and second step trials (range p-values from p = .0001 to p < .0001; Bonferroni-corrected  $\alpha = .005$ ). There was no significant main effect of the condition on the movement duration ( $F_{2,46} = 1.89$ , p =.162,  $\eta_G^2$  =.019), or an interaction effect (F\_{8,184} = 0.75, p =.644,  $\eta_G^2$  =.004). Similarly, the maximum absolute steering wheel angle differed significantly across trials in all conditions ( $F_{L92}$  = 92.17, p <.001,  $\eta_G^2$  =.205), with a significantly larger maximum absolute steering wheel angle on the baseline trial than on all four step trials (all p-values <.001; Bonferroni-corrected  $\alpha$ =.005). The maximum absolute steering wheel angle continued to decrease significantly across the first three step trials (all p-values <.001; Bonferronicorrected  $\alpha = .005$ ). There was no significant main effect of the condition on the maximum absolute steering wheel angle ( $F_{2.46} = 3.01$ , p = .059,  $\eta_G^2 = .020$ ), or an interaction effect between the trial and the condition ( $F_{8,186} = 0.79$ , p = .611,  $\eta_G^2$  = .003). Participants seemed to fine-tune their steering behavior after the large jump in the gain by increasing the movement duration again slightly and continuing to decrease the maximum absolute steering wheel angle across the step trials, thereby minimizing the displacement error while simultaneously adhering to the imposed time window.

The similarity in the correction across conditions and the fine-tuning of the steering behavior across the step trials is also shown in Figure 4.5. In this figure, the steering wheel angle as a function of time is normalized relative to the baseline trials. For each participant and trial block, we first resampled the steering wheel angles of the baseline and the four step trials to 200 samples per trial using linear interpolation. The movement duration and steering wheel angles on these trials were then normalized by dividing them by the movement duration and the maximum absolute steering wheel angle of the corresponding baseline trial, respectively. Normalized steering wheel angles were averaged across trial blocks and participants, and a corresponding linearly spaced time vector of 200 samples was created for each trial running from zero, representing movement onset, to the mean normalized movement duration across trial blocks and participants.

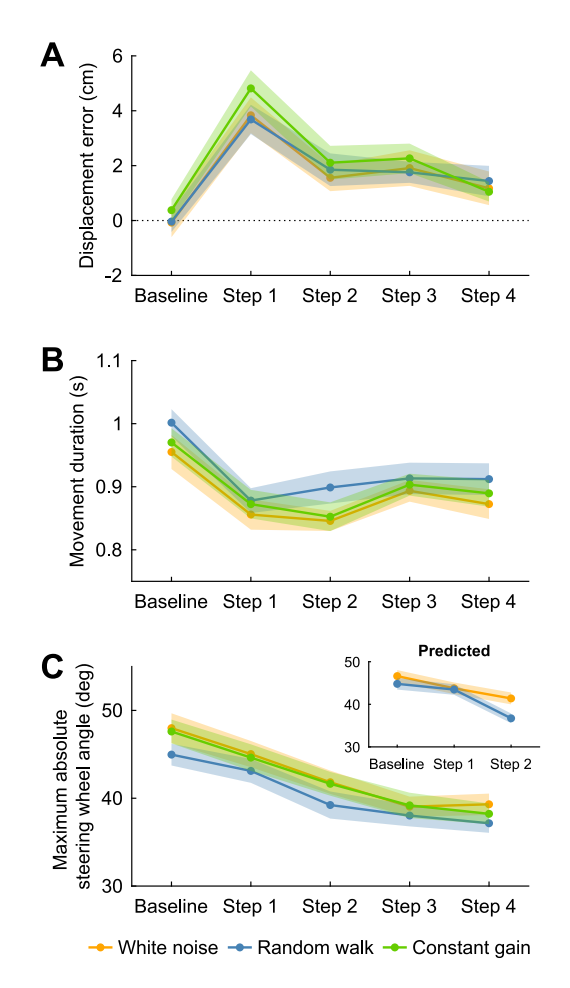


Figure 4.4. Displacement error, movement duration and maximum absolute steering wheel angle on baseline and step trials. A) Mean displacement error across trial blocks and participants as a function of the trial grouped based on the experimental condition (colored lines). Negative numbers represent undershoots; positive numbers represent overshoots. Colored shaded areas represent between-subjects means ± SE. B) Same configuration as in A, but with the mean movement duration across trial blocks and participants. C) Same configuration as in A, but with the mean maximum absolute steering wheel angle across trial blocks and participants. Inset shows the maximum absolute steering wheel angles for the baseline and first and second step trials of the white noise and random walk conditions, predicted based on the results of the trial series regression model.

As described above, participants decreased both the movement duration and the maximum absolute steering wheel angle in response to the increase in the gain from the baseline to the first step trial. They did this already early on within the first step trial. Even though the responses to the higher gain are similar across conditions, the decrease in the maximum absolute steering wheel angle

from the baseline trial to the first step trial seems to be slightly smaller in the random walk condition, as also shown in Figure 4.4C. Participants continued to decrease the maximum absolute steering wheel angle across the subsequent step trials, while slightly increasing the movement duration again towards the baseline movement duration.

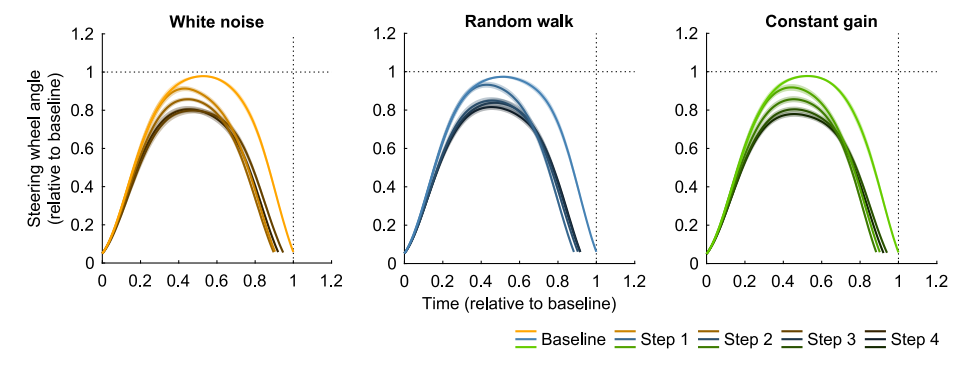


Figure 4.5. Steering behavior on the baseline and step trials. Average absolute steering wheel angle as a function of time across trial blocks and participants for the baseline and step trials grouped based on the experimental condition (panels). Values were normalized relative to baseline. Colored shaded areas represent between-subjects means  $\pm$  SE.

Based on the results of the regression model fitted to the condition-specific trials, we made predictions for the steering wheel angle as a function of time for the baseline and the first two step trials in the white noise and random walk condition. Figure 4.6A shows the mean experimentally observed absolute steering wheel angles as a function of time for the baseline and the first two step trials. These steering wheel profiles are the same as the profiles shown in Figure 4.5, but without the baseline normalization. Overall, the steering wheel angles were slightly smaller in the random walk condition than in the white noise condition, and this difference is accurately predicted based on the regression model, as shown in the right panel in Figure 4.6A.

We could additionally separate the effects of the current and the previous gain on the changes in the steering wheel profiles across the baseline and the first two step trials. Figure 4.6B shows the products of the regression coefficients for the current and the previous gain and the z-scored gains as a function of time for each of the three trials. For the baseline trials, the z-scored current gain was close to zero, as the gain on the baseline trial was always 1.0 cm/s per deg and the mean gain across the condition-specific trials within a trial block was set to be close to the baseline gain. Additionally, since the gain on the trial before the

4

baseline trial varied across trial blocks and participants, the average contribution of the previous gain is also close to zero for the baseline trial. The steering wheel angle as a function of time on this trial was thus similar to the constant in the regression model, representing the average steering wheel angle as a function of time across the condition-specific trials within the trial block.

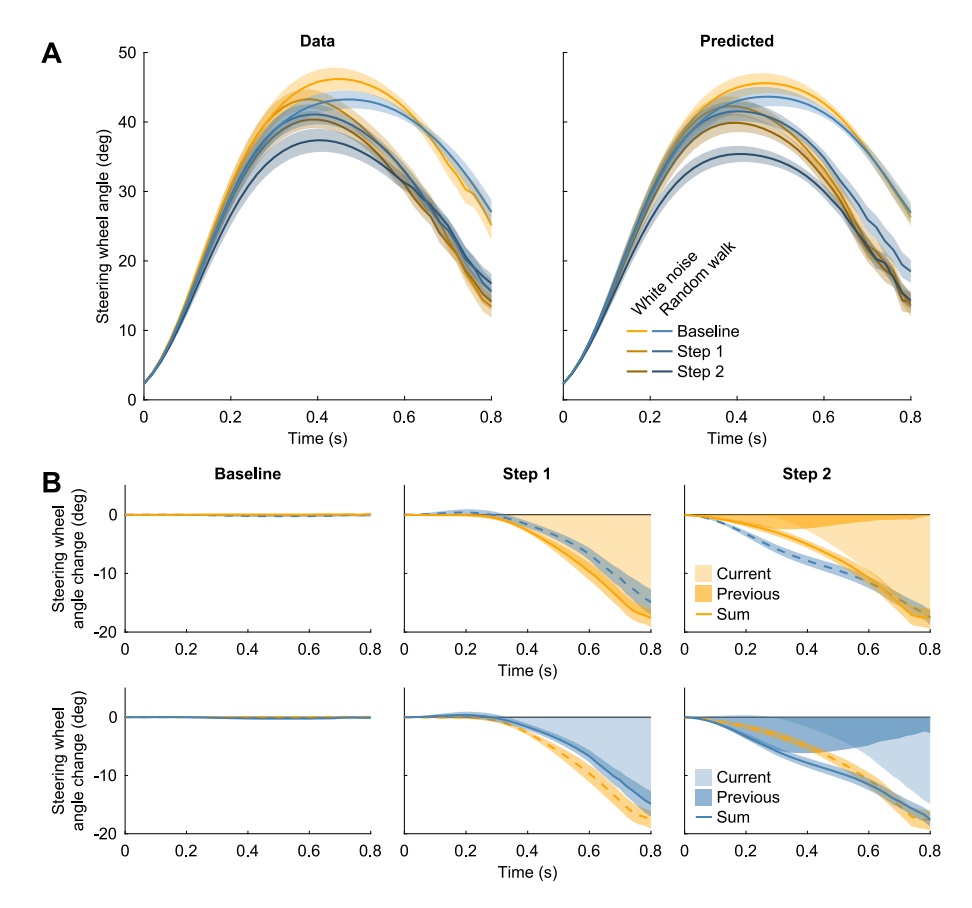


**Figure 4.6.** Predicted steering behavior on the baseline and step trials, based on the trial series regression model. A) Mean absolute steering wheel angle as a function of time across trial blocks and participants for the baseline and the first two step trials in the white noise and random walk conditions (left panel), and the predicted values based on the regression coefficients of the regression model (right panel). Steering wheel angles were predicted for the baseline trial and the first two step trials, per trial block and participant. Colored shaded areas represent between-subjects means  $\pm$  SE. B) Mean predicted change in the steering wheel angle relative to the average steering wheel profile, represented by the constant of the regression model, based on the current and previous gain (shaded areas) as well as the sum (solid colored lines, colored shaded areas represent between-subjects means  $\pm$  SE) for the baseline and the first two step trials (horizontal panels) of the white noise and random walk conditions (upper and lower panels, respectively) across trial blocks and participants. Dashed colored lines show the sum of the predicted change in the same trial for the other condition as a reference line.

On the first step trial, the effect of the gain experienced on the previous trial, the baseline trial, on the steering wheel angle is again very close to zero. The effect of the gain on the current trial is however large in both conditions. The predicted change in the steering wheel angle relative to the average angle is slightly greater in the white noise condition due to the slightly more negative value for regression coefficient  $\beta_{11}$  as shown in Figure 4.3B. On the second step trial, there is an effect of the gain on both the previous and the current trial on the steering wheel angle. In the random walk condition, the effect of the previous gain is larger than in the white noise condition due to a significantly more negative value for regression coefficient  $\beta_{2}$  as shown in Figure 4.3C. This leads to a greater overall reduction in the steering wheel angle over time relative to the mean angle, starting rather early on in the movement. This can also be observed, albeit a little less pronounced, from the greater reduction in the maximum absolute steering wheel angle in the random walk condition from the first to the second step trial in Figure 4.4C (see the inset for the predicted maximum absolute steering wheel angle), and the greater difference between the steering wheel profiles of the first and the second step trial in the random walk condition in Figure 4.5. Hence, there are differences in the steering behavior across the white noise and random walk conditions, which can be mainly observed on the second step trial, due to different effects of the gain on the previous and current trial on the steering wheel angle.

# 4.4 Discussion

In this study, participants used a steering wheel to move their body to a memorized visual target location. They were exposed to three experimental conditions, in which the gain between the steering wheel angle and the velocity of the linear motion platform varied with different levels of predictability from one trial to the next. In the white noise condition, the steering gain varied randomly from trial to trial (i.e., not predictable), in the random walk condition it was moderately predictable, and in the constant gain condition it remained constant across trials (i.e., highly predictable). The goal was to examine whether participants took the predictability of the gain into account in their steering behavior, by forming and relying on an internal model of the steering dynamics, or whether they simply relied on the vestibular feedback in their steering, as in path integration.

Using a trial series regression analysis, we have shown that participants used a different steering strategy for the white noise and random walk conditions

(Fig. 4.3). The average steering wheel angle and the regression coefficient for the current gain were similar across conditions throughout the trial, but the regression coefficient for the previous gain was significantly more negative in the random walk condition from 180 to 600 ms after movement onset. This suggests that participants decreased the steering wheel angle more in the random walk condition than in the white noise condition if the gain on the previous trial was higher than the average gain, and vice versa. Based on the results of the regression model, we also predicted the subtle differences between the white noise and random walk condition in the changes in the steering behavior from the baseline to step trials, in which the gain was suddenly higher for four consecutive trials (Fig. 4.6). Participants thus took the previous gain into account in the random walk condition, which is a useful strategy given the high autocorrelation in the gains. We conclude that participants formed an internal representation of the steering dynamics, which is in line with the internal model hypothesis.

In all conditions, including the constant gain condition, participants decreased the maximum absolute steering wheel angle and the movement duration on the first step trial. Across the subsequent step trials (Fig. 4.5), participants improved their adaptation to the new steering dynamics by simultaneously increasing the movement duration and decreasing the maximum absolute steering wheel angle to adhere to the time window imposed in the experiment, similar as in van Helvert et al. (2022). These tactful changes in the steering behavior underline the idea that participants built and updated an internal model of the steering dynamics and the associated self-motion based on the vestibular feedback. In principle, we could have also predicted the steering behavior on the third and fourth step trial based on the fitted regression model. For these trials, both the gain on the current and the previous trial would be the same as for the second step trial, and the prediction would thus be that the steering behavior remains the same across these three trials. Even though the changes in the steering behavior are relatively small across these step trials, see for example Figure 4.4 and 4.5, it seems plausible that participants revised their steering strategy on these trials, given that the dynamics on the step trials were different from the dynamics experienced during the condition-specific trials.

In our previous study (van Helvert et al., 2022), participants performed a similar steering experiment but the steering gain changed only twice during the whole experiment, comparable with the constant gain condition in the current experiment. We found that participants responded rapidly to these changes in the steering dynamics, suggesting that participants had some expectations about their velocity and the steering dynamics, but we could not further distinguish between the internal model hypothesis and the path integration hypothesis. Here, we dissociate the contribution of vestibular feedback and predictions by changing the steering dynamics across trials with different levels of predictability. We show that participants use the vestibular feedback during the trial to estimate their self-motion, but also that their steering behavior depends on the predictability of the steering gain. Important to note, this conclusion is based mainly on the results of the regression model. in which the data from the constant gain condition could not be included. Due to the high predictability of the steering gain, we expected participants to respond slowest on the step trials in the constant gain condition, but the data did not support this notion. To study steering behavior with a high predictability of the steering gain, future studies could include white noise and random walk conditions with varying levels of variability, similar to Burge et al. (2008) who studied the trade-off between prediction and estimation based on sensory feedback in reach adaptation.

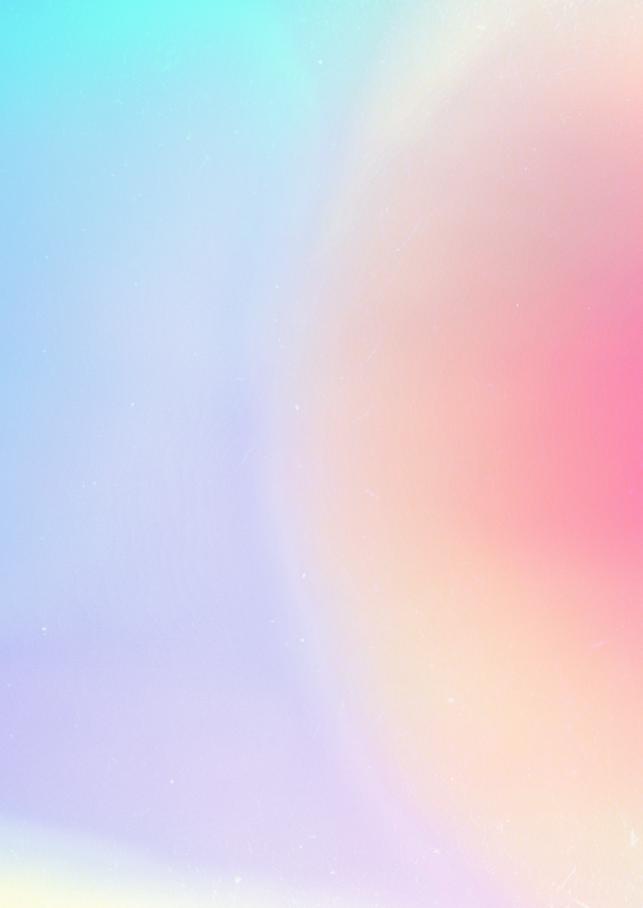
Stavropoulos et al. (2022) also used a closed-loop steering experiment to study the role of vestibular feedback and predictions in self-motion estimation. Participants used a joystick to navigate to a target while the steering dynamics changed from trial to trial following a bounded random walk. They found that the steering behavior was biased with responsive steering control and concluded that participants were not able to accurately steer and build an internal model of the steering dynamics based on the vestibular feedback alone. Our previous results suggested that participants can accurately estimate their self-motion and suggest that they build an internal model of the steering dynamics based on just vestibular feedback (van Helvert et al., 2022), and here we show that they can even do this under steering dynamics that change from trial to trial. This discrepancy between the results might be explained by the fact that the velocity of the motion platform used by Stavropoulos et al. (2022) was close to constant. This may have made it more difficult for participants to estimate their self-motion, as the vestibular organs and more specifically the otoliths, which process information about translational motion, are known to be mainly sensitive to acceleration (Benson, Spencer, & Stott, 1986; Fernandez & Goldberg, 1976; Fitze, Mast, & Ertl, 2023). Also, participants in our experiments received feedback about their performance at the end of each trial, which is likely to have removed any possible biases in participants' selfmotion estimates.

The present study is based on previous studies of visuomotor and force field adaptation in reaching movements that examined the role of sensory feedback and predictions (Burge et al., 2008; Gonzalez Castro et al., 2014; Wei & Körding, 2010). These studies showed that participants respond faster to perturbations if the mapping between the reaching movement and the sensory feedback is more uncertain, due to a greater reliance on the feedback. Additionally, Gonzalez Castro et al. (2014) examined motor adaptation when the force field perturbation strength varied randomly across trials and when it varied according to a random walk. They showed that participants relied more on predictions of the perturbation in the random walk condition. This is in line with our finding that the effect of the previous gain on the steering behavior is more pronounced in the random walk condition than in the white noise condition.

Our results suggest that participants build an internal model of the steering dynamics to estimate their self-motion during active steering. Multiple studies have looked for neural markers of such an internal model and have tried to unravel its location in the vestibular processing pathway (Egger & Britten, 2013; Jacob & Duffy, 2015; Lakshminarasimhan, Avila, Pitkow, & Angelaki, 2023; Page & Duffy, 2008; Roy & Cullen, 2001). In general, the cerebellum is thought to play an important role in the internal model computations for selfmotion estimation (Brooks et al., 2015; Cullen, 2023; Laurens & Angelaki, 2017; Rineau, Bringoux, Sarrazin, & Berberian, 2023), also because of its projections to the vestibular nuclei. Neurons in the vestibular nuclei are known to distinguish between active and passive self-motion, being less sensitive to actively generated, and thus predictable, self-motion (Cullen et al., 2011). However, these neurons respond similarly to passive selfmotion and self-motion generated by a steering movement (Roy & Cullen, 2001). One explanation for this may be that the monkeys in the experiment were not trained enough to build an internal model of the steering dynamics. Another explanation may be that the cerebellum does not predict the sensory consequences of the steering movement, and that the internal model of the steering movement is located more downstream in the vestibular processing pathway (Alefantis et al., 2022). Similarly, during the processing of the visual reafference of steering movements in monkeys, markers for an internal model were found in the medial superior temporal area (Page & Duffy, 2008) and the posterior parietal cortex (Lakshminarasimhan et al., 2023).

The sensorimotor processes that underlie driving have gained additional interest with the development of automated vehicles (Nash & Cole, 2020; Nash, Cole, & Bigler, 2016). Nash and Cole (2016) have described these sensorimotor processes in detail, and have shown that a driver model that includes an internal model of the mapping between the steering wheel angle and the sensory feedback accurately describes human steering behavior in their experimental set up (Nash & Cole, 2020). Our results are in line with these findings. Based on the predictions of such an internal model, feedforward control actions can be made, which can be extremely important in driving given the delays in the sensorimotor system (Nash et al., 2016). Along these lines, the present results may also stimulate novel concepts for artificial navigation systems, e.g., those providing independent mobility to sensory-deprived people and vehicle control.

In conclusion, our results show that participants take the predictability of changes in the steering dynamics into account during driving. This suggests that participants build an internal model of the gain between the steering wheel angle and their self-motion, and use this model to predict the vestibular reafference in driving and self-motion estimation.



# Chapter 5

# General discussion

Natural environments are continuously changing and full of action opportunities. Yet, we seem to effortlessly move around and interact with objects in the environment in daily life. In this thesis, I aimed to unravel how the central nervous system so smoothly selects and controls our movements in rich and dynamic environments. In **Chapter 2**, I investigated the neural processes underlying action selection and movement planning by examining hand choice. In **Chapter 3 and 4**, I focused on the computational processes for online movement control, examining the role of vestibular sensory feedback and predictions in the control of self-motion during steering. In this chapter, I will summarize and discuss these findings. I will additionally consider their broader implications for sensorimotor control and make suggestions for future research.

# 5.1 Action selection and movement planning

In **Chapter 2**, I focused on the neural processes underlying hand selection and reach planning. In 2005, Cisek and Kalaska reported that the neural activity in the motor cortex of nonhuman primates simultaneously represents multiple potential reach targets before the actual target is specified. This was taken to suggest that the brain prepares multiple movement plans in parallel, while they compete for selection and execution. Whether this idea of competition and parallel planning also applies to the selection of left and right hand reaches has been a topic of debate (Bernier et al., 2012; Oliveira et al., 2010).

To examine whether deciding between using the left or right hand in a reach leads to the specification of parallel movement plans that compete for execution, participants were asked to perform a hand choice reaching task while recording the activity of groups of neurons in central cortical regions using electroencephalography (EEG; see Box 1 in **Chapter 1**). To be able to measure the neural activity during reach planning, the location of the reach target was announced by a cue presented 1000 to 1500 ms before the actual target. The cue additionally indicated whether participants were supposed to reach with the hand of their choice, or whether they had to use the left or right hand. Reach reaction times were longer when participants were free to choose which hand to use compared to when the reaching hand was instructed by the cue. This supports the notion of a competitive process for hand selection. Additionally, the power of neural oscillations in the beta band during movement preparation decreased less when participants had to choose which

hand to use compared to when the hand was predetermined. Lower levels of beta-band power have been associated with a readiness to move (Khanna & Carmena, 2017), and these results therefore suggest that participants were less prepared to move when they had to choose which hand to use. I conclude that hand choice is governed by a competitive process between movement plans for the left and right hand, and that this competitive process modulates beta-band power during reach planning.

Surprisingly, I did not find an effect of the location of the reach target on reaction times and beta-band power. I expected the competition between movement plans for the left and right hand to be highest for reaches to the target location for which participants have an equal probability of using the left and the right hand (the point of subjective equality or PSE). This lack of an effect of the target location could be explained by the fact that the location of the upcoming target was cued incorrectly in half of the trials. These incorrect cues were introduced to be able to demonstrate that participants started preparing the movement before target onset, and thus that the neural activity before target onset was related to reach planning. However, it might have resulted in participants not fully committing to preparing a movement with a single hand during the cueing phase.

#### 5.1.1 Serial and parallel processing

While these results are in line with the idea that movement plans for the left and right hand are prepared in parallel and compete for execution, the idea of parallel processing is not undebated. Dekleva et al. (2018) recorded activity from neurons in the motor cortex while monkeys prepared reaching movements towards two potential targets. They replicated the trial-averaged findings of Cisek and Kalaska (2005), showing that the neuronal activity represents both targets before the actual reach target is specified. However, an additional analysis showed that the activity at the level of a single trial only represents a single reach plan. This can be taken to suggest that the brain processes information in a serial manner and decides on the action to execute before planning the action, instead of preparing multiple potential action plans in parallel.

Similar to the results described by Cisek and Kalaska (2005), my results are based on data that were averaged across trials. Unfortunately, the signal-tonoise ratio of my data was too low to investigate the neural oscillations at the single-trial level. To assess whether beta-band power during reach preparation represents movement plans for a single hand or both hands at the single-trial level, future studies could try to improve the signal-to-noise ratio of the data, for example by applying more sophisticated artifact removal techniques or by reducing muscle artifacts introduced by the reaching movements. The latter could perhaps be achieved by reducing the distance between the start positions of the hands and the reach targets. In my experiment, this distance was approximately 30 cm. Reducing the size of the reaching movement might make it more likely that the motion remains confined within the arms and hands. Additionally, if the signal-to-noise ratio is sufficiently high to analyze the betaband power at the single-trial level, it may be possible to associate it with the behavior demonstrated during the trial. For example, a negative correlation between the decrease in beta-band power during reach planning and reach reaction times would strengthen the idea that both reflect competition between left and right hand reach plans during hand choice.

#### 5.1.2 Hand choice during body motion

In general, the decision to reach with the left or right hand is thought to be based on the desirability and the costs of the two options (Shadmehr et al., 2016; Trommershäuser et al., 2009; Wolpert & Landy, 2012). In daily life, we often reach while our body is moving. In this situation, the biomechanical costs of the potential movements depend on the inertial forces exerted on the arms (Cos et al., 2011). Researchers in my lab have previously investigated how hand choice is affected by passive body motion, and found that hand choice is modulated by sinusoidal body motion (Bakker et al., 2019, 2017; Oostwoud Wijdenes et al., 2022). This sinusoidal modulation of choice behavior was also visible in a read-out of the corticospinal excitability (Oostwoud Wijdenes et al., 2022), and might also be visible in beta-band power during reach planning. To examine this in a future study, participants could perform a hand choice experiment during body motion while their neural activity is recorded using EEG. Previous studies have shown that EEG can be reliably recorded during body motion (Gutteling & Medendorp, 2016; Gutteling, Selen, & Medendorp, 2015).

The observation that hand choice and corticospinal excitability are modulated by sinusoidal body motion suggests that participants continuously monitor the sensory feedback about their body motion and take it into account when deciding which hand to use. In **Chapter 3 and 4**, I built upon these studies and examined the role of vestibular feedback, but also predictions of the vestibular feedback, in the online control of movements.

# Online control of movements and motor learning and adaptation

In Chapter 3 and 4, I focused on the online control of movements and examined the role of vestibular feedback and vestibular predictions in self-motion estimation in a closed-loop steering experiment. Of note, our movements can be the result of our own actions, but they can also be passively imposed. During active movements, the sensory consequences of the movement can be predicted by an internal forward model based on efference copies of the motor commands (von Holst & Mittelstaedt, 1950). For self-motion estimation, the computations underlying active and passive movements have been formalized with a single mathematical model (Cullen, 2019; Laurens & Angelaki, 2017). In this model, active self-motion estimates rely both on sensory feedback and predictions, whereas passive self-motion estimates rely on sensory feedback only. However, the model leaves open the possibility that sensory predictions can be made based on motor signals that have an indirect relationship with self-motion cues, such as the motor signals that occur when driving a car. It is unknown whether the brain can also predict the sensory feedback based on such motor signals. In principle, the sensory feedback could be predicted if an accurate internal forward model of the steering dynamics is available.

In Chapter 3, I examined if participants could construct an accurate internal model of the mapping between a steering movement and the vestibular reafference. Participants were asked to translate their body to a memorized visual target using a steering wheel that controlled the velocity of the linear motion platform they were seated on (see Box 2 in **Chapter 1**). They were able to learn to control the motion platform and made fast within-trial changes to their steering behavior in response to unexpected changes in the mapping between the steering wheel angle and the platform velocity. They additionally gradually improved their adaptation to the new control dynamics. I compared their steering behavior to that of participants who remained stationary during the experiment, and thus did not receive any online sensory feedback. These participants responded more slowly to the unexpected changes in the mapping, and I therefore conclude that the online vestibular feedback plays an important role in the online control of the steering movement.

The finding that participants who received online vestibular feedback responded rapidly to the unexpected changes in the mapping between the steering wheel angle and the platform velocity suggests that these participants had expectations about the sensory feedback. This in turn implies that they constructed an internal model of the mapping between the steering movement and the vestibular reafference. However, these results could in principle also be explained in the context of path integration, in which participants keep track of their position by integrating the vestibular feedback over time without taking predictions of the sensory feedback into account (Grasso et al., 1999). In my experiment, participants could have simply stopped the platform motion when their path integration derived position had reached the memorized location of the target, independent of the mapping between the steering wheel angle and the platform velocity.

In **Chapter 4**, I therefore investigated the role of sensory feedback and predictions during steering in more detail. I aimed to manipulate the contribution of sensory feedback and predictions by changing the consistency of the mapping between the steering wheel angle and the platform velocity across trials. I compared three conditions with varying levels of the predictability of the mapping across trials: predictable (constant gain), moderately predictable (random walk), and unpredictable (white noise). Again, as described in Chapter 3, participants made fast within-trial changes to their steering behavior on trials with a large jump in the mapping between the steering wheel angle and the platform velocity irrespective of the predictability of the mapping. This suggests that online vestibular feedback plays an important role in the online control of the steering movement. I additionally found that participants took the mapping between the steering wheel angle and the platform velocity of the previous trial into account more when it followed a random walk across trials than when it varied unpredictably across trials. Given that the autocorrelation in the mapping across trials was relatively high in the random walk condition, this is a useful strategy. I conclude that participants consider the predictability of changes in the control dynamics during steering, which suggests that they construct an internal model to predict the vestibular reafference.

## 5.2.1 Trial series regression analysis

In **Chapter 4**, I show that participants take the previous mapping between the steering movement and their self-motion into account more when the mapping is more predictable across trials. This conclusion is based on the results of a trial series regression analysis, in which the steering wheel angle at a certain time point is modelled as a linear combination of the average steering wheel angle across trials, the mapping on the current trial, the mapping on the previous trial and a residual error. Even though this relatively simple model

could reliably show differences across two of the experimental conditions (moderately predictable and unpredictable mapping), a more complex model could perhaps uncover more subtle differences in the steering behavior across conditions. Such a model could for example take the dependencies between data points within a trial into account (the steering wheel angle at time point t+1 depends on the steering wheel angle at time point t), and could describe in more detail how participants relied on the mapping within and across trials (e.g., how much of what participants learned about the mapping during the trial do they transfer to the next trial?). Additionally, the use of a regression model prohibited us from including the data from one of the experimental conditions due to the constant mapping across trials. Perhaps a more complex model could describe the steering behavior with a constant gain. Alternatively, future studies could use the trial series regression model to compare steering behavior across multiple experimental conditions with a changing mapping across trials but with different levels of variability (i.e., more or less overall spread in the mapping) to examine the effect of the reliability of the mapping on the steering behavior.

#### 5.2.2 Neural correlates of internal models in closed-loop steering experiments

Whether humans and nonhuman primates are able to build an internal model during steering has been a topic of debate (see for example Angelaki & Cullen, 2008; Danz, 2021; Nash & Cole, 2020). Roy and Cullen (2001) recorded neural responses in the vestibular nuclei of monkeys during vestibular self-motion caused by active steering and passive rotations of the body. Neurons in the vestibular nuclei are known to respond to passive movements of the body but show decreased firing during active movements. This neural activity is therefore thought to reflect sensory predictions errors. They found that neural activity during active steering was similar to that observed during passive rotations. This suggests that sensory feedback was not correctly predicted during active steering based on the steering motor commands, and sensory prediction errors remained. Even though the monkeys were able to make accurate steering movements, it has been suggested that the monkeys were not exposed to enough training to build an internal model of the control dynamics of the steering wheel (Angelaki & Cullen, 2008). Perhaps the activity of neurons in the vestibular nuclei would decrease during active steering after more extensive training.

Alternatively, predictions based on motor signals that have an indirect relationship with the sensory feedback might be processed at a more downstream level within the vestibular pathway (Alefantis et al., 2022). Typically, the cerebellum is suggested to house internal models of the motor system (Wolpert, Miall, & Kawato, 1998), and more specifically the internal model for the estimation of active self-motion (Cullen et al., 2011). During visual self-motion in monkeys, neurons in the medial superior temporal area have been shown to respond differently to optic flow cues during active steering and passive viewing (Jacob & Duffy, 2015; Page & Duffy, 2008; but see also Egger & Britten, 2013). Similarly, in humans, Schmitt et al. (2022) found that neural activity at the cortical level recorded with EEG differed between passive viewing of an optic flow stimulus and active reproduction of that same stimulus using a joystick. These differences in neural activity suggest that the visual sensory feedback was predicted during active reproduction based on the motor commands generated during the steering movement, and that these predictions were processed at a relatively downstream level of the visual processing pathway.

To look for a neural correlate of the internal model of the mapping between the steering movement and the sensory feedback during vestibular self-motion, future studies could build upon the experiments described in **Chapter 3 and 4** and use EEG to compare neural activity across conditions that differ in the expected weights on sensory feedback and sensory predictions (e.g., varying levels of predictability of the mapping between the steering movement and the vestibular reafference, or active versus passive self-motion).

## 5.2.3 Reweighting sources of (noisy) information

In **Chapter 4**, I aimed to manipulate the relative contributions of sensory feedback and sensory predictions for online control by changing the steering dynamics across trials. This idea was based on studies in reach adaptation, in which the experimenters changed the reliability of the sensory feedback and the mapping between the reach endpoint and the sensory feedback by blurring the visual feedback and perturbing it with specific statistical regularities, respectively (Burge et al., 2008; Wei & Körding, 2010). A similar approach has been used in a steering experiment in virtual reality in which monkeys and humans used a joystick to steer to a memorized target location using optic flow cues (Alefantis et al., 2022). During the experiment, the reliability of the visual feedback was manipulated by changing the density of the optic flow elements. The reliability of the mapping between the steering movement and the sensory feedback was manipulated by perturbing the optic flow and changing the gain of the joystick.

In the framework of Bayesian inference, the brain is thought to combine information from multiple sources and weigh the information according to its

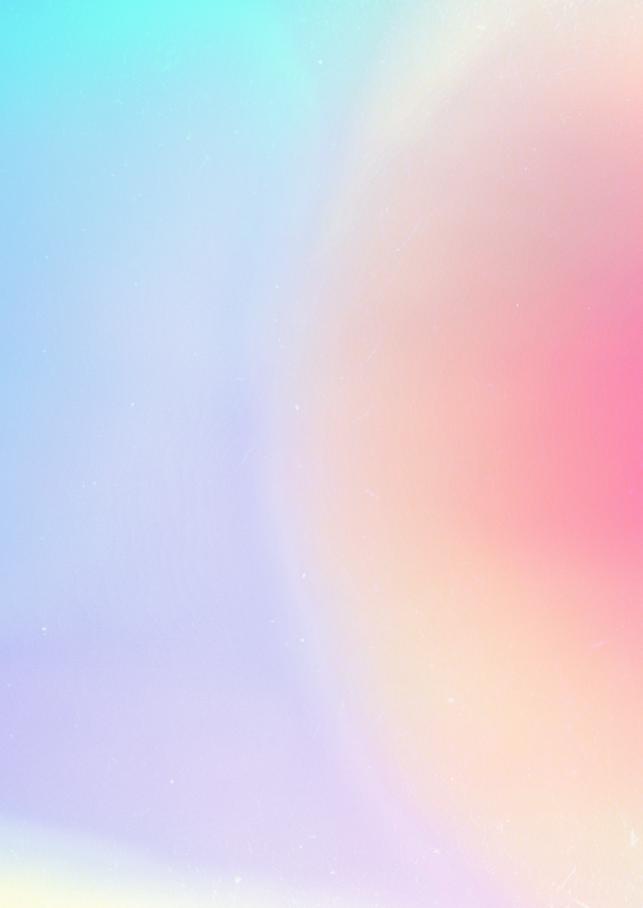
reliability (Körding & Wolpert, 2004). In patients with a sensory deprivation, the reliability of the information from a certain source might be decreased or the information might be missing completely. In such a situation, the brain is thought to build a percept based on the remaining sources of information (Angelaki & Laurens, 2020; Medendorp et al., 2018). Angelaki and Laurens (2020) examined this by training monkeys to report the direction of gravity in a visual orientation task, after which the monkeys underwent surgery that led to a complete vestibular loss. Three weeks after the surgery, the monkeys were able to perform the task almost as well as before the surgery, suggesting that the monkeys learned to use the remaining sources of sensory information to estimate the direction of gravity.

In a pilot study that has not been included in this thesis, I similarly tried to examine the mechanisms of multisensory reweighting in vestibular patients. I was specifically interested to see how patients with a congenital loss of vestibular function weigh the remaining sensory (i.e., visual and somatosensory) and prior information to estimate the direction of gravity. Previously, researchers from my lab have shown that participants who have slowly developed a vestibular impairment rely almost entirely on visual information when estimating the direction of gravity (Alberts, Selen, Verhagen, & Medendorp, 2015; Alberts, Selen, Verhagen, Pennings, & Medendorp, 2018). I tried to generalize these findings to the situation where the participant had never had a functioning vestibular system. Three participants with Usher syndrome (type 1) were asked to perform a rod-and-frame task, during which they indicated whether a line that was briefly flashed inside a square frame was rotated clockwise or counterclockwise relative to the orientation of gravity. I expected them to show a larger effect of the orientation of the square frame on the judged orientation of the line than healthy control participants due to an increased weight on visual information (Alberts et al., 2018). Preliminary results suggest that this is indeed true for two out of the three participants, but further research is needed to confirm this in a larger group. However, building on these experiments, in which the reliability of sources of information is altered (i.e., actively manipulated or due to loss), would be an interesting approach for future research to more elaborately study the role of sensory feedback and predictions in sensorimotor control.

## 5.3 Conclusion

In this thesis, I have studied the processes underlying action selection and movement planning, on the one hand, and the online control of movements, necessitating motor learning and adaptation, on the other hand, as if they are distinct. However, the brain is thought to continuously and parallelly select, plan, execute, control and learn from our actions. To describe these processes, Pezzulo and Cisek (2016) proposed the hierarchical affordance competition theory, which combines the ideas of parallel processing of movement plans and feedback control. More specifically, due to the ability of the brain to predict the consequences of actions, the brain is thought to select and control upcoming actions by taking directly available action opportunities into account, as well as those that might become available during or after execution. This process is continuous and relies heavily on the online sensory feedback, as the potential actions change over time due to changes in the environment and due to our own actions. To enable us to smoothly interact with our environment, the brain is thus thought to continuously define the best upcoming action and to check whether it is executed properly through continuous feedback control.

In summary, in the first part of this thesis I investigated the neural processes underlying action selection and movement planning and showed that reach plans for the left and right hand are prepared in parallel during hand choice and compete for execution. This competition is reflected in neural oscillations over central cortical regions during movement preparation. In the second part of this thesis, I investigated the computational processes for online movement control and demonstrated that both online vestibular feedback and vestibular predictions play an important role in the online control of steering. These vestibular predictions are based on an internal model of the mapping between the steering movement and the self-motion. The results of the present thesis give insight into the processes that underlie the selection and control of our actions in rich and dynamic natural environments.



# **Appendices**

References

**Dutch summary** 

Research data management

About the author

**Donders Graduate School** 

Acknowledgements

## References

- Alberts, B. B. G. T., Selen, L. P. J., Bertolini, G., Straumann, D., Medendorp, W. P., & Tarnutzer, A. (2016). Dissociating vestibular and somatosensory contributions to spatial orientation. *Journal of Neurophysiology*, 116(1), 30–40. https://doi.org/10.1152/jn.00056.2016
- Alberts, B. B. G. T., Selen, L. P. J., Verhagen, W. I. M., & Medendorp, W. P. (2015). Sensory substitution in bilateral vestibular a-reflexic patients. *Physiological Reports*, 3(5), e12385. https://doi.org/10.14814/phy2.12385
- Alberts, B. B. G. T., Selen, L. P. J., Verhagen, W. I. M., Pennings, R. J. E., & Medendorp, W. P. (2018). Bayesian quantification of sensory reweighting in a familial bilateral vestibular disorder (DFNA9). *Journal of Neurophysiology*, 119(3), 1209-1221. https://doi.org/10.1152/jn.00082.2017
- Alefantis, P., Lakshminarasimhan, K. J., Avila, E., Noel, J.-P., Pitkow, X., & Angelaki, D. E. (2022). Sensory evidence accumulation using optic flow in a naturalistic navigation task. *Journal of Neuroscience*, 42(27), 5451–5462. https://doi.org/10.1523/JNEUROSCI.2203-21.2022
- Angelaki, D. E., & Cullen, K. E. (2008). Vestibular system: The many facets of a multimodal sense. *Annual Review of Neuroscience*, 31, 125–150. https://doi.org/10.1146/annurev.neuro.31.060407.125555
- Angelaki, D. E., & Laurens, J. (2020). Time course of sensory substitution for gravity sensing in visual vertical orientation perception following complete vestibular loss. *eNeuro*, 7(4), 1–12. https://doi.org/10.1523/ENEURO.0021-20.2020
- Angelaki, D. E., Shaikh, A. G., Green, A. M., & Dickman, J. D. (2004). Neurons compute internal models of the physical laws of motion. *Nature*, 430(6999), 560–564. https://doi.org/10.1038/nature02754
- Bakeman, R. (2005). Recommended effect size statistics for repeated measures designs. Behavior Research Methods, 37(3), 379–384. https://doi.org/10.3758/BF03192707
- Bakker, R. S., Selen, L. P. J., & Medendorp, W. P. (2018). Reference frames in the decisions of hand choice. *Journal of Neurophysiology*, 119(5), 1809–1817. https://doi.org/10.1152/jn.00738.2017
- Bakker, R. S., Selen, L. P. J., & Medendorp, W. P. (2019). Transformation of vestibular signals for the decisions of hand choice during whole body motion. *Journal of Neurophysiology*, 121(6), 2392-2400. https://doi.org/10.1152/jn.00470.2018
- Bakker, R. S., Weijer, R. H. A., van Beers, R. J., Selen, L. P. J., & Medendorp, W. P. (2017). Decisions in motion: passive body acceleration modulates hand choice. *Journal of Neurophysiology*, 117(6), 2250–2261. https://doi.org/10.1152/jn.00022.2017
- Basso, M. A., & Wurtz, R. H. (1997). Modulation of neuronal activity by target uncertainty. *Nature*, 389(6646), 66–69. https://doi.org/10.1038/37975
- Batcho, C. S., Gagné, M., Bouyer, L. J., Roy, J. S., & Mercier, C. (2016). Impact of online visual feedback on motor acquisition and retention when learning to reach in a force field. *Neuroscience*, 337, 267–275. https://doi.org/10.1016/j.neuroscience.2016.09.020
- Benson, A. J., Spencer, M. B., & Stott, J. (1986). Thresholds for the detection of the direction of whole-body, linear movement in the horizontal plane. *Aviation Space and Environmental Medicine*, 57(11), 1088–1096.
- Bernier, P. M., Cieslak, M., & Grafton, S. T. (2012). Effector selection precedes reach planning in the dorsal parietofrontal cortex. *Journal of Neurophysiology*, 108(1), 57–68. https://doi.org/10.1152/jn.00011.2012

- Blouin, J., Bresciani, J. P., Guillaud, E., & Simoneau, M. (2015). Prediction in the vestibular control of arm movements. *Multisensory Research*, 28(5-6), 487-505. https://doi.org/10.1163/22134808-00002501
- Britten, K. H. (2008). Mechanisms of self-motion perception. *Annual Review of Neuroscience*, 31(1), 389-410. https://doi.org/10.1146/annurev.neuro.29.051605.112953
- Britton, Z., & Arshad, Q. (2019). Vestibular and multi-sensory influences upon self-motion perception and the consequences for human behavior. *Frontiers in Neurology*, 10, 63. https://doi.org/10.3389/fneur.2019.00063
- Brooks, J. X., Carriot, J., & Cullen, K. E. (2015). Learning to expect the unexpected: Rapid updating in primate cerebellum during voluntary self-motion. *Nature Neuroscience*, 18(9), 1310–1317. https://doi.org/10.1038/nn.4077
- Brooks, J. X., & Cullen, K. E. (2019). Predictive sensing: The role of motor signals in sensory processing. *Biological Psychiatry: Cognitive Neuroscience and Neuroimaging*, 4(9), 842–850. https://doi.org/10.1016/j.bpsc.2019.06.003
- Bryden, P. J., Pryde, K. M., & Roy, E. A. (2000). A performance measure of the degree of hand preference. *Brain and Cognition*, 44(3), 402–414. https://doi.org/10.1006/brcg.1999.1201
- Burge, J., Ernst, M. O., & Banks, M. S. (2008). The statistical determinants of adaptation rate in human reaching. *Journal of Vision*, 8(4), 20. https://doi.org/10.1167/8.4.20
- Campos, J. L., & Bülthoff, H. H. (2012). Multimodal integration during self-motion in virtual reality. In *The Neural Bases of Multisensory Processes* (pp. 603–627). Boca Raton: CRC Press/Taylor & Francis. https://doi.org/10.1201/b11092-38
- Campos, J. L., Butler, J. S., & Bülthoff, H. H. (2012). Multisensory integration in the estimation of walked distances. *Experimental Brain Research*, 218(4), 551–565. https://doi.org/10.1007/s00221-012-3048-1
- Carriot, J., Brooks, J. X., & Cullen, K. E. (2013). Multimodal integration of self-motion cues in the vestibular system: Active versus passive translations. *Journal of Neuroscience*, 33(50), 19555–19566. https://doi.org/10.1523/JNEUROSCI.3051-13.2013
- Cheng, Z., & Gu, Y. (2018). Vestibular system and self-motion. *Frontiers in Cellular Neuroscience*, 12, 456. https://doi.org/10.3389/fncel.2018.00456
- Cisek, P. (2006). Integrated neural processes for defining potential actions and deciding between them: A computational model. *Journal of Neuroscience*, 26(38), 9761–9770. https://doi.org/10.1523/JNEUROSCI.5605-05.2006
- Cisek, P. (2007). Cortical mechanisms of action selection: the affordance competition hypothesis. *Philosophical Transactions of the Royal Society B: Biological Sciences*, 362(1485), 1585. https://doi.org/10.1098/RSTB.2007.2054
- Cisek, P., & Kalaska, J. F. (2005). Neural correlates of reaching decisions in dorsal premotor cortex: Specification of multiple direction choices and final selection of action. *Neuron*, 45(5), 801–814. https://doi.org/10.1016/j.neuron.2005.01.027
- Cisek, P., & Kalaska, J. F. (2010). Neural Mechanisms for Interacting with a World Full of Action Choices. *Annual Review of Neuroscience*, 33(1), 269–298. https://doi.org/10.1146/annurev.neuro.051508.135409

- Clemens, I. A. H., De Vrijer, M., Selen, L. P. J., Van Gisbergen, J. A. M., & Medendorp, W. P. (2011). Multisensory processing in spatial orientation: An inverse probabilistic approach. *Journal of Neuroscience*, 31(14), 5365–5377. https://doi.org/10.1523/JNEUROSCI.6472-10.2011
- Cohen, J. (1988). Statistical power analysis for the behavioral sciences (2nd ed.). New York: Routledge.
- Cohen, M. X. (2014a). Advantages and limitations of time- and time-frequency-domain analyses. In *Analyzing neural time series data: Theory and practice* (pp. 15–30). Cambridge, MA: MIT Press.
- Cohen, M. X. (2014b). Interpreting and asking questions about time-frequency results. In *Analyzing neural time series data: Theory and practice* (pp. 31–42). Cambridge, MA: MIT Press.
- Cohen, M. X. (2014c). The discrete time Fourier transform, the FFT, and the convolution theorem. In *Analyzing neural time series data: Theory and practice* (pp. 121–140). Cambridge, MA: MIT Press.
- Cos, I., Bélanger, N., & Cisek, P. (2011). The influence of predicted arm biomechanics on decision making. *Journal of Neurophysiology*, 105(6), 3022–3033. https://doi.org/10.1152/jn.00975.2010
- Crevecoeur, F., Thonnard, J. L., & Lefèvre, P. (2020). A very fast time scale of human motor adaptation: Within movement adjustments of internal representations during reaching. eNeuro, 7(1). https://doi.org/10.1523/ENEURO.0149-19.2019
- Cui, H., & Andersen, R. A. (2011). Different representations of potential and selected motor plans by distinct parietal areas. *Journal of Neuroscience*, 31(49), 18130–18136. https://doi.org/10.1523/JNEUROSCI.6247-10.2011
- Cullen, K. E. (2012). The vestibular system: multimodal integration and encoding of self-motion for motor control. *Trends in Neurosciences*, *35*, 185–196. https://doi.org/10.1016/j. tins.2011.12.001
- Cullen, K. E. (2019). Vestibular processing during natural self-motion: Implications for perception and action. Nature Reviews Neuroscience, 20(6), 346-363. https://doi. org/10.1038/s41583-019-0153-1
- Cullen, K. E. (2023). Internal models of self-motion: Neural computations by the vestibular cerebellum. *Trends in Neurosciences*. https://doi.org/10.1016/J.TINS.2023.08.009
- Cullen, K. E., Brooks, J. X., Jamali, M., Carriot, J., & Massot, C. (2011). Internal models of self-motion: Computations that suppress vestibular reafference in early vestibular processing. Experimental Brain Research, 210, 377–388. https://doi.org/10.1007/s00221-011-2555-9
- Dadarlat, M. C., O'Doherty, J. E., & Sabes, P. N. (2015). A learning-based approach to artificial sensory feedback leads to optimal integration. *Nature Neuroscience*, 18(1), 138-144. https://doi.org/10.1038/nn.3883
- Dancause, N., & Schieber, M. H. (2010). The impact of head direction on lateralized choices of target and hand. *Experimental Brain Research*, 201(4), 821-835. https://doi.org/10.1007/s00221-009-2097-6
- Danz, A. D. (2021). Predictive steering control and neural representation of heading in macaques. University of Rochester.
- de Winkel, K. N., Soyka, F., Barnett-Cowan, M., Bülthoff, H. H., Groen, E. L., & Werkhoven, P. J. (2013). Integration of visual and inertial cues in the perception of angular self-motion. Experimental Brain Research, 231(2), 209-218. https://doi.org/10.1007/s00221-013-3683-1
- DeAngelis, G., & Angelaki, D. (2011). Visual-vestibular integration for self-motion perception. In M. M. Murray & M. T. Wallace (Eds.), *The Neural Bases of Multisensory Processes* (pp. 629-650). CRC Press/Taylor & Francis. https://doi.org/10.1201/9781439812174-39

- Dekleva, B. M., Kording, K. P., & Miller, L. E. (2018). Single reach plans in dorsal premotor cortex during a two-target task. *Nature Communications*, 9(1), 1–12. https://doi.org/10.1038/s41467-018-05959-y
- Dokka, K., MacNeilage, P. R., DeAngelis, G. C., & Angelaki, D. E. (2011). Estimating distance during self-motion: A role for visual-vestibular interactions. *Journal of Vision*, 11(13), 2-2. https://doi.org/10.1167/11.13.2
- Donders, F. C. (1869/1969). On the speed of mental processes. *Acta Psychologica*, 30(C), 412–431. https://doi.org/10.1016/0001-6918(69)90065-1
- Dufour, B., Thénault, F., & Bernier, P. M. (2018). Theta-band EEG activity over sensorimotor regions is modulated by expected visual reafferent feedback during reach planning. *Neuroscience*, 385, 47-58. https://doi.org/10.1016/j.neuroscience.2018.06.005
- Egger, S. W., & Britten, K. H. (2013). Linking sensory neurons to visually guided behavior: Relating MST activity to steering in a virtual environment. *Visual Neuroscience*, 30(5-6), 315-330. https://doi.org/10.1017/S0952523813000412
- Fernandez, C., & Goldberg, J. M. (1976). Physiology of peripheral neurons innervating otolith organs of the squirrel monkey. III. Response dynamics. *Journal of Neurophysiology*, 39(5), 996–1008. https://doi.org/10.1152/jn.1976.39.5.996
- Fetsch, C. R., Turner, A. H., DeAngelis, G. C., & Angelaki, D. E. (2009). Dynamic reweighting of visual and vestibular cues during self-motion perception. *Journal of Neuroscience*, 29(49), 15601–15612. https://doi.org/10.1523/JNEUROSCI.2574-09.2009
- Fitze, D. C., Mast, F. W., & Ertl, M. (2023). Human vestibular perceptual thresholds—A systematic review of passive motion perception. *Gait & Posture*, 107, 83–95. https://doi.org/10.1016/J. GAITPOST.2023.09.011
- Fitzpatrick, A. M., Dundon, N. M., & Valyear, K. F. (2019). The neural basis of hand choice: An fMRI investigation of the Posterior Parietal Interhemispheric Competition model. *NeuroImage*, 185, 208–221. https://doi.org/10.1016/j.neuroimage.2018.10.039
- Franklin, D. W., So, U., Burdet, E., & Kawato, M. (2007). Visual feedback is not necessary for the learning of novel dynamics. *PLOS ONE*, 2(12), e1336. https://doi.org/10.1371/journal.pone.0001336
- Franklin, D. W., & Wolpert, D. M. (2011). Computational mechanisms of sensorimotor control. Neuron, 72(3), 425–442. https://doi.org/10.1016/j.neuron.2011.10.006
- Gabbard, C., & Rabb, C. (2000). What determines choice of limb for unimanual reaching movements? *Journal of General Psychology*, 127(2), 178–184. https://doi.org/10.1080/00221300009598577
- Genzel, D., Firzlaff, U., Wiegrebe, L., & MacNeilage, P. R. (2016). Dependence of auditory spatial updating on vestibular, proprioceptive, and efference copy signals. *Journal of Neurophysiology*, 116(2), 765–775. https://doi.org/10.1152/jn.00052.2016
- Glasauer, S., Amorim, M. A., Viaud-Delmon, I., & Berthoz, A. (2002). Differential effects of labyrinthine dysfunction on distance and direction during blindfolded walking of a triangular path. Experimental Brain Research, 145(4), 489-497. https://doi.org/10.1007/s00221-002-1146-1
- Glasauer, S., Schneider, E., Grasso, R., & Ivanenko, Y. P. (2007). Space-time relativity in self-motion reproduction. *Journal of Neurophysiology*, 97(1), 451-461. https://doi.org/10.1152/jn.01243.2005
- Glaser, J. I., Perich, M. G., Ramkumar, P., Miller, L. E., & Kording, K. P. (2018). Population coding of conditional probability distributions in dorsal premotor cortex. *Nature Communications*, 9(1), 1–14. https://doi.org/10.1038/s41467-018-04062-6

- Goldberg, M. E., Walker, M. F., & Hudspeth, A. J. (2000). The vestibular system. In *Principles of Neural Science* (Fifth edit, pp. 917–934). New York: McGraw-Hill.
- Gonzalez-Moreno, A., Aurtenetxe, S., Lopez-Garcia, M.-E., del Pozo, F., Maestu, F., & Nevado, A. (2014). Signal-to-noise ratio of the MEG signal after preprocessing. *Journal of Neuroscience Methods*, 222, 56-61. https://doi.org/10.1016/j.jneumeth.2013.10.019
- Gonzalez Castro, L. N., Hadjiosif, A. M., Hemphill, M. A., & Smith, M. A. (2014). Environmental consistency determines the rate of motor adaptation. *Current Biology*, 24(10), 1050–1061. https://doi.org/10.1016/j.cub.2014.03.049
- Gordon, G., Kaplan, D. M., Lankow, B., Little, D. Y. J., Sherwin, J., Suter, B. A., & Thaler, L. (2011). Toward an integrated approach to perception and action: Conference report and future directions. Frontiers in Systems Neuroscience, 5, 20. https://doi.org/10.3389/FNSYS.2011.00020
- Grasso, R., Glasauer, S., Georges-François, P., & Israël, I. (1999). Replication of passive whole-body linear displacements from inertial cues: Facts and mechanisms. *Annals of the New York Academy of Sciences*, 871(1), 345–366. https://doi.org/10.1111/J.1749-6632.1999.TB09197.X
- Grent-'t-Jong, T., Oostenveld, R., Jensen, O., Medendorp, W. P., & Praamstra, P. (2014). Competitive interactions in sensorimotor cortex: oscillations express separation between alternative movement targets. *Journal of Neurophysiology*, 112(2), 224–232. https://doi.org/10.1152/jn.00127.2014
- Grent-'t-Jong, T., Oostenveld, R., Medendorp, W. P., & Praamstra, P. (2015). Separating visual and motor components of motor cortex activation for multiple reach targets: A visuomotor adaptation study. *Journal of Neuroscience*, 35(45), 15135–15144. https://doi.org/10.1523/JNEUROSCI.1329-15.2015
- Gu, Y., Watkins, P. V., Angelaki, D. E., & DeAngelis, G. C. (2006). Visual and nonvisual contributions to three-dimensional heading selectivity in the medial superior temporal area. *The Journal of Neuroscience*, 26(1), 73–85. https://doi.org/10.1523/JNEUROSCI.2356-05.2006
- Gutteling, T. P., & Medendorp, W. P. (2016). Role of Alpha-Band Oscillations in Spatial Updating across Whole Body Motion. *Frontiers in Psychology*, 7, 194486. https://doi.org/10.3389/fpsyq.2016.00671
- Gutteling, T. P., Selen, L. P. J., & Medendorp, W. P. (2015). Parallax-sensitive remapping of visual space in occipito-parietal alpha-band activity during whole-body motion. *Journal of Neurophysiology*, 113, 1574–1584. https://doi.org/10.1152/jn.00477.2014
- Guyot, J. P., Perez Fornos, A., Guinand, N., van de Berg, R., Stokroos, R., & Kingma, H. (2016). Vestibular assistance systems: Promises and challenges. *Journal of Neurology*, 263(S1), 30–35. https://doi.org/10.1007/s00415-015-7922-1
- Haggard, P. (2008). Human volition: Towards a neuroscience of will. *Nature Reviews Neuroscience*, 9(12), 934–946. https://doi.org/10.1038/nrn2497
- Hamel-Thibault, A., Thénault, F., Whittingstall, K., & Bernier, P. M. (2018). Delta-band oscillations in motor regions predict hand selection for reaching. *Cerebral Cortex*, 28(2), 574–584. https://doi.org/10.1093/cercor/bhw392
- Heed, T., Beurze, S. M., Toni, I., Röder, B., & Medendorp, W. P. (2011). Functional rather than effector-specific organization of human posterior parietal cortex. *Journal of Neuroscience*, 31(8), 3066–3076. https://doi.org/10.1523/JNEUROSCI.4370-10.2011
- Helmholtz, H. (1867). Handbuch der Physiologischen Optik. Leipzig: Leopold Voss.
- Jacob, M. S., & Duffy, C. J. (2015). Steering transforms the cortical representation of self-movement from direction to destination. *Journal of Neuroscience*, 35(49), 16055–16063. https://doi.org/10.1523/JNEUROSCI.2368-15.2015

- Jasper, H., & Penfield, W. (1949). Electrocorticograms in man: Effect of voluntary movement upon the electrical activity of the precentral gyrus. *Archiv Für Psychiatrie Und Nervenkrankheiten*, 183(1), 163–174. https://doi.org/10.1007/BF01062488
- Jeffreys, H. (1961). Theory of probability. Oxford, UK: Oxford University Press.
- Kandel, E. R., & Hudspeth, A. J. (2000). The Brain and Behavior. In *Principles of Neural Science* (Fifth edit, pp. 5–20). New York: McGraw-Hill.
- Kaski, D., Quadir, S., Nigmatullina, Y., Malhotra, P. A., Bronstein, A. M., & Seemungal, B. M. (2016). Temporoparietal encoding of space and time during vestibular-guided orientation. *Brain*, 139(2), 392–403. https://doi.org/10.1093/brain/awv370
- Kawato, M. (1999). Internal models for motor control and trajectory planning. *Current Opinion in Neurobiology*, 9(6), 718–727. https://doi.org/10.1016/S0959-4388(99)00028-8
- Keshavarzi, S., Velez-Fort, M., & Margrie, T. W. (2023). Cortical integration of vestibular and visual cues for navigation, visual processing, and perception. *Annual Review of Neuroscience*, 46(1), 301–320. https://doi.org/10.1146/annurev-neuro-120722-100503
- Khanna, P., & Carmena, J. M. (2017). Beta band oscillations in motor cortex reflect neural population signals that delay movement onset. *ELife*, 6, e24573. https://doi.org/10.7554/eLife.24573
- Kilavik, B. E., Zaepffel, M., Brovelli, A., MacKay, W. A., & Riehle, A. (2013). The ups and downs of beta oscillations in sensorimotor cortex. *Experimental Neurology*, 245, 15–26. https://doi.org/10.1016/J.EXPNEUROL.2012.09.014
- Kim, H. E., Avraham, G., & Ivry, R. B. (2021). The psychology of reaching: Action selection, movement implementation, and sensorimotor learning. Annual Review of Psychology, 72, 61–95. https://doi.org/10.1146/ANNUREV-PSYCH-010419-051053
- Klaes, C., Westendorff, S., Chakrabarti, S., & Gail, A. (2011). Choosing goals, not rules: Deciding among rule-based action plans. *Neuron*, 70(3), 536-548. https://doi.org/10.1016/j.neuron.2011.02.053
- Körding, K. P., & Wolpert, D. M. (2004). Bayesian integration in sensorimotor learning. *Nature*, 427(6971), 244–247. https://doi.org/10.1038/nature02169
- Lakshminarasimhan, K. J., Avila, E., Pitkow, X., & Angelaki, D. E. (2023). Dynamical latent state computation in the male macaque posterior parietal cortex. *Nature Communications*, 14(1), 1–20. https://doi.org/10.1038/s41467-023-37400-4
- Lakshminarasimhan, K. J., Petsalis, M., Park, H., DeAngelis, G. C., Pitkow, X., & Angelaki, D. E. (2018). A dynamic Bayesian observer model reveals origins of bias in visual path integration. *Neuron*, 99(1), 194–206. https://doi.org/10.1016/j.neuron.2018.05.040
- Lappe, M., Jenkin, M., & Harris, L. R. (2007). Travel distance estimation from visual motion by leaky path integration. *Experimental Brain Research*, 180(1), 35–48. https://doi.org/10.1007/s00221-006-0835-6
- Laurens, J., & Angelaki, D. E. (2017). A unified internal model theory to resolve the paradox of active versus passive self-motion sensation. *ELife*, 6, e28074. https://doi.org/10.7554/ eLife.28074
- Laurens, J., & Droulez, J. (2007). Bayesian processing of vestibular information. *Biological Cybernetics*, 96(4), 389-404. https://doi.org/10.1007/s00422-006-0133-1
- Lawrence, M. A. (2016). ez: Easy analysis and visualization of factorial experiments. Retrieved from https://cran.r-project.org/package=ez
- Little, D. Y., & Sommer, F. T. (2013). Learning and exploration in action-perception loops. Frontiers in Neural Circuits, 7, 37. https://doi.org/10.3389/fncir.2013.00037

- Loomis, J. M., Klatzky, R. L., Golledge, R. G., Cicinelli, J. G., Pellegrino, J. W., & Fry, P. A. (1993). Nonvisual navigation by blind and sighted: Assessment of path integration ability. *Journal of Experimental Psychology: General*, 122(1), 73–91. https://doi.org/10.1037/0096-3445.122.1.73
- MacNeilage, P. R., Ganesan, N., & Angelaki, D. E. (2008). Computational approaches to spatial orientation: From transfer functions to dynamic Bayesian inference. *Journal of Neurophysiology*, 100(6), 2981–2996. https://doi.org/10.1152/jn.90677.2008
- Maris, E., & Oostenveld, R. (2007). Nonparametric statistical testing of EEG- and MEGdata. *Journal of Neuroscience Methods*, 164(1), 177–190. https://doi.org/10.1016/j. jneumeth.2007.03.024
- Marr, D. (1982). Vision: A computational investigation into the human representation and processing of visual information. San Francisco: W.H. Freeman.
- McMenamin, B. W., Shackman, A. J., Maxwell, J. S., Bachhuber, D. R. W., Koppenhaver, A. M., Greischar, L. L., & Davidson, R. J. (2010). Validation of ICA-based myogenic artifact correction for scalp and source-localized EEG. *NeuroImage*, 49(3), 2416–2432. https://doi.org/10.1016/j.neuroimage.2009.10.010
- Medendorp, W. P. (2011). Spatial constancy mechanisms in motor control. *Philosophical Transactions of the Royal Society B: Biological Sciences*, 366(1564), 476–491. https://doi.org/10.1098/rstb.2010.0089
- Medendorp, W. P., Alberts, B. B. G. T., Verhagen, W. I. M., Koppen, M., & Selen, L. P. J. (2018). Psychophysical evaluation of sensory reweighting in bilateral vestibulopathy. *Frontiers in Neurology*, 9, 377. https://doi.org/10.3389/fneur.2018.00377
- Medendorp, W. P., & Heed, T. (2019). State estimation in posterior parietal cortex: Distinct poles of environmental and bodily states. *Progress in Neurobiology*, 183, 101691. https://doi.org/10.1016/j.pneurobio.2019.101691
- Medendorp, W. P., & Selen, L. J. P. (2017). Vestibular contributions to high-level sensorimotor functions. *Neuropsychologia*, 105, 144-152. https://doi.org/10.1016/j.neuropsychologia.2017.02.004
- Merfeld, D. M., Zupan, L., & Peterka, R. J. (1999). Humans use internal models to estimate gravity and linear acceleration. *Nature*, *398*(6728), 615–618. https://doi.org/10.1038/19303
- Nagel, S. (2019). Towards a home-use BCI: fast asynchronous control and robust non-control state detection. Universität Tübingen. https://doi.org/10.15496/PUBLIKATION-37739
- Nash, C. J., & Cole, D. J. (2020). Identification and validation of a driver steering control model incorporating human sensory dynamics. *Vehicle System Dynamics*, *58*(4), 495–517. https://doi.org/10.1080/00423114.2019.1589536
- Nash, C. J., Cole, D. J., & Bigler, R. S. (2016). A review of human sensory dynamics for application to models of driver steering and speed control. *Biological Cybernetics*, 110(2), 91–116. https://doi.org/10.1007/S00422-016-0682-X
- Oldfield, R. C. (1971). The assessment and analysis of handedness: The Edinburgh inventory. Neuropsychologia, 9(1), 97–113. https://doi.org/10.1016/0028-3932(71)90067-4
- Oliveira, F. T. P., Diedrichsen, J., Verstynen, T., Duque, J., & Ivry, R. B. (2010). Transcranial magnetic stimulation of posterior parietal cortex affects decisions of hand choice. *Proceedings of the National Academy of Sciences of the United States of America*, 107(41), 17751–17756. https://doi.org/10.1073/pnas.1006223107
- Oostenveld, R., Fries, P., Maris, E., & Schoffelen, J. M. (2011). FieldTrip: Open source software for advanced analysis of MEG, EEG, and invasive electrophysiological data. *Computational Intelligence and Neuroscience*, 2011. https://doi.org/10.1155/2011/156869

- Oostwoud Wijdenes, L., Ivry, R. B., & Bays, P. M. (2016). Competition between movement plans increases motor variability: Evidence of a shared resource for movement planning. *Journal of Neurophysiology*, 116(3), 1295–1303. https://doi.org/10.1152/jn.00113.2016
- Oostwoud Wijdenes, L., Wynn, S. C., Roesink, B. S., Schutter, D. J. L. G., Selen, L. P. J., & Medendorp, W. P. (2022). Assessing corticospinal excitability and reaching hand choice during whole body motion. *Journal of Neurophysiology*, 128(1), 19–27. https://doi.org/10.1152/JN.00699.2020
- Page, W. K., & Duffy, C. J. (2008). Cortical neuronal responses to optic flow are shaped by visual strategies for steering. *Cerebral Cortex*, 18(4), 727–739. https://doi.org/10.1093/cercor/bhm109
- Pape, A.-A., & Siegel, M. (2016). Motor cortex activity predicts response alternation during sensorimotor decisions. *Nature Communications*, 7(1), 1–10. https://doi.org/10.1038/ncomms13098
- Perfetti, B., Moisello, C., Landsness, E. C., Kvint, S., Pruski, A., Onofrj, M., Tononi, G., Ghilardi, M. F. (2011). Temporal evolution of oscillatory activity predicts performance in a choice-reaction time reaching task. *Journal of Neurophysiology*, 105(1), 18–27. https://doi.org/10.1152/jn.00778.2010
- Perrotta, M. V., Asgeirsdottir, T., & Eagleman, D. M. (2021). Deciphering sounds through patterns of vibration on the skin. *Neuroscience*, 458(1), 77-86. https://doi.org/10.1016/j.neuroscience.2021.01.008
- Petzschner, F. H., & Glasauer, S. (2011). Iterative Bayesian estimation as an explanation for range and regression effects: A study on human path integration. *Journal of Neuroscience*, 31(47), 17220–17229. https://doi.org/10.1523/JNEUROSCI.2028-11.2011
- Pezzulo, G., & Cisek, P. (2016). Navigating the affordance landscape: Feedback control as a process model of behavior and cognition. *Trends in Cognitive Sciences*, 20(6), 414–424. https://doi.org/10.1016/j.tics.2016.03.013
- Pfurtscheller, G. (1992). Event-related synchronization (ERS): an electrophysiological correlate of cortical areas at rest. *Electroencephalography and Clinical Neurophysiology*, 83(1), 62–69. https://doi.org/10.1016/0013-4694(92)90133-3
- Poulton, E. C. (1975). Observer bias. *Applied Ergonomics*, 6(1), 3-8. https://doi.org/10.1016/0003-6870(75)90204-5
- Prsa, M., Jimenez-Rezende, D., & Blanke, O. (2015). Inference of perceptual priors from path dynamics of passive self-motion. *Journal of Neurophysiology*, 113(5), 1400–1413. https://doi.org/10.1152/jn.00755.2014
- R Core Team. (2017). R: A language and environment for statistical computing. Vienna, Austria: R Foundation for Statistical Computing. Retrieved from https://www.r-project.org/
- Rhodes, E., Gaetz, W. C., Marsden, J., & Hall, S. D. (2018). Transient alpha and beta synchrony underlies preparatory recruitment of directional motor networks. *Journal of Cognitive Neuroscience*, 30(6), 867–875. https://doi.org/10.1162/jocn\_a\_01250
- Rineau, A. L., Bringoux, L., Sarrazin, J. C., & Berberian, B. (2023). Being active over one's own motion: Considering predictive mechanisms in self-motion perception. *Neuroscience & Biobehavioral Reviews*, 146, 105051. https://doi.org/10.1016/J.NEUBIOREV.2023.105051
- Rouder, J. N., Morey, R. D., Speckman, P. L., & Province, J. M. (2012). Default Bayes factors for ANOVA designs. *Journal of Mathematical Psychology*, 56(5), 356-374. https://doi.org/10.1016/j.jmp.2012.08.001

- Roy, J. E., & Cullen, K. E. (2001). Selective processing of vestibular reafference during selfgenerated head motion. *The Journal of Neuroscience*, *21*(6), 2131–2142. https://doi. org/10.1523/JNEUROSCI.21-06-02131.2001
- Sanders, M. C., Chang, N. Y. N., Hiss, M. M., Uchanski, R. M., & Hullar, T. E. (2011). Temporal binding of auditory and rotational stimuli. *Experimental Brain Research*, 210(3-4), 539-547. https://doi.org/10.1007/s00221-011-2554-x
- Sarwary, A. M. E., Selen, L. P. J., & Medendorp, W. P. (2013). Vestibular benefits to task savings in motor adaptation. *Journal of Neurophysiology*, 110(6), 1269-1277. https://doi.org/10.1152/jn.00914.2012
- Schmitt, C., Krala, M., & Bremmer, F. (2022). Neural signatures of actively controlled self-motion and the subjective encoding of distance. *eNeuro*, 9(6), 1–18. https://doi.org/10.1523/ENEURO.0137-21.2022
- Schoffelen, J. M., Oostenveld, R., & Fries, P. (2005). Neuronal coherence as a mechanism of effective corticospinal interaction. *Science*, 308(5718), 111–113. https://doi.org/10.1126/SCIENCE.1107027
- Schroeder, C. E., Wilson, D. A., Radman, T., Scharfman, H., & Lakatos, P. (2010). Dynamics of active sensing and perceptual selection. *Current Opinion in Neurobiology*, 20(2), 172–176. https://doi.org/10.1016/J.CONB.2010.02.010
- Schumann, F., & O'Regan, J. K. (2017). Sensory augmentation: Integration of an auditory compass signal into human perception of space. Scientific Reports, 7(1), 42197. https:// doi.org/10.1038/srep42197
- Schweighofer, N., Xiao, Y., Kim, S., Yoshioka, T., Gordon, J., & Osu, R. (2015). Effort, success, and nonuse determine arm choice. *Journal of Neurophysiology*, 114(1), 551–559. https://doi.org/10.1152/jn.00593.2014
- Scott, S. H. (2004). Optimal feedback control and the neural basis of volitional motor control.

  Nature Reviews Neuroscience 2004 5:7, 5(7), 532–545. https://doi.org/10.1038/nrn1427
- Shadmehr, R., Huang, H. J., & Ahmed, A. A. (2016). A representation of effort in decision-making and motor control. *Current Biology*, 26, 1929–1934. https://doi.org/10.1016/j.cub.2016.05.065
- Smith, M. A., Ghazizadeh, A., & Shadmehr, R. (2006). Interacting adaptive processes with different timescales underlie short-term motor learning. *PLOS Biology*, 4(6), e179. https://doi.org/10.1371/JOURNAL.PBIO.0040179
- Snyder, D. B., Beardsley, S. A., & Schmit, B. D. (2019). Role of the cortex in visuomotor control of arm stability. *Journal of Neurophysiology*, 122(5), 2156–2172. https://doi.org/10.1152/JN.00003.2019
- Stavropoulos, A., Lakshminarasimhan, K. J., Laurens, J., Pitkow, X., & Angelaki, D. (2022). Influence of sensory modality and control dynamics on human path integration. *ELife*, 11. https://doi.org/10.7554/eLife.63405
- Stoloff, R. H., Taylor, J. A., Xu, J., Ridderikhoff, A., & Ivry, R. B. (2011). Effect of reinforcement history on hand choice in an unconstrained reaching task. *Frontiers in Neuroscience*, *5*, 41. https://doi.org/10.3389/fnins.2011.00041
- ter Horst, A. C., Koppen, M., Selen, L. P. J., & Medendorp, W. P. (2015). Reliability-based weighting of visual and vestibular cues in displacement estimation. *PLOS ONE*, 10(12), e0145015. https://doi.org/10.1371/journal.pone.0145015
- Todorov, E., & Jordan, M. I. (2002). Optimal feedback control as a theory of motor coordination. Nature Neuroscience 2002 5:11, 5(11), 1226–1235. https://doi.org/10.1038/nn963

- Tramper, J. J., & Medendorp, W. P. (2015). Parallel updating and weighting of multiple spatial maps for visual stability during whole body motion. *Journal of Neurophysiology*, 114(6), 3211–3219. https://doi.org/10.1152/jn.00576.2015
- Tresilian, J. (2012). Sensorimotor control and learning: An introduction to the behavioral neuroscience of action. London: Bloomsbury Publishing.
- Trommershäuser, J., Maloney, L. T., & Landy, M. S. (2009). The expected utility of movement. In *Neuroeconomics* (pp. 95–111). Academic Press. https://doi.org/10.1016/B978-0-12-374176-9.00008-7
- Tzagarakis, C., Ince, N. F., Leuthold, A. C., & Pellizzer, G. (2010). Beta-band activity during motor planning reflects response uncertainty. *Journal of Neuroscience*, 30(34), 11270-11277. https://doi.org/10.1523/JNEUROSCI.6026-09.2010
- Tzagarakis, C., West, S., & Pellizzer, G. (2015). Brain oscillatory activity during motor preparation: effect of directional uncertainty on beta, but not alpha, frequency band. *Frontiers in Neuroscience*, 9(JUN), 246. https://doi.org/10.3389/fnins.2015.00246
- van Beers, R. J., Haggard, P., & Wolpert, D. M. (2004). The Role of Execution Noise in Movement Variability. *Journal of Neurophysiology*, *91*(2), 1050–1063. https://doi.org/10.1152/jn.00652.2003
- van de Berg, R., Guinand, N., Ranieri, M., Cavuscens, S., Nguyen, T. A. K., Guyot, J. P., Lucieer, F., Starkov, D., Kingma, H., van Hoof, M., Perez-Fornos, A. (2017). The vestibular implant input interacts with residual natural function. *Frontiers in Neurology*, 8, 644. https://doi.org/10.3389/FNEUR.2017.00644
- Van Der Werf, J., Jensen, O., Fries, P., & Medendorp, W. P. (2010). Neuronal synchronization in human posterior parietal cortex during reach planning. *Journal of Neuroscience*, 30(4), 1402–1412. https://doi.org/10.1523/JNEUROSCI.3448-09.2010
- van Helvert, M. J. L., Selen, L. P. J., van Beers, R. J., & Medendorp, W. P. (2022). Predictive steering: Integration of artificial motor signals in self-motion estimation. *Journal of Neurophysiology*, 128(6), 1395–1408. https://doi.org/10.1152/jn.00248.2022
- van Wijk, B. C. M., Daffertshofer, A., Roach, N., & Praamstra, P. (2009). A role of beta oscillatory synchrony in biasing response competition? *Cerebral Cortex*, 19(6), 1294–1302. https://doi.org/10.1093/CERCOR/BHN174
- von Holst, E., & Mittelstaedt, H. (1950). The principle of reafference: Interactions between the central nervous system and the peripheral organs. Retrieved from https://courses.cit.cornell.edu/bionb4240/Documents/Holst\_Mittelsteadt\_1950\_English.pdf
- Wei, K., & Körding, K. (2010). Uncertainty of feedback and state estimation determines the speed of motor adaptation. *Frontiers in Computational Neuroscience*, 4, 11. https://doi.org/10.3389/fncom.2010.00011
- Westbrook, G. L. (2000). Seizures and epilepsy. In *Principles of Neural Science* (Fifth edit, pp. 1116–1139). New York: McGraw-Hill.
- Wichmann, F. A., & Hill, N. J. (2001). The psychometric function: I. Fitting, sampling, and goodness of fit. *Perception and Psychophysics*, 63(8), 1293–1313. https://doi.org/10.3758/BF03194544
- Wolpert, D. M., & Bastian, A. J. (2021). Principles of sensorimotor control. In *Principles of Neural Science* (Sixth edit, pp. 713–736). New York: McGraw-Hill.
- Wolpert, D. M., & Landy, M. S. (2012). Motor control is decision-making. *Current Opinion in Neurobiology*, 22(6), 996–1003. https://doi.org/10.1016/j.conb.2012.05.003

- Wolpert, D. M., Miall, R. C., & Kawato, M. (1998). Internal models in the cerebellum. *Trends in Cognitive Sciences*, 2(9), 338–347. https://doi.org/10.1016/S1364-6613(98)01221-2
- Wolpert, D. M., Pearson, K. G., & Ghez, C. P. J. (2000). The organization and planning of movement. In *Principles of Neural Science* (Fifth edit, pp. 743–767). New York: McGraw-Hill.
- Worchel, P. (1952). The role of the vestibular organs in space orientation. *Journal of Experimental Psychology*, 44(1), 4–10. https://doi.org/10.1037/h0058791
- Zaidel, A., Turner, A. H., & Angelaki, D. E. (2011). Multisensory calibration is independent of cue reliability. *Journal of Neuroscience*, 31(39), 13949–13962. https://doi.org/10.1523/JNEUROSCI.2732-11.2011
- Zhou, L., & Gu, Y. (2023). Cortical mechanisms of multisensory linear self-motion perception. Neuroscience Bulletin, 39(1), 125–137. https://doi.org/10.1007/s12264-022-00916-8

# **Dutch summary**

In ons dagelijks leven lijken we moeiteloos door onze omgeving te bewegen terwijl we daarbij interacteren met voorwerpen om ons heen. Hoewel onze omgeving continu verandert en ontelbare mogelijkheden voor interacties bevat, gaat ons dit meestal gemakkelijk af. Op de achtergrond spelen er echter complexe en onbewuste hersenprocessen die de noodzakelijke koppeling tussen perceptie en actie voor interactie met de omgeving tot stand brengen. In dit proefschrift heb ik een aantal van deze processen onderzocht.

In **Hoofdstuk 2** heb ik onderzocht hoe onze hersenen bewegingen selecteren en voorbereiden. Met behulp van elektro-encefalografie, een methode om de elektrische activiteit van de hersenen te meten, heb ik bekeken of onze hersenen tijdens het kiezen van een beweging met de linker- of de rechterhand in eerste instantie beide bewegingen voorbereiden. De resultaten laten zien dat proefpersonen langer nodig hadden om met de beweging te beginnen wanneer ze zelf mochten kiezen tussen de linker- of de rechterhand dan wanneer de te bewegen hand vooraf bepaald was. Ook zag ik dat de sterkte van bètagolven, trillingen met een frequentie van 13 tot 30 Hz, in de hersenactiviteit voorafgaand aan de beweging sterker afnam als de te bewegen hand vooraf bepaald was, wat geassocieerd kan worden met een betere voorbereiding van de beweging. Deze resultaten suggereren dat de hersenen gelijktijdig meerdere bewegingen voorbereiden als er gekozen moet worden voor de linker- of de rechterhand.

In **Hoofdstuk 3 en 4** heb ik onderzocht hoe de hersenen er tijdens een beweging voor zorgen dat de beweging efficiënt verloopt op basis van zintuiglijke terugkoppeling en verwachtingen over de beweging. Hiervoor heb ik gebruik gemaakt van experimenten waarbij de proefpersonen op een bewegend platform zaten en een stuur gebruikten om de beweging van het platform te controleren. In **Hoofdstuk 3** heb ik het stuurgedrag van proefpersonen die op het bewegende platform zaten vergeleken met het stuurgedrag van proefpersonen die tijdens het experiment niet zelf bewogen maar wel het resultaat op een scherm zagen. De proefpersonen die zelf bewogen reageerden sneller op plotselinge veranderingen in de relatie tussen de beweging van het stuur en het platform dan proefpersonen waar het stuur alleen tot een visuele verandering leidde. Dit suggereert dat de proefpersonen de informatie van het evenwichtsorgaan vergeleken met de verwachtingen die ze over de beweging hadden op basis van hun stuurgedrag.

In **Hoofdstuk 4** ging ik dieper in op de rol van verwachtingen in stuurgedrag door te onderzoeken of proefpersonen meer vertrouwen op verwachtingen over de beweging van het platform als de relatie tussen de beweging van het stuur en de beweging van het platform voorspelbaarder is. Hiervoor heb ik het stuurgedrag van proefpersonen vergeleken in drie experimentele condities. In één conditie bleef de relatie tussen de beweging van het stuur en de beweging van het platform constant. In de andere twee condities veranderde deze relatie van beweging tot beweging en was de voorspelbaarheid van de relatie relatief hoog ("random walk" of "dronkemanswandeling") of laag ("witte ruis"). Wanneer de voorspelbaarheid van de relatie relatief hoog was, bleken proefpersonen in hun stuurgedrag meer rekening te houden met de relatie tussen de beweging van het stuur en de beweging van het platform tijdens de voorgaande beweging dan wanneer de voorspelbaarheid van de relatie relatief laag was. Dit suggereert dat de proefpersonen in de hersenen een interne representatie, of een intern model, gevormd hadden van de relatie tussen de beweging van het stuur en de zintuiglijke terugkoppeling over de beweging van het platform, waarmee ze voorspellingen maakten om de beweging van het platform beter in te schatten.

# Research data management

This research followed the applicable laws and ethical guidelines. Research Data Management was conducted according to the FAIR principles. The paragraphs below specify in detail how this was achieved.

#### Ethics

This thesis is based on the results of human studies, which were conducted in accordance with the principles of the Declaration of Helsinki. The Ethical Committee of the faculty of Social Sciences (ECSS) has given a positive advice to conduct these studies to the Dean of the Faculty, who formally approved the conduct of these studies (ECSW2017-0805-504 and ECSW-2022-082). Data collection was performed at the Donders Centre for Cognition. Informed consent was obtained on paper following the Centre procedure. The forms are archived in the central archive of the Centre for 10 years after termination of the studies. This research was funded by an internal grant from the Donders Centre for Cognition.

#### Findable and accessible

The table below details where the data and research documentation for each chapter can be found on the Donders Repository. All data archived as a Data Sharing Collection (DSC) remain available for at least 10 years after termination of the studies.

Chapter	DAC	RDC	DSC	DSC License
2	DAC_2017.00123_568	RDC_2017.00123_052	DSC_2017.00123_365	RU-DI- HD-1.0
3	DAC_2019.00064_438	RDC_2019.00064_388	DSC_2019.00064_640	RU-DI- NH-1.0
4	DAC_2023.00037_058	RDC_2023.00037_928	DSC_2023.00037_462	

DAC = Data Acquisition Collection, RDC = Research Documentation Collection, DSC = Data **Sharing Collection** 

The manuscript of **Chapter 4** is currently under review, and the data are shared with the reviewers in a DSC and will be made publicly available once the article has been published. It will then be shared under the CC-BY-4.0 license.

The raw data are stored in the Data Acquisition Collection (DAC) in their original form. For the Research Documentation Collection (RDC) and DSC long-lived file formats have been used, ensuring that data remains usable in the future. We provide a description of the experimental setup, raw data (DAC and DSC), and the analysis scripts (RDC and DSC) in the readme files to make sure that the results are reproducible.

#### **Privacy**

The privacy of the participants in this thesis has been warranted using random individual subject codes. A pseudonymization key linked this random code with the personal data. This pseudonymization key was stored on a network drive that was only accessible to members of the project who needed access to it because of their role within the project. The pseudonymization key was stored separately from the research data. The pseudonymization keys were destroyed within one month after finalization of these projects.

## About the author

Milou van Helvert was born in Eindhoven, the Netherlands, on September 24, 1994. In 2012, she started the bachelor's program in Psychobiology at the University of Amsterdam. She wrote her thesis on the effectiveness of a cueing device to improve walking in people with Parkinson's disease, which she investigated during an internship in the Neural Movements Disorders lab of the Donders Institute for Brain, Cognition and Behaviour. After obtaining her bachelor's degree in 2015. Milou took a gap year and worked as a teaching assistant for the Psychobiology bachelor's program and as a research assistant at the Spinoza Centre for Neuroimaging in Amsterdam. In 2016, she started the master's program in Cognitive Neuroscience at Radboud University, and did an internship in the Sensorimotor lab of the Donders Institute for Brain, Cognition and Behaviour. Here, she studied neural activity during hand choice. After obtaining her master's degree in 2018, she continued her career as a PhD candidate in the Sensorimotor lab. Her PhD project focused on the neural control of reaching and steering movements. Milou currently works as a postdoctoral researcher in the Sensorimotor lab on a project that aims to improve home rehabilitation in children with neurological disorders.

## Donders Graduate School

For a successful research Institute, it is vital to train the next generation of scientists. To achieve this goal, the Donders Institute for Brain, Cognition and Behaviour established the Donders Graduate School in 2009. The mission of the Donders Graduate School is to guide our graduates to become skilled academics who are equipped for a wide range of professions. To achieve this, we do our utmost to ensure that our PhD candidates receive support and supervision of the highest quality.

Since 2009, the Donders Graduate School has grown into a vibrant community of highly talented national and international PhD candidates, with over 500 PhD candidates enrolled. Their backgrounds cover a wide range of disciplines, from physics to psychology, medicine to psycholinguistics, and biology to artificial intelligence. Similarly, their interdisciplinary research covers genetic, molecular, and cellular processes at one end and computational, system-level neuroscience with cognitive and behavioral analysis at the other end. We ask all PhD candidates within the Donders Graduate School to publish their PhD thesis in de Donders Thesis Series. This series currently includes over 600 PhD theses from our PhD graduates and thereby provides a comprehensive overview of the diverse types of research performed at the Donders Institute. A complete overview of the Donders Thesis Series can be found on our website: https://www.ru.nl/donders/donders-series.

The Donders Graduate School tracks the careers of our PhD graduates carefully. In general, the PhD graduates end up at high-quality positions in different sectors, for a complete overview see https://www.ru.nl/donders/ destination-our-former-phd. A large proportion of our PhD alumni continue in academia (>50%). Most of them first work as a postdoc before growing into more senior research positions. They work at top institutes worldwide, such as University of Oxford, University of Cambridge, Stanford University, Princeton University, UCL London, MPI Leipzig, Karolinska Institute, UC Berkeley, EPFL Lausanne, and many others. In addition, a large group of PhD graduates continue in clinical positions, sometimes combining it with academic research. Clinical positions can be divided into medical doctors, for instance, in genetics, geriatrics, psychiatry, or neurology, and in psychologists, for instance as healthcare psychologist, clinical neuropsychologist, or clinical psychologist. Furthermore, there are PhD graduates who continue to work as researchers outside academia, for instance at non-profit or government organizations, or in pharmaceutical companies. There are also PhD graduates who work in education, such as teachers in high school, or as lecturers in higher education. Others continue in a wide range of positions, such as policy advisors, project managers, consultants, data scientists, web- or software developers, business owners, regulatory affairs specialists, engineers, managers, or IT architects. As such, the career paths of Donders PhD graduates span a broad range of sectors and professions, but the common factor is that they almost all have become successful professionals.

For more information on the Donders Graduate School, as well as past and upcoming defenses please visit: http://www.ru.nl/donders/ graduate-school/phd/.

# Acknowledgements

Throughout my PhD, many people have supported me in various ways. Without their help, this work would not have been possible. Given that you are reading this part of the thesis, I suspect you are one of them. Thank you! I would also like to take this opportunity to extend special thanks to a few people.

Luc, Rob and Pieter, thank you very much for being great supervisors. You have guided me on this journey and gave me the opportunity to learn a lot over the past years. I think we made a good team! Luc, I appreciate it that you checked in with me regularly and dared to play the devil's advocate from time to time. Fortunately, you also always took the time to help me get back on track when the advocate had a point, be it in the lab or on a more conceptual level. Rob, in such situations you always remained calm, and you were able to keep both the bigger picture and tiny details in mind to find a solution. Thank you for encouraging me to take the time to develop my skills and helping me out. Pieter, you always remained positive and saw the glass half full and fortunately enough this was contagious. I admire your enthusiasm and pragmatism. Thank you for your patience when I missed another deadline. I am very happy that you dared to take on another project with me!

Leonie and Linda, thank you both very much for your help during and after my internship. At the start of my PhD I did not expect our hand choice experiment to be included in this thesis, but I am very happy that we managed to get a grasp on the data during COVID. You both are very inspiring people, serious about science in a (seemingly) relaxed way!

I would like to thank all other (former and current) members of the Sensorimotor lab for their feedback and for thinking along, but also for the chats, lunch breaks, game nights and fun trips: Antonella, Aslan, Bart, Brandon, Debora, Erik, Florian, Hüseyin, James, Janny, Johannes, Judith, Katrin K., Katrin S., Kevin, Lonneke, Luke, Mathieu, Mathilde, Nika, Noel, Nynke, Palak, Sonal, Sophie, Valeria and Yvonne. Erik, thank you for being my fun officemate in the Spinoza building, distracting me with crazy questions! Debora, thank you for allowing me to be your supervisor during your internship, even though I had only just finished mine. Yvonne, I am very happy that we got to do quite some things together during our PhDs, such as teaching and being a member of the same peer coaching group. I enjoy your company a lot, and admire your drive to be a great scientist. Judith and Katrin, thank you for all the fun coffee

and lunch breaks, and for being great friends. You set a very good example for me by "just" finishing your thesis (even though I did not manage to do this as smoothly as the two of you did). I am very happy to have met you!

I knocked on the doors of the members of the Technical Support Group a lot. Wilbert, thank you very much for taking the time to rewrite the sled library and for all the trouble shooting over the years. Being able to use the sled in the velocity mode has opened up a lot of opportunities for cool experiments, I hope this makes it all worth it! Gerard, thank you for all your help and for all the fun chats on guiet Friday afternoons. You have really helped me out a lot, and I really appreciate it! Also thanks to Hubert, Maarten, Norbert, Pascal, Philip, Truus and Twan for their help throughout the years.

Miriam, thank you for all your help and for the fun times during our meetings for my PhD job. You involved me in all kinds of activities and committees, and I really enjoyed it and learned a lot! Also, Pauline, Jiska and Ronny, thank you for your help. Vanessa, Karin and Jolanda, thank you for always answering my questions, for all the chats, and for turning every day into a party! Charlotte and Randi, thank you for being such nice colleagues. Marlijn, I could indeed have never imagined that we would both still be working at the Donders Institute almost ten years after starting our master's, but I am very happy that we are! Thank you for being such a good and fun friend, and I am very curious to see what we will be doing ten years from now!

During my PhD, I was also involved in a project on Usher syndrome. Wim and Ronald, thank you for making this possible and for thinking along. Mirthe, thank you for your help with participant recruitment. Aniek, thank you for helping out with the code for the eye tracker. Also, thanks a lot to the people who participated in the experiment!

I would also like to thank my peer coaching group. Knowing that we all faced similar smaller problems and being there for each other through larger struggles was really nice. Thank you for being there!

Nina, Jeroen, Anne, Hari, Florence and Clémence, thank you for the fun discussions and the good times during NCM in Dublin. Nina, I am very happy that you agreed to being a member of my defense committee! Anne, Hari and Clémence, thank you showing us around in Brussels!

Ook buiten het werk om heb ik veel steun gekregen van de mensen om me heen. Wikke, Anne-Sophie, Veerle, Ruth, Gesina, Susanne en Thijmen, bedankt dat jullie zulke lieve vrienden zijn. Wikke, bedankt dat je mij fit hebt gehouden en dat ik altijd bij jou en Tom mag komen logeren. Anne-Sophie, bedankt voor je flauwe grapjes en je betrokkenheid. Veerle, bedankt dat je al zo lang lief bent en dat ook blijft. Ruth, bedankt voor al je tripjes naar Nijmegen en je zeer gewaardeerde mening. Gesina, bedankt voor je gezelligheid en het een feestje maken van dingen. Susanne, bedankt voor je aanstekelijke lach, ik ben blij dat die "just a call away" is. Thijmen, bedankt voor de gezellige koffiepauzes en het (huil)lachen over onze PhDs.

Alexandra, Jan, Joyce, Jack, Stephanie, Rik, Lotte en Timo, bedankt dat jullie zo'n lieve schoonfamilie voor mij zijn. Ik ben heel blij dat ik jullie met Kris erbij heb gekregen. Lieve ooms en tantes en neefjes en nichtjes, heel erg bedankt dat jullie er zijn. Ik vind het heel bijzonder dat we zo close zijn. Luuk en Margot, bedankt dat jullie mijn liefste vriendjes zijn. Ik ben heel blij dat we zo dichtbij elkaar staan (letterlijk en figuurlijk), en dat jullie erbij zijn tijdens mijn verdediging. Boris, Zowi en Monti, ik vind jullie lief. Pappa en mamma, ik ben heel erg blij met jullie, heel erg bedankt dat jullie zo lief zijn, alles goed vinden en ons dingen zelf laten ontdekken. Kris, bedankt dat je mijn grootste cheerleader bent en dat je van alles wat ik doe denkt dat het goed is, gewoon omdat ik het ben. Ik mag alles van jou, en jij geeft mij ook het gevoel dat ik alles kan! Tuur, ik ben gewoon superblij dat jij er bent!

Dit boekje wil ik graag officieus opdragen aan mijn lieve opa en oma's. Oma Wies, ik denk aan je! Opa Piet en oma Joek, heel erg bedankt dat jullie zo lief zijn en dat jullie altijd zo geïnteresseerd zijn in mijn werk. Jullie weten altijd precies wat er in de krant staat of op tv komt als het met mijn werk te maken heeft, hebben mijn opname voor een congres meerdere keren bekeken en hebben zelfs een keer meegedaan aan een onderzoek. En dat terwijl jullie er toch niks van begrijpen (grapje)!



